Materials & Design 270 (2026) 116872

Contents lists available at ScienceDirect

Materials & Design

journal homepage: www.elsevier.com/locate/matdes

A systematic review on interlocking structures to enhance dissimilar materials joining by additive manufacturing

Federica Valenza [a,c,d], Eleonora Atzeni [a,c,d], Alberta Aversa [b,c,d,*], Sara Biamino [b,c,d], Alessandro Salmi [a,c,d]

[a] Politecnico di Torino, Department of Management and Production Engineering, Corso Duca degli Abruzzi 24, 10129 Torino, Italy
[b] Politecnico di Torino, Department of Applied Science and Technology, Corso Duca degli Abruzzi 24, 10129 Torino, Italy
[c] Politecnico di Torino, Interdepartmental Center of Integrated Additive Manufacturing (IAM@PoliTO), Corso Castelfidardo 51, 10129 Torino, Italy
[d] National Interuniversity Consortium of Materials Science and Technology, INSTM, Via G. Giusti 9, 50121 Firenze, Italy

ARTICLE INFO

Keywords:
Mechanical interlocking
Additive manufacturing
Multi-material systems
Dissimilar materials joining
Interface engineering

ABSTRACT

Multi-material systems are increasingly pursued to meet industrial demands for lightweight, high-performance structures. However, reliable joining remains critical. In recent years, mechanical interlocking has emerged as a promising strategy to overcome limitations of conventional joining methods such as adhesive bonding, mechanical fastening, and welding. By exploiting the geometric freedom of Additive Manufacturing (AM), interlocking structures can be directly integrated into the interface, enabling new opportunities for multi-material integration. Yet, the literature remains fragmented and lacks transferable design principles. This study reframes AM-enabled interlocking as a design-driven interface strategy and, through a PRISMA-guided literature review, introduces a unified design-material-process-performance mapping of the field. Interlocking structures are classified across scales as micro-features, macro-pins, and macro-lattices, and further interpreted through a common set of mechanism-based descriptors. These design categories are then examined alongside dominant material combinations, AM and joining processes, reported mechanical response and failure modes. Sector-specific requirements in aerospace, mobility, biomedical, robotics, and electronics applications are mapped onto the proposed framework, and the main barriers to industrial uptake – lack of standardization, limited non-destructive inspection, scalability, and sustainability – are translated into concrete research directions.

1. Introduction

The industry is increasingly interested in multi-material components, particularly in the aerospace, automotive, and defense fields. These multi-material components help integrate different functions into a single component, achieve customizable properties, and outperform single-material parts. By strategically selecting materials, highly functional and lightweight components can be developed. The resulting weight reduction significantly decreases fuel and energy consumption, contributing to the mitigation of emissions required to meet the increasingly stringent climate targets. Different techniques allow obtaining multi-material components, including using functionally graded materials. A special scenario arises when different materials are joined to combine their properties, as in the case of sandwich structures,

Abbreviations: ABS, Acrylonitrile Butadiene Styrene; AI, Artificial Intelligence; AM, Additive Manufacturing; ASA, Acrylonitrile Styrene Acrylate; BCC, Body-Centered Cubic; BCCZ, Body-Centered Cubic Reinforced along Z-direction; BFRP, Basalt Fiber Reinforced Polymer; CFRP, Carbon Fiber Reinforced Polymer; DED, Directed Energy Deposition; DIC, Digital Image Correlation; EBSD, Electron Backscatter Diffraction; EDS, Energy Dispersive Spectroscopy; FCC, Face-Centered Cubic; FEM, Finite Element Modelling; FFF, Fused Filament Fabrication; FRP, Fiber Reinforced Polymer; GFRP, Glass Fiber Reinforced Polymer; HYPER, Hybrid Penetrative Reinforcement; MEX, Material Extrusion; μCT, Micro-Computed Tomography; MJT, Material Jetting; MMAM, Multi-Material Additive Manufacturing; OM, Optical Microscopy; PA, Polyamide; PAEK, Polyaryletherketone; PBF, Powder Bed Fusion; PBF-EB, Powder Bed Fusion with Electron Beam; PBF-LB, Powder Bed Fusion with Laser Beam; PC, Polycarbonate; PE, Polyethylene; PEEK, Polyether Ether Ketone; PET, Polyethylene Terephthalate; PH-SS, Precipitation-Hardening Stainless Steel; PLA, Polylactic Acid; PMMA, Polymethyl Methacrylate; PP, Polypropylene; PRISMA, Preferred Reporting Items for Systematic Reviews and Meta-Analyses; PTFE, Polytetrafluoroethylene; PU, Polyurethane; SEM, Scanning Electron Microscopy; TPMS, Triply Periodic Minimal Surface; VARI, Vacuum Assisted Resin Infusion; VPP, Vat Photopolymerization; XRD, X-Ray Diffraction.

* Corresponding author at: Politecnico di Torino, Department of Applied Science and Technology, Corso Duca degli Abruzzi 24, 10129 Torino, Italy.
E-mail address: alberta.aversa@polito.it (A. Aversa).

https://doi.org/10.1016/j.matdes.2026.116872
Received 24 March 2026; Received in revised form 5 August 2026; Accepted 23 August 2026
Available online 24 August 2026

where stiff face sheets and lightweight cores are integrated to achieve enhanced structural efficiency [1,2], or in the case of fan blades for aero-engines, where metallic leading edges are combined with composite airfoils to improve impact resistance while reducing weight [3]. In such an application, the performance of multi-material components is highly dependent on the quality of the interfacial bond between the materials to be joined, especially when joining materials characterized by different coefficients of thermal expansion, stiffness, and chemical properties. The interface is typically a critical area requiring appropriate processing, dimensioning, and design.

Several technologies can be applied to join dissimilar materials, including adhesive bonding, mechanical fastening, welding, or a combination of them, such as adhesive-bolt hybrid joints. Each of these techniques presents well-known intrinsic limitations [4]: adhesive bonding suffers from costly surface pre-treatments and uncertain long-term durability [5,6]; mechanical fastening introduces additional weight and stress concentrations around the fixing holes [7]; welding is restricted by material compatibility and, for dissimilar pairs such as metals and polymers, typically yields porosity, thermal degradation and weak interfacial adhesion [8]. Hybrid solutions can partially mitigate these issues, but they also inherit the drawbacks of the combined techniques, while adding manufacturing complexity and cost [6]. Consequently, novel joining strategies have been recently explored to overcome these limitations.

Among the emerging methods for joining dissimilar materials to create a multi-material component, this review examines the strategy of mechanical interlocking. This technique relies on the principle of physically interlocking components by properly designed structures on the surface of the materials involved. A noteworthy advantage of this approach is that it enhances the mechanical strength and toughness at the interface, preventing catastrophic failure when compared with adhesive joints [9]. Additionally, it enables mechanical load transfer between the two materials, removing the need for additional locking elements in contrast to mechanical fastening, while also addressing the issues associated with the thermal resistance in welding [10]. New challenges, though, arise with regard to end-of-life procedures, particularly the separation of multi-material structures in the light of recyclability and sustainability.

Various techniques can be employed to produce interlocking structures, including molding, machining, and Additive Manufacturing (AM). This review focuses on interlocking structures produced by AM, taking advantage of the design freedom that this technology permits. AM enables the direct fabrication of geometrically tailored interfacial features, with a level of complexity that is difficult or impossible to achieve through conventional processes. This could enable the interlocking structures to be adapted to the material combination, manufacturing strategy, and expected loading condition, while also simplifying the assembly phase and potentially reducing costs and time required.

Despite the growing interest in the field, the current literature on AM-enabled interlocking remains highly fragmented, thereby slowing technological maturation. This review aims to systematically present the state of the art of mechanical interlocking joints produced using AM technologies, offering a structured map that integrates interlocking structures design, material combinations and manufacturing strategies, joint performance, and emerging application scenarios. In particular, Section 2 explains the methodology and approach of the research. Section 3 investigates the nature and design of interlocking structures, while Section 4 provides an in-depth analysis of materials and manufacturing techniques. The properties of multi-material components are heavily influenced by the interface quality, and Section 5 examines the destructive and non-destructive test applied to interlocked joints and the main characteristics reported in the literature. Section 6 explores the possible applications, while Section 7 examines the current limitations of this joining strategy and outlines future research directions. The acquired knowledge on mechanical interlocking joints will promote the widespread use of multi-material components, enabling a more resource-efficient approach with reduced environmental impact.

2. Methodology and approach of the research

A systematic literature review was performed to address the research question: “How AM has been deployed to build mechanical interlocking structures?”. Two categories of keywords were therefore included in the search query:

(1) Related to the production method: additive manufacturing, 3D printing;
(2) Related to the product class: interlocking structures.

The selected search terms were combined using Boolean operators “AND” to narrow the results (e.g. “interlock*” AND “additive manufacturing”), and “OR” to include word variants (e.g. “additive manufacturing” OR “3D print*”). These queries were used for title, abstract, and keywords search on Scopus and Web of Science databases. The search was limited to English-language sources without any date range restrictions. The sources included published peer-reviewed research papers, proceedings of renowned conferences, and book chapters available online, as summarized in Table 1. The initial search yielded 658 articles, which were then reduced to 357 after removing duplicates (Fig. 1). Additionally, 103 relevant articles were identified in the reference lists through forward and backward searches.

The included records underwent a multi-stage screening process (Fig. 1). In the first step, potentially eligible studies were identified by screening titles and abstracts following predetermined inclusion/exclusion criteria related to both the production method and product class. Specifically, records were excluded when AM was not used as the production method, or when the interlocking structures were not intended as a joining strategy between two materials. Studies in which interlocking was employed as an architectural or structural principle governing a monolithic or modular system were therefore omitted. Of the 460 records analyzed, 260 were excluded at this stage. Finally, a comprehensive eligibility assessment was conducted through in-depth reading, verifying the same inclusion/exclusion criteria in greater detail. As a result, 117 studies were selected, which investigated the design, materials, manufacturing techniques, properties, and applications of additively manufactured mechanical interlocking structures.

The methodology employed in this review adheres to several recommendations of the Preferred Reporting Items for Systematic Reviews and Meta-Analyses (PRISMA) [11] to ensure transparency in data selection. The data shows an increasing trend in the number of articles published each year, suggesting a growing significance of the research (Fig. 2).

Table 1
Summary of literature searching criteria followed in the review.

Literature searching criteria	
Search time frame	Up to February 2026
Language	English
Publication period	No restrictions
Bibliography sources	Scopus; Web of Science
Search keywords	Additive manufacturing; 3D printing; interlocking structures
Search syntax	(“interlock* structure*” AND “additive manufacturing*”) OR (“interlock*” AND “additive manufacturing*”) OR (“interlock* structure*” AND “3D print*”)
Publication type	Peer-reviewed articles; proceedings of conferences; book chapters
Scope	Design, materials, technologies, testing, properties, and applications of additively manufactured mechanical interlocking structures

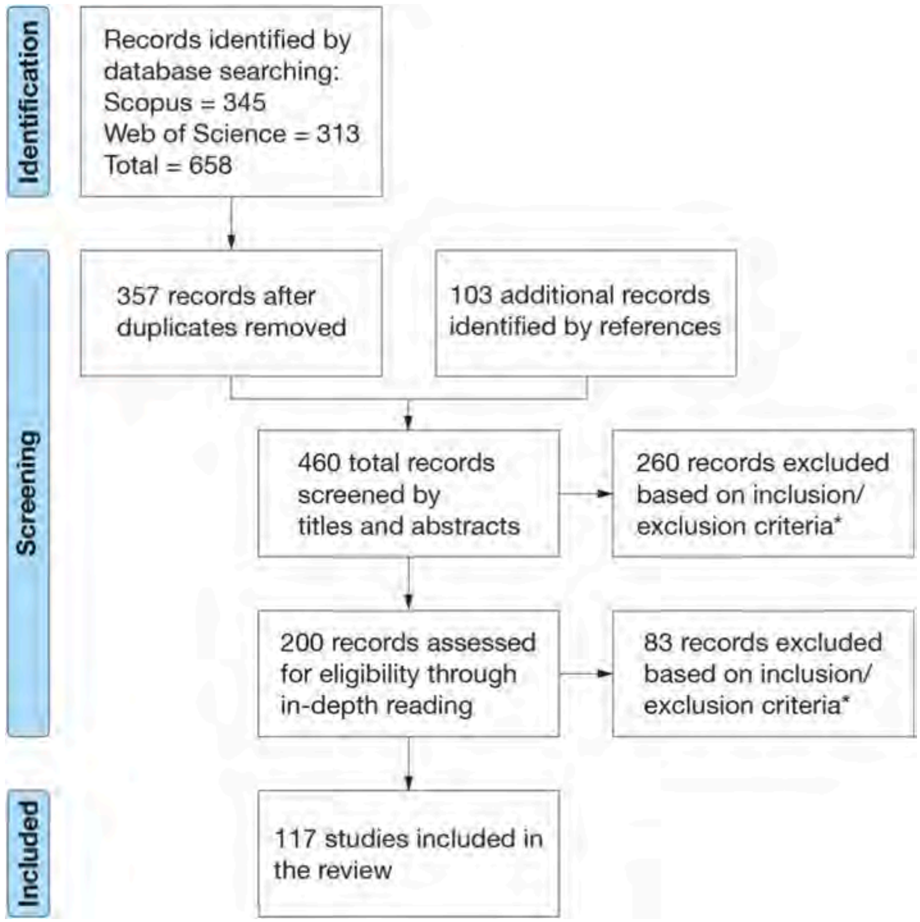

Fig. 1. Flow diagram of the review adapted from PRISMA guidelines [12]. * Records excluded if AM was not used as the production method, or if interlocking structures were not intended as a joining technique between two materials.

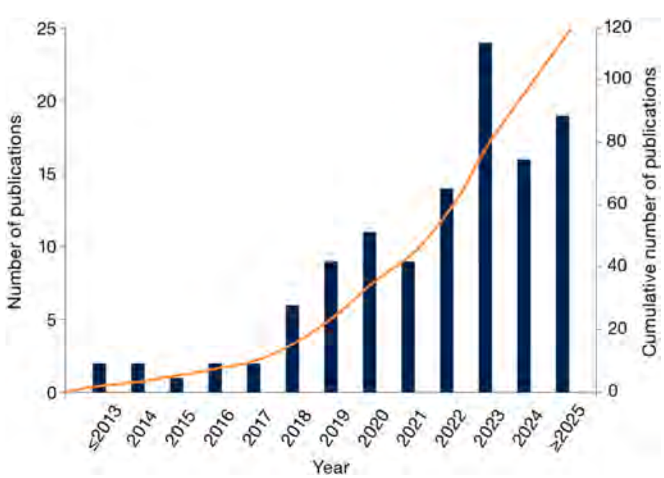

Fig. 2. Temporal distribution of the published studies on additively manufactured mechanical interlocking structures included in the review. The curve represents the cumulative growth of the literature over time.

3. Design of mechanical interlocking structures

The mechanical interlocking mechanism is primarily governed by geometric interference, wherein the shape of the structure is employed to lock materials in one or multiple directions. Consequently, detailed geometric and design considerations are essential to improve the effectiveness of the joints. Multiple studies have, in fact, demonstrated that the bonding performance between dissimilar materials is heavily reliant on the interlocking structure design [13,14].

In the following sections, a systematic analysis of the design of interlocking structures is presented. It is important to specify that mechanical interlocking structures produced by AM can be classified into two categories: micro-interlocking structures, involving features at the submillimeter scale, and macro-interlocking structures, which encompass larger-scale features (Fig. 3). Although the categories are introduced here on a geometric scale basis, they are not exclusively dimensional: each category is associated with a dominant interlocking mechanism and with characteristic design descriptors that influence joint performance. Micro-interlocking structures, presented in Section 3.1, include surface topology, wherein surface irregularities in terms of roughness and porosity are deployed to interlock components, and surface texture, which refers to designed surface patterns or micro-geometrical features introduced to enhance mechanical interlocking at the interface. Micro-interlocking structures operate predominantly via surface anchoring, intended here as the penetration of the material into surface irregularities or designed features. Macro-interlocking structures, which have been more extensively reported in the literature, are outlined in Sections 3.2 and 3.3. In this context, interlocking structures can be arrays of features, hereafter referred to as "pins", which have specific geometries and protrude from the material surfaces, exploiting single-feature geometric interference through their shape. Additionally, arrays of cells, such as lattice structures, are also included within this category. These are hollow structures comprising periodically arranged three-dimensional unit-cells that exhibit high strength-to-weight ratio properties [15] and allow three-dimensional volumetric interference across the unit-cell network. Table 2 provides a summarized comparison

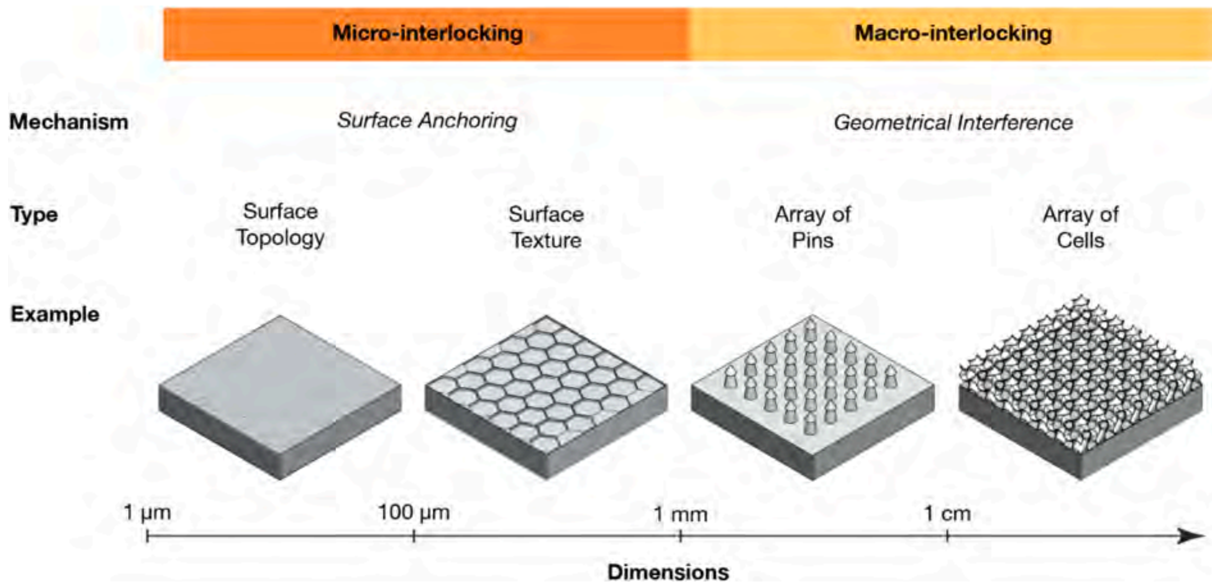

Fig. 3. Classification of mechanical interlocking structures produced by AM.

of these categories, reporting the main examples from the literature, and introduces a design-oriented framework that is recalled in the corresponding sections.

For nomenclature clarity throughout this review, micro-interlocking structures are hereafter collectively referred to as *micro-features*; macro-interlocking structures with arrays of pins, instead, are referred to as *macro-pins*; finally, macro-interlocking structures with arrays of cells are defined as *macro-lattices*. Furthermore, the material hosting the interlocking structures is designated as the *primary material*, while the interacting material that engages with these structures is referred to as the *secondary material*.

3.1. Micro-features

The micro-interlocking mechanism operates at the submillimeter scale and, as illustrated in Fig. 3, can be divided into two subcategories: surface topology and surface texture. A comparative overview of the main characteristics of micro-features is provided in Table 2 together with macro-pins and macro-lattices. Surface topology is the most referenced class, referring to the intrinsic characteristics of AM surfaces, such as roughness and open porosity. Surface texture involves modifying the top layers to form specifically designed features in the submillimeter range. It is important to underline that, although adhesion phenomena often co-exist at this scale, micro-interlocking is conceptually distinct from specific adhesion-dominated mechanisms [23]. In specific adhesion-dominated interfaces, load is transferred through molecular or atomic scale interactions, and the interfacial strength is largely chemistry-driven. In micro-interlocking mechanisms, instead, the secondary material physically penetrates into surface topology irregularities or designed surface texture, and load is transferred through geometric interference. A more detailed discussion of these mechanisms is provided in Section 5.1.

Within the surface topology class, roughness is frequently highlighted, as it enhances the contact area between the two materials, allowing the secondary material to penetrate the surface irregularities of the primary material and promote mechanical interlocking [24]. For AM surfaces, roughness is commonly described through profile parameters such as R_a, which may range from a few micrometers to several tens of micrometers depending on the process, material, build orientation, and processing parameters. As an example, Nguyen et al. [17] reported an average roughness R_a of approximately 12 µm on Ti6Al4V surfaces produced through Powder Bed Fusion with Laser Beam (PBF-LB) technique, showing that the AM surface morphology can provide an effective mechanical interlocking. In the study conducted by Marques et al. [24], the bonding between CuNi2SiCr and Ti6Al4V, produced via a multi-material Powder Bed Fusion (PBF) process, was shown to be strongly influenced by the surface topology of the Ti6Al4V. In particular, morphological observations of the interface showed that the AM-induced roughness of as-built Ti6Al4V surfaces promoted mechanical interlocking by enabling the molten CuNi2SiCr to penetrate surface irregularities, whereas polished Ti6Al4V surfaces lead to poor adhesion due to insufficient roughness. This AM-induced roughness can be attributed to the presence of partially melted particles (Fig. 4), whose formation is influenced by the process parameters.

Surface roughness can be categorized into macro-, micro-, and nano-scale roughness [25]. Different strategies can be employed to enhance it. In particular, two solutions are often proposed: the implementation of surface treatments [16,26] or the modification of process parameters [27,28]. The surface treatments can be classified into two categories: mechanical surface treatments and chemical/laser-based processes. Mechanical treatments include the use of emery papers, media blasting, abrasive abrading and allow the formation of macro- and micro-scale roughness [29]. These treatments are generally low-cost and easily scalable, but can introduce residual compressive stresses and offer limited control on feature shape. Chemical and laser-based treatments encompass laser texturing, anodizing, acid etching, pickling, and reactive gas processes for polymeric materials and allow the formation of nano-scale roughness [16,30–32]. Laser texturing provides the highest geometric control, on the negative site it requires dedicated equipment, may induce a heat-affected zone, and processing time scales linearly with surface area. Parkes et al. [31] provided evidence that laser-induced nano-scale roughness, produced on PBF-LB Ti6Al4V surfaces, resulted in improved adhesion to Carbon Fiber Reinforced Polymer (CFRP) surfaces in comparison to micro- and macro-roughness, with a 25% higher load required to initiate failure compared to grit-blasted components. In addition, a recent investigation [32] demonstrated that laser-induced nano-scale roughness, when superimposed on micro-scale roughness, creates a morphology that enhances mechanical interlocking in Ti6Al4V-Ti6Al4V joints produced by PBF-LB process. This resulted in up to 162% higher quasi-static shear strength and 130% longer fatigue life compared with the as-built surface condition (Fig. 5). Anodizing treatments have also been found to be highly effective in generating nano-scale roughness and can be carried out using a variety of chemical solutions [16]. The most utilized include chromic,

Table 2
Comparison of the three interlocking categories, summarizing the main literature trends and linking design, material combinations, testing conditions, and joint performance.

Category	scale	Dominant mechanism	Design descriptors	Typical material combinations (primary–secondary)	Testing conditions	Main reported performance
Micro-features	< 1 mm	Surface anchoring	• Surface roughness parameters (e.g., Ra), size and morphology • Pore size • Texture and micro-features geometry (e.g., height, depth, diameter)	• Metal–Composite • Metal–Polymer	Lap-shear, tensile/pull-out, and fracture toughness tests, often combined with surface characterization before and after joining	• AlSi10Mg-BFRP: anodized nano-porous surfaces increased maximum shear load by up to 30% compared with as-built surfaces [16] • Ti6Al4V-CFRP: semi-cylindrical grooves increased Mode I Fracture toughness by up to 50% compared with the flat joint, by deflecting the crack path and promoting mixed-mode crack growth [17]
Macro-pins	1 ÷ 10 mm	Single-feature geometric interference	• Tip/body/root shape • Pin geometry (height, width, diameter, aspect ratio) • Pin spacing and distribution pattern • Pin orientation/offset angle	• Polymer–Polymer • Metal–Composite	Lap-shear, tensile/pull-out, and fracture toughness tests. Less frequently, fatigue and impact/damage-tolerance tests	• 316 L-GFRP: cylindrical pins increased quasi-static strength by approximately 50–60% in double-lap joints and about 99% in single-lap joints compared with flat joints, while promoting progressive failure and high energy absorption [18] • Co-Cr/PMMA: Y-shaped pins increased interfacial tensile strength by 15 times compared with the flat interface and improved stiffness [19] • Ti6Al4V-CFRP: grooved pins increased the contact area between materials by 30%, resulting in a 14% higher maximum pull-out load and a 60% higher absorbed energy compared with cylindrical pins [3]
Macro-lattices	≥ 10 mm	Volumetric interference across the unit cell network	• Unit cell topology • Cell size • Strut diameter or wall thickness • Porosity and relative density • Number of lattice layers • Lattice orientation	• Polymer–Polymer • Metal–Composite	Tensile/pull-out and compression tests	• 316 L-AV651: BCCZ, FCC, and Kelvin lattices exhibited tensile strength values 2–3 times higher than those obtained through conventional surface modification, with BCCZ showing the highest interfacial strength [20] • PLA-PP: dovetail planar-based lattices improve bonding, but remain limited by in-plane deformation/disassembly [21] • VeroClear-PDMS: diamond TPMS lattices led to bonding strength 28 times higher and fracture energy up to 217 times higher than flat joints [22]

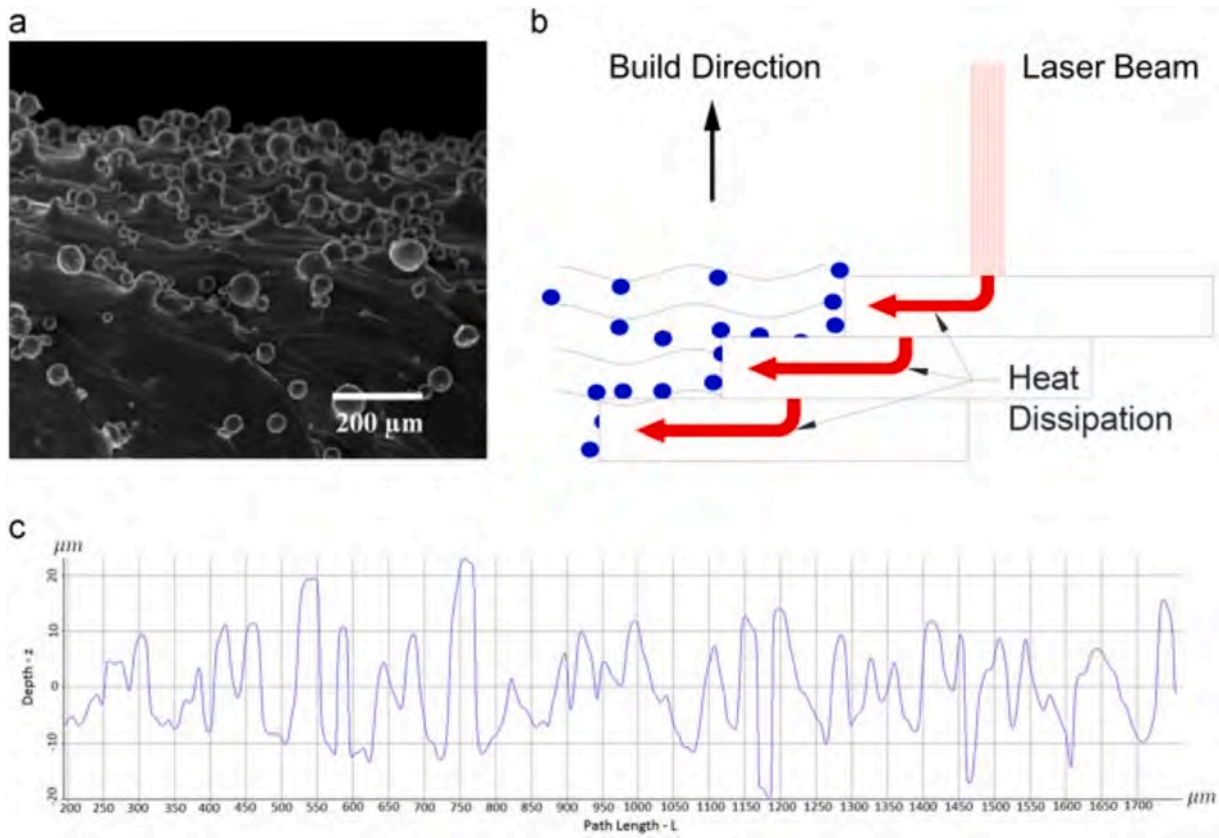

Fig. 4. (a and b) Surface morphology of a PBF-LB part, characterized by adhered and partially fused particles, resulting from process-related thermal effects; (c) the corresponding roughness profile. Reprinted from [17], Copyright (2016), with permission from Elsevier.

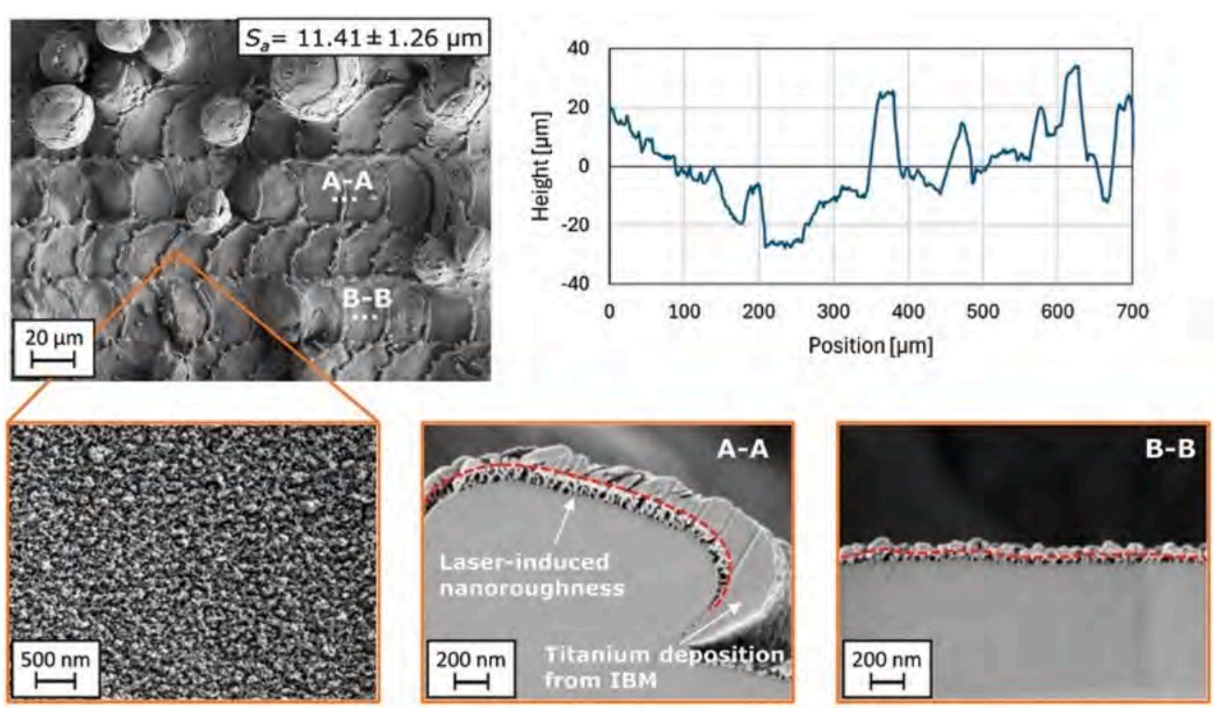

Fig. 5. SEM micrographs and surface height profile of a laser-treated surface. Laser processing generates nano-scale roughness at both the pulse edge (A-A) and pulse depression (B-B), superimposed on the underlying micro-scale roughness, contributing to enhanced mechanical interlocking. Reprinted from [32], under the terms of the Creative Commons CC BY 4.0 license.

phosphoric, and sulphuric acids. Miranda et al. [16] reported increases in maximum shear load of up to 30% for anodized AlSi10Mg manufactured through PBF-LB and joined with Basalt Fiber Reinforced Polymer (BFRP) compared to as-built conditions, attributed to the formation of nano-porous oxide layers on the primary material surface that enhance mechanical interlocking. However, this approach can be time-consuming and involves the use of environmentally hazardous chemicals [33]. Acid etching, pickling and reactive-gas treatments for polymers may represent simpler alternatives, but are strongly material-dependent and provide less control over the resulting surface morphology. The selection of an appropriate treatment is therefore dependent upon the specific requirements of the intended application and the materials involved. In general, mechanical treatments may be preferred when cost and scalability dominate, laser texturing when controlled local morphology is critical, anodizing when uniform nano-porosity over complex shapes is needed, and acid etching, pickling or reactive-gas treatments when chemical activation is required but geometric control is less critical.

With regard to process parameters, Chueh et al. [27] introduced micro-features by adjusting the process parameters of the PBF-LB technique. The surface roughness and open porosity were controlled through the utilization of different laser-scanning parameters and strategies, avoiding laser re-melting to create craters and pores on 316 L surfaces. In another approach, Goetzendorfer et al. [28] reduced the energy density during PBF-LB processing of tool steel to a level insufficient for complete melting of the layer, resulting in the formation of roughness, cavities, and channels that enhanced interlocking with PA12.

The effectiveness of surface treatments and process parameter modifications is highly dependent on the specific process involved for both the fabrication of micro-features and the joining process of the materials. Multiple studies [17,25,34] concluded that the roughness of components produced by PBF-LB, for instance, can be sufficient for adhesion in certain applications, negating the necessity for any surface treatment processes. Considering the joining process, instead, in processes like injection molding, when high thermal loads are involved, particularly in polymer-based systems, the interface layers may undergo local remelting or thermal degradation, thereby reducing the effectiveness of roughness [35]. Consequently, alternative techniques are proposed, including the combination of roughness with surface textures or macro-interlocking structures. A comparison of micro and macro-interlocking structures revealed that the latter have a more considerable impact than roughness itself [35]. Therefore, combining both mechanisms is often recommended. Macro-interlocking structures are discussed in the following section.

In the context of surface textures, the geometry of the designed features and their characteristic dimensions, such as height, depth, and diameter, control the available bonding area, the filling efficiency of the secondary material, and the degree of geometric interference generated at the interface. Dai et al. [36] investigated surface textures printed on zirconia ceramic core through Vat Photopolymerization (VPP) and joined with veneering porcelain, showing that these features can enhance the shear bond strength by increasing the roughness and the

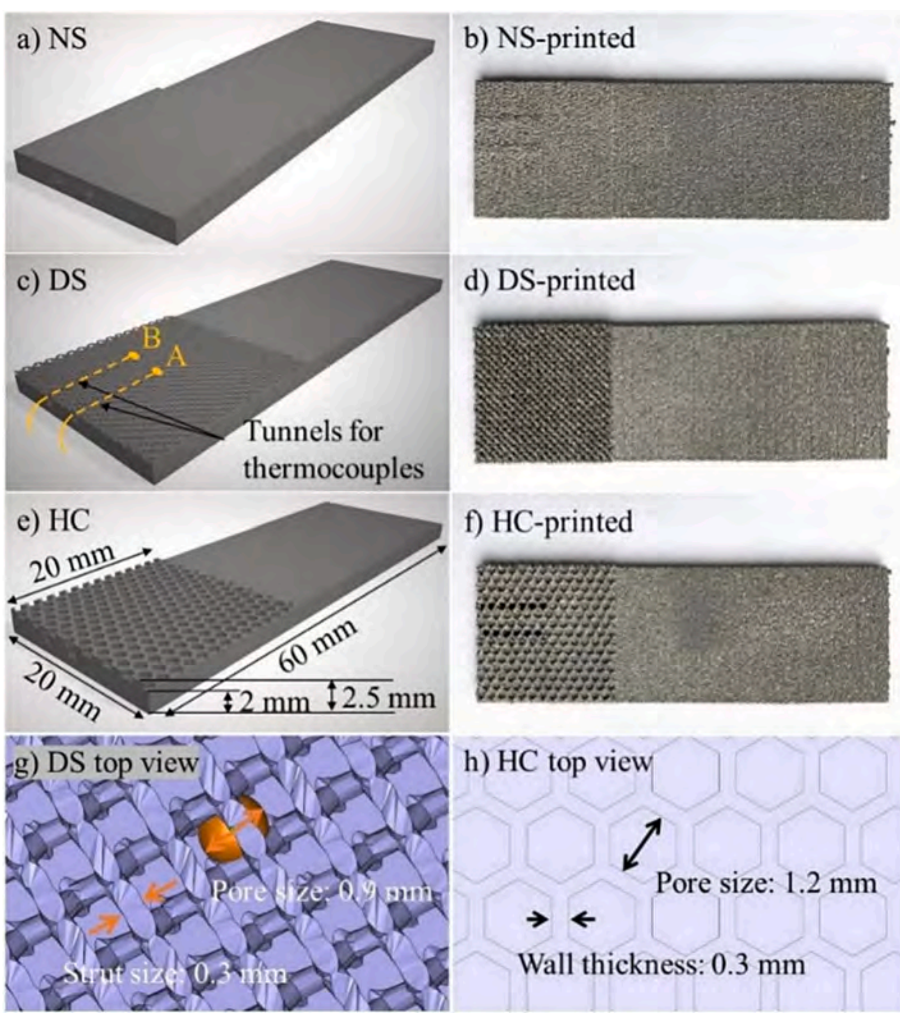

Fig. 6. Examples of different surface textures: (a and b) non-structured surface; (c and d) rectangular/diamond-shaped texture; (e and f) hexagonal/honeycomb texture. Top views (g and h) illustrate the characteristic geometric parameters of each texture. Reprinted from [37], under the terms of the Creative Commons CC BY 4.0 license.

effective bonding area of the primary material. In their study, two designs were proposed: a hexagonal grid and a rectangular grid. The hexagonal grid, with a height of 0.09 mm, was demonstrated to significantly enhance the shear bond performance. Furthermore, the grid design exerted an influence on the failure mode. The implementation of hexagonal grids resulted in an increase of cohesive failure, observed through microscopy analyses, thereby indicating a more robust bond in comparison to the use of rectangular grids. Similarly, Zou et al. [37] compared hexagonal and rectangular grids, fabricated by Powder Bed Fusion with Electron Beam (PBF-EB) and designated as honeycomb and diamond-shaped, respectively, for Ti6Al4V-UHMWPE joints (Fig. 6). The honeycomb architecture consisted of regular hexagonal prisms, with a strut diameter of 0.3 mm, while the diamond-shaped configuration comprised a rectangular tetrahedron as the unit cell, with the same strut diameter. Both structures had a height of 0.5 mm. Results showed that the ultimate shear force was markedly improved in both cases; however, the structural complexity must be taken into account. Indeed, in comparison to the diamond-shaped configuration, the simplified honeycomb structure improved the filling efficiency, showing better stability. It was thus established that the hexagonal configuration represents an optimal solution.

Among surface textures, spherical protrusions have been investigated [38–40]. Wang et al. [38] proposed spherical 316 L protrusions produced by PBF-LB with diameters ranging from 160 to 450 μm (Fig. 7), as preliminary route for metal-polymer or metal-CFRP joining. In this case, the morphology and size were selected with the objective of facilitating the disassembly between materials. The authors emphasized the necessity for micron-sized features rather than macro-sized ones, as the latter could potentially lead to damage if joined with composite materials containing fibers, resulting in delamination and making disassembly a challenging process. Additionally, larger features may induce thermal stress on the primary material during the manufacturing process due to the significant heat input. Kim et al. [41] suggested the formation of particle-shaped protrusions on A5052 aluminum alloy substrates, which remained within the range of spherical features, by spreading a special mix of Al-Ti-C powder on the substrate of the primary material in a thin layer of 50 μm and subsequently utilizing a laser to create micro-features. The resulting A5052 surfaces were joined with PA6 sheets and tested under lap shear loading. It was established that, for the investigated system, the chemical composition of the Al-Ti-C powder mixture, expressed through the C/Ti molar ratio, controls the morphology and adhesion of the protrusions and, consequently, the lap shear strength of the joints. The highest joint strength was obtained for a C/Ti molar ratio of 0.6, owing to the high fraction of well-bonded protrusions.

Finally, Nguyen et al. [17] introduced the bio-inspired concept of hierarchical structures, which are characterized by the incorporation of features at varying length scales. Such structures are observed in biological materials, such as lotus leaves and mosquito legs [42]. These can assist in enhancing joint performance, as the interfering hierarchical features could deflect the straight crack path. The researchers proposed the use of hemi-spherical and semicylindrical features with a diameter ranging between 100 and 200 μm produced through PBF-LB. However, they found that these features did not result in an improvement when bonding similar metallic materials (Ti6Al4V-Ti6Al4V). Instead, the semi-cylindrical features protruding from the surface increased Mode I fracture toughness by up to 50% between dissimilar materials (TI6Al4V-CFRP). This proves the influence of the materials composition on the effectiveness of surface textures.

In summary, the following can be stated:

- Within the micro-features category, two main approaches are identified: surface topology and surface texture. In surface topology, three levels of roughness can be distinguished according to their scale: macro-, micro-, and nano-scale roughness.
- Surface roughness has a significant impact on joining strength, providing a larger bonding area and promoting micro-interlocking. Although a systematic quantitative correlation between roughness parameters and mechanical performance is still lacking, the reviewed studies allow a qualitative comparison among roughness scales and morphologies. This comparison highlights that both the size and morphology of the roughness are of critical importance. In

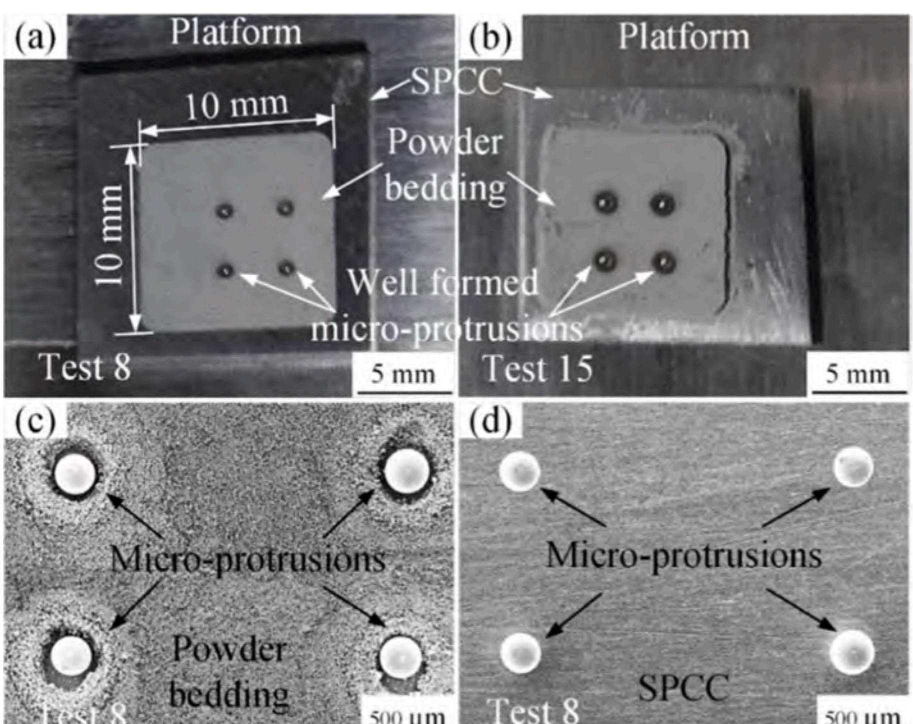

Fig. 7. Spherical micro-protrusions on the primary material substrate at 5 × (a-b) and 30 × (c-d) magnification, before and after removal of the un-melted powder. Reprinted from [38], under the terms of the Creative Commons CC-BY-NC-ND license.

particular, nano-scale roughness, achievable through laser texturing and anodizing treatments, has frequently been reported to be the most effective.
- Surface texture can be classified according to the geometry and dimensional characteristics of the designed features, including height, depth, and diameter. Reported examples include hexagonal and rectangular grids, spherical features, and semicylindrical features. It emerged that hexagonal grids facilitate filling and structural stability; spherical features allow for easy disassembly; and semi-cylindrical features enhance adhesion. However, the compatibility of these surface textures with the secondary material must be considered.
- Manufacturing considerations, including both the production of the micro-features and joining processes with the secondary material, as well as material combinations, and application requirements are fundamental in order to select the most appropriate interlocking strategy.

3.2. Macro-pins

Macro-pins constitute the first macro-interlocking configuration analyzed in this section. An overview of the main characteristics of this category, including scale, dominant mechanism, design descriptors, material combinations, testing conditions, and reported performance, is provided in Table 2. These structures consist of arrays of protruding features, referred to as pins, fabricated on the primary material surface, with dimensions ranging from submillimeter to several millimeters (Fig. 3). The discussion is organized into two subsections: the first proposes a geometric classification of pin profiles (Section 3.2.1), while the second presents representative macro-pin implementations reported in the literature (Section 3.2.2).

3.2.1. Pin profiles

The geometric profile of a pin plays a key role in defining the mechanical interlocking mechanism and the overall joint performance. Accordingly, a schematic classification of pin profiles is proposed. Three fundamental regions can be identified – the tip, which is the upper part of the pin; the body, which forms the main structure; and the root, which is the final part of the pin, connecting the body to the substrate (Fig. 8). For each of the mentioned regions (tip, body, and root), the shapes found in the literature were summarized into three main classes according to their geometrical complexity: straight, expanding, and profiled (Fig. 8). The classes are presented in a progressive order of complexity, with an explanation of the effects of the different shapes. It is important to note that all class combinations across the three regions are possible, e.g., it is possible to find a pin with a straight tip, an expanding body, and a profiled root.

The *straight class* is characterized by pins that exhibit a consistent linear shape without any significant changes or expansions throughout their length. Within this class, the tip may adopt a flat or a conical configuration, extending directly from the body. The conical shape is suggested to facilitate the embedding of the pin into the secondary material [31]. Cylindrical or rectangular bodies are represented in this class, typically exhibiting a uniform section through the entire structure. The root is a sharp edge, hence a direct connection between the body and the substrate is created. In this class, the majority of published studies report pins characterized by an axis of symmetry perpendicular to the component surface. Nevertheless, alternative configurations have also been described, in which the axis of symmetry is inclined at an offset angle relative to the surface [3]. For the straight class, interlocking is achieved by geometric interference in the x-y plane.

As the complexity of the pin increases, the *expanding class* can be considered. In this setup, the tip, body, and root do not align linearly; rather, they gradually increase or decrease in size or diameter with respect to the component surface. For the tip, the connection with the body may expand in a perpendicular direction to the axis of symmetry, creating a T-shape if the tip ends in a flat configuration or resembling an arrow shape if the tip converges to a point. The undercuts created by the material expansion play a crucial role, causing a dual effect. Firstly, they enhance the interlocking mechanism between primary and secondary materials, increasing grip and producing geometric interference along the z-direction. However, their effectiveness depends on whether the secondary material can adequately fill them [43]. Regarding the body, the expanding configuration can resemble a truncated cone or an inverse truncated cone. Therefore, the angle formed between the profile of the pin and the horizontal plane is significant. As for the root, the body may be connected to the substrate with a chamfer or a fillet. In this class, interlocking is achieved through geometric interference along all three axes.

The last group is the *profiled class*, which includes all the geometries that cannot be described as straight or expanding due to their complexity. Examples include an elliptical tip, a tip that combines straight and expanding features, or an irregularly shaped tip. The body may have a helical shape, a grooved surface, or other irregular shapes. The same applies to the root. These experimental shapes are frequently proposed to investigate the impact of the geometry on joint performances [3]. In this case, interlocking is accomplished through geometric interference in one or multiple axes, in function of the shape realized.

The interlocking behavior for macro-pins is governed by design descriptors such as pin height, width or diameter, their ratio, and the geometry of the tip, body, and root. Considering these design characteristics and the different degrees of mechanical constraint provided by each pin profile, suitable load scenarios can be summarized as follows. Straight pins, such as cylindrical or rectangular pins, are generally more suitable for shear-dominated, in-plane load cases with a limited normal component, where their simple and cost-effective fabrication can compensate for the comparatively low pull-out resistance. Expanding pins, such as T-shape or arrow-shape pins, are more

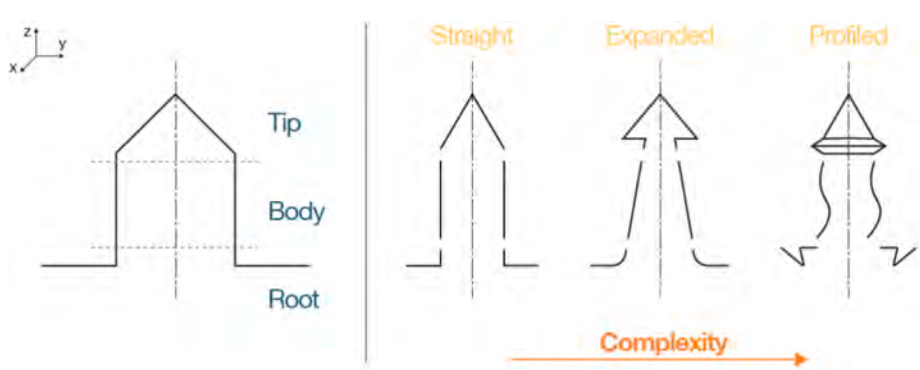

Fig. 8. Schematic representation of pin profiles, identifying the three fundamental regions (tip, body, and root) and the three profile classes (straight, expanded, and profiled), arranged in increasing order of geometrical complexity.

effective under tension/pull-out dominated loading, including peel-prone configurations, because the undercut geometry generates mechanical interference along the z-direction. Profiled pins, such as helical or grooved pins, are particularly attractive for combined shear/tension loading and for conditions requiring enhanced energy dissipation, since tailored surface features can modify the pull-out response, redistribute stresses, and promote progressive damage mechanisms along the pin length. However, the increased fabrication complexity and process-related constraints of these geometries should also be considered.

It should be noted that the distinction between straight, expanding, and profiled classes in this classification is intended as a design-oriented schematization, since geometrical features of different classes may coexist within the same pin. Nevertheless, the aim is to provide qualitative guidelines for relating specific design features to dominant loading scenarios, given the lack of standardized methods for quantitatively comparing the influence of different classes and their descriptors on performance.

Extending the discussion from the single pin to pin arrays, two configurations can be identified. The first, and most widely reported, consists of arrays of pins protruding from the primary material surface and engaging the secondary material (Fig. 9a). The second corresponds to a *complementary interlocking* configuration, also referred to in the literature as *male–female* or *mortise-and-tenon* [45,46]. In contrast to the previous case, both materials are geometrically structured: each protrusion on the primary material is matched by a corresponding negative geometry in the secondary material, and vice versa (Fig. 9b). Mechanical interlocking is therefore achieved through the mutual engagement of these geometrically matched features on both materials. This configuration draws inspiration from several biological systems, such as cranial and shell sutures or the elytra of certain beetles (Fig. 9b), where interdigitated protrusions and cavities connect dissimilar tissues, promoting enhanced load transfer and toughness [44,47].

Overall, the proposed classification aims to guide the design of pins produced by AM. The following section presents representative examples reported in the literature, corresponding to each of the profile classes discussed above.

3.2.2. *Macro-pin examples*

Based on the proposed schematization of pin profiles, a structured analysis of the literature is conducted. Initiating the examination of the straight class, Ribeiro et al. [48] introduced a fully straight pin characterized by a flat tip, a rectangular body, and an edge root, with both width and height equal to 2 mm, referred to as *U-shape* in their study (Fig. 10b).This configuration represents the most elementary pin case. The authors investigated PLA-PLA and PLA-TPU material pairs, produced through Fused Filament Fabrication (FFF), under tensile loading and emphasized that, for this geometry, the contribution of mechanical interlocking was limited, and the joint strength was mainly governed by interfacial adhesion between the materials. Consequently, two additional geometries were introduced in their work: the so-called *T-shape* (Fig. 10a), consisting of a straight rectangular body 2 mm in width with an expanding tip approximately 3 mm wide, and the *dovetail shape* (Fig. 10c), featuring an inverted truncate-cone body 1.4 mm in height with a flat tip of 2 mm diameter. These geometries represent a hybrid

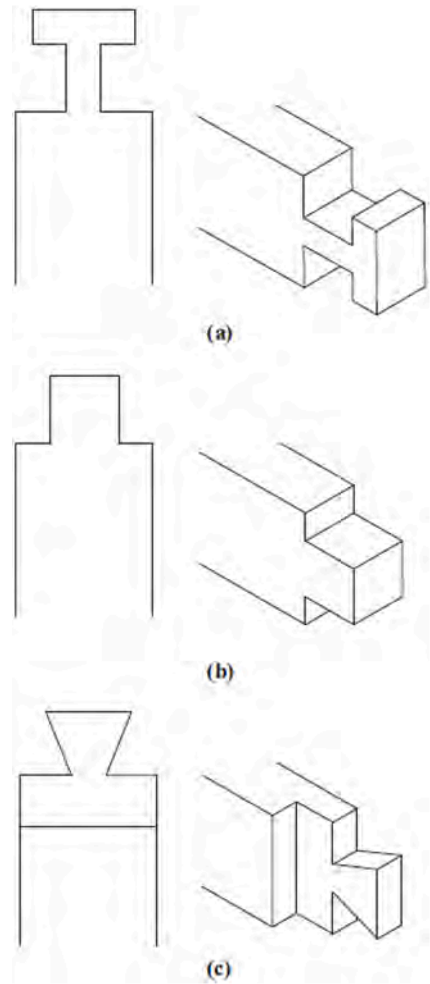

Fig. 10. Pin geometries proposed by Ribeiro et al. [48]: (a) T-shape; (b) U-shape; (c) dovetail. Geometries (a) and (c) represent hybrid straight-expanding classes, while (b) is the simplest reference of the straight class. Reprinted with permission from [48]. Copyright 2019 Emerald Publishing. Permission conveyed through Copyright Clearance Center, Inc.

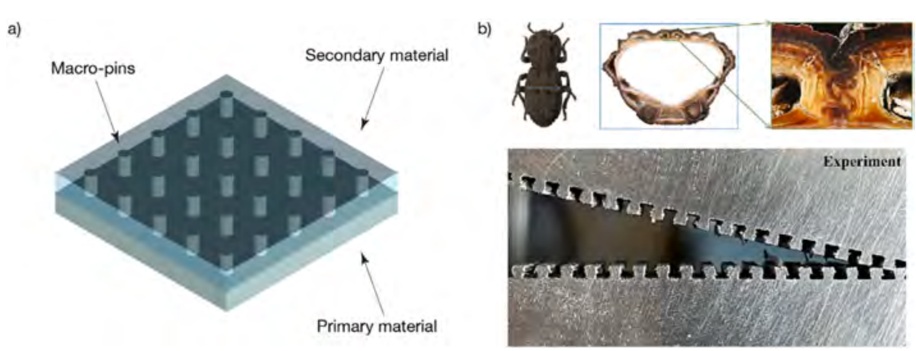

Fig. 9. Schematic representation of macro-pin configurations: (a) the most widely reported interlocking configuration, with pins protruding from the primary material and engaging the secondary material; (b) complementary interlocking configuration, in which both materials are geometrically structured with conjugated positive and negative features, drawing inspiration from biological systems such as beetle elytra. Panel (b) adapted from [44], Copyright (2023), with permission from Elsevier.

between the straight and the expanding class, which is analyzed later in this section. Comparative analysis of the three shapes revealed that the T-shape interface provided the highest mechanical performance among the tested geometries, particularly in terms of Young's modulus and tensile stress. This was especially evident for the low-compatibility PLA-TPU pair, for which the T-shape geometry increased the ultimate tensile stress by approximately 35–50% compared with the U-shape and dovetail interfaces. A further noteworthy study in the straight class was conducted by Peralta Marino et al. [49], who demonstrated the impact of pin geometry and distribution on stress concentrations along the bond length. A complementary interlocking configuration was utilized in this work. Starting from a simple straight pin with a flat tip, a cylindrical body, and an edge root, the researchers progressively modified specific pin regions through Finite Element Modelling (FEM) to tailor its response under different load conditions. Modifications included adjustments to pin length based on shear stress diagrams, optimization of pin distribution on the interface to redistribute stress concentrations, and exploration of tip configurations, transitioning from flat to hook shape to mitigate stress induced by peeling. The experimental validation was carried out on FFF-manufactured PLA components. The results of the test, executed on compression-loaded single-lap configurations, showed that the interlocked geometries shifted the stress peak from the overlap edges toward the interlocked region and enabled higher load-bearing capability than the non-modified reference geometry. The complementary interlocking configuration was adopted also by Silva et al. [46], who investigated aluminum-aluminum and aluminum-polymer joints. They showed that the compression of a protruding pin within its corresponding negative geometry amplifies the interlocking mechanisms, acting similarly to mechanical fastenings and withstanding pull-out forces of approximately 8 kN and 6 kN, respectively.

In the category of straight pins, a significant subcategory is constituted by pins with a conical tip. As previously reported, the conical tip facilitates the embedding of the secondary material, thereby enhancing the interlocking mechanism. An example is provided by the works of Graham et al. [18,50], who proposed pointed cylindrical pins with a diameter of 1 mm and a nominal height of 3 mm, produced on 316 L substrates and embedded into Glass Fiber Reinforced Polymer (GFRP) secondary material. The authors demonstrated that these features enable the benefits of bonded and bolted joints without an increase in weight. In quasi-static tests, the joints showed an increase in strength of approximately 50–60% in double-lap configurations and about 99% in single-lap configurations compared with flat control joints. Moreover, the pins promoted a more progressive failure response, increasing energy absorption. Bagnato et al. [51] adopted a similar overall pin geometry for Ti6Al4V-CFRP joints, but introduced a 0.5 mm fillet at the root, aimed at reducing stress concentration, representing an example of a pin with a straight body and tip, but an expanding root. The PBF-LB titanium pins markedly enhanced interfacial toughness: the Mode I and Mode II propagation toughness values were approximately 18.5 and 6.3 times higher, respectively, than those of the flat control joint. Finally, Nguyen et al. [52] proposed straight cylindrical Ti6Al4V pins manufactured by PBF-LB and embedded into CFRP, incorporating both a 0.5 mm fillet and a 45° chamfer at the tip. The inclusion of the chamfer was intended to facilitate the joining of the two materials. As a result, the integration of the pins led to Mode I initiation fracture toughness and Mode I steady-state fracture toughness values approximately 3.5 and 4.6 times higher, respectively, than those of the unpinned control configuration. Moreover, the length-to-diameter ratio was shown to be a crucial factor governing the transition between pin pull-out and pin failure under different loading conditions [52,53]. The influence of pin length was further highlighted by Huelsbusch et al. [53], who investigated Ti6Al4V-CFRP joints with different pin lengths and reported that 2.0 mm pins resulted in tensile shear strength and fatigue strength values approximately 6.0 and 3.5 times higher, respectively, than those of the solely adhesive reference.

Exploring the expanding class, one of the most frequently cited examples is the work of Parkes et al. [55]. The researchers developed pins with a conical expanding tip forming undercut geometries, referred to hereafter as *arrow-shaped* tip, a truncated-cone body, and a fillet at the root. These pins, which are part of a joining technology patented by Airbus Group Innovations, are known as *HYPER* (*Hybrid Penetrative Reinforcement*). The pins were additively manufactured from Ti6Al4V and embedded into CFRP laminates in a single-lap shear configuration. The research demonstrated that the pins delayed failure initiation, slowed damage propagation, and significantly increased ultimate strength compared to joints without pins. In particular, the limit load was 21% higher than the ultimate load of the joints without pins, while the ultimate load was up to 6.5 times higher. Final failure occurred catastrophically by shear failure of the pins at their bases. Consequently, in a further study [31], the authors investigated an alternative pin geometry with a 17% larger root diameter. This modification increased the resisting area of the pins and resulted in a 25% improvement in joint shear strength. However, more recent findings seem to suggest that pin diameter must be selected also considering the type of secondary material. In particular, when the secondary material is a composite, reducing the pin diameter from 1 mm to 0.5 mm was shown to significantly mitigate damage in the composite, while maintaining comparable interfacial performance [54]. Raimondi et al. [54] introduced PBF-LB manufactured double arrow-shaped pins (Fig. 11b), produced from Precipitation-Hardening Stainless Steel (PH-SS) and embedded into CFRP, showing increased pull-out strength compared with cylindrical straight pins and improved repeatability of the mechanical response. Focusing on arrow-shaped tips, Sarantinos et al. [13] performed a systematic numerical optimization to tailor the pin geometry according to the mechanical response under different loading conditions. The titanium pins were manufactured by PBF-EB and joined to CFRP laminates. Three geometries were proposed, encompassing diameters ranging from 0.28 mm to 1.5 mm: the *spiked μpin*, a simple cylindrical shape that represents the straight pin class; the HYPER μpin, previously mentioned; and the *Mode I optimized* μpin with the numerically optimized expanding profile. The latter exhibited a 3.5-fold higher maximum pull-out force and an 8.2-fold higher energy absorption to failure compared to the cylindrical straight pin.

It is important to acknowledge that a considerable number of macro-pin designs draw inspiration from natural structures. Indeed, over millions of years of evolution, natural structures have developed unique features that provide excellent examples of multi-functional components. Alsheghri et al. [19], for example, proposed a *Y-shaped* geometry inspired by mangrove root systems for Co-Cr/PMMA joints. The interlocking features, produced by PBF-LB, led to a 15-fold increase in interfacial tensile strength compared with the flat interface, while also improving interfacial stiffness through geometric redistribution of stresses. Similarly, Yunzhu et al. [44] took inspiration from the jigsaw-like suture of the diabolical ironclad beetle elytra [56]. The authors proposed PBF-LB manufactured AlSi10Mg pins, with an inverted truncated-cone body, in a complementary interlocking configuration. The investigated geometries were characterized by a height of 1.25 mm and different interlocked angles, namely 76°, 70°, and 63°, defined as the angle formed between the profile of the pin and the horizontal plane. The study demonstrated that interface strength, toughness, and failure mechanisms can be tuned by varying the design descriptors of the interlocking feature. In particular, the analysis indicated that an interlocked angle of 70° provides the most favorable fracture performance.

Finally, the most complex and least diffuse category is represented by the profiled class. The first proposed work is that of Nguyen et al. [3]. The authors proposed Ti6Al4V pins, produced through PBF-LB, joined to CFRP laminates. Pins had lengths between 2 mm and 4.5 mm, diameters ranging from 0.5 mm to 1 mm, and four shapes: a cylindrical reference pin and the so-called *grooved*, *pyramidal*, and *helical* pins (Fig. 12). With regard to the cylindrical pin, an offset angle ranging between 0° and 30° was used to offset the pin axis with respect to the primary material surface in order to investigate the mechanical behavior of the pin. The

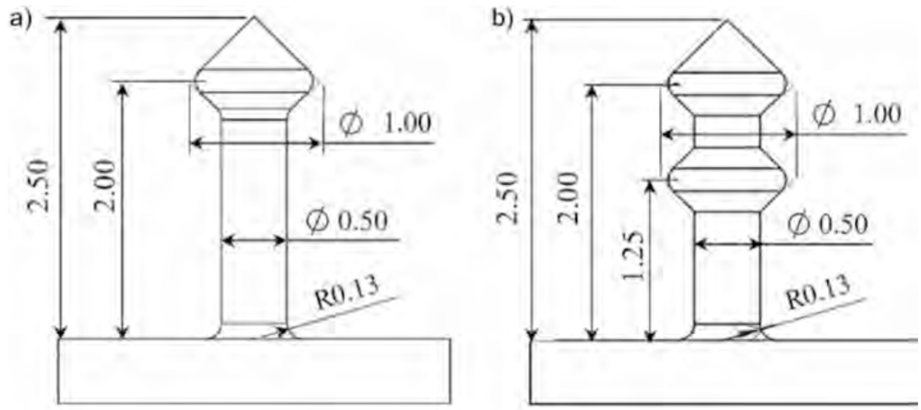

Fig. 11. Pin geometries proposed by Raimondi et al. [54]: (a) pin with arrow-shaped expanding tip; (b) pin with double arrow-shaped expanding tip. Adapted from [54], under the terms of the Creative Commons CC BY 4.0 license.

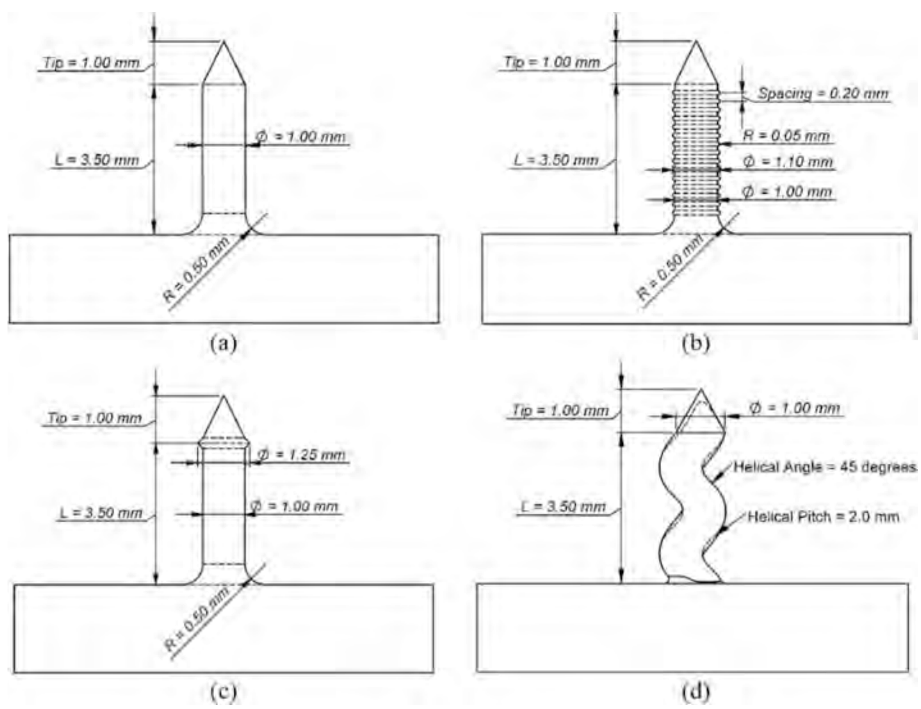

Fig. 12. Pin geometries proposed by Nguyen et al. [3]: (a) cylindrical reference pin; (b) grooved pin; (c) pyramidal pin; and (d) helical pin. Geometries (b) and (d) feature a profiled body, whereas (c) is characterized by a profiled tip. Reprinted from [3], Copyright (2017), with permission from Elsevier.

results indicated that higher offset angles led to increased friction and energy absorption, although at the expense of localized stress concentrations that could promote earlier failure. The grooved pin represents a combination of the three aforementioned classes. It presents a straight conical tip, a profiled body with a series of evenly spaced, parallel grooves, and a fillet in the expanding root region (Fig. 12b). The pyramidal pin has a profiled tip with a sudden change in inclination: the tip widens before narrowing, creating an outward and inward sloping surface, and then converges to a point (Fig. 12c). It then has a cylindrical body and a fillet. The final geometry is characterized by a conical tip and a 45° helical rib along the body (Fig. 12d). The introduction of surface profiling elements, such as pyramidal tips or helical ribs, was shown to improve the interlocking mechanism by increasing the contact area between materials and modifying the pull-out response. However, these pins exhibit unique failure patterns; for example, cracking can occur around the tip for pyramidal pins and midway along the surface for helical pins. In particular, the grooved pins increased the contact area by 30%, resulting in a 14% higher maximum pull-out load and a 60% higher absorbed energy compared with cylindrical pins, while preserving a progressive pull-out failure mode. Conversely, pyramidal and helical pins increased the maximum load by 20% and promoted composite fracture. Frascio et al. [57] proposed a profiled tip with a lobate geometry, referred to as *Mickey Mouse* geometry, for multi-material PET/PLA components produced by FFF. Compared with the expanding T-shape tip, they found that the lobate shape reduced stress concentrations around sharp tip edges. However, tensile tests showed that the Mickey Mouse geometry provided only a 7% increase in ultimate tensile strength compared with a flat interface, whereas the T-shape geometry achieved a 58% improvement. Focusing on profiled root regions, Chueh et al. [27] presented an *anchor root* and a *tree-shaped root* in pins with a height and width of about 2 mm. In this work, SS 316 L interlocking structures were manufactured by PBF-LB and subsequently filled with PET by FFF. The anchor root consisted of two converging straight lines forming an inverted V-shape, whereas the tree-shaped root adopted a trapezoidal profile. These geometries were designed to facilitate the penetration and enhance the adhesion and connection with the secondary material, thereby preventing detachment. Tensile and shear tests confirmed reliable metal/polymer joint strength, with tensile failure occurring mainly in the polymer component rather than at the interface.

In conclusion, the following considerations emerge from the analysis of the available literature:

- There is a lack of standardization in pin design, despite its decisive role in governing joint performance. The same authors frequently present different pin geometries in their works, progressing from one class to another or mixing them.
- From a comparative perspective, the straight class provides a simpler solution, mainly suited to shear-dominated load transfer, whereas the expanding class, which is the most recurrent, enhances pull-out and peel resistance through undercuts and enlarged contact areas. The profiled class introduces additional surface features that further tailor stress distribution and mitigate energy dissipation under combined loading, although often at the cost of increased manufacturing complexity.
- Certain geometric features, such as conical tips, undercut geometries, and root fillets, recur across multiple studies and consistently demonstrate a stronger influence on joint performance than more elaborate surface modifications.
- In terms of dimensions, variability exists among proposed designs; however, pins with widths and heights in the 2–3 mm range are most commonly reported. Geometric parameters such as length-to-diameter ratio, as well as pin distribution along the interface, are repeatedly identified as critical variables. A more detailed analysis of their effect is provided in Section 5.4.

3.3. *Macro-lattices*

Macro-lattices constitute the most geometrically complex macro-interlocking configuration, typically characterized by dimensions in the millimeter range and above (Fig. 3). An overview of the main characteristics of this category is reported in Table 2. Macro-lattices consist of arrays of periodically arranged three-dimensional unit-cells, commonly referred to as *lattice* structures [15], fabricated on the primary material surface. Their inherent porosity can facilitate the infiltration of the secondary material, thereby promoting mechanical interlocking through volumetric engagement [20]. Compared to micro-features and macro-pins, the literature on macro-lattices presents significantly fewer studies. However, the underlying mechanism in all three approaches remains the same: each design strategy aims to increase the contact area, enhancing the bond between materials.

Considering the limited number of studies, macro-lattice implementation appears circumscribed to two main design cases. The first involves their adoption as a geometric alternative to conventional surface modification techniques, such as plasma activation or chemical pretreatments, typically employed to bond materials with poor chemical compatibility, commonly defined as *hard to bond*. In such cases, conventional methods may prove insufficient, while macro-lattices have been shown to significantly enhance bonding strength, with reported values fivefold those of conventional methods [58,59]. The second scenario involves the integration of macro-lattices with structural adhesives [58,60]. In this configuration, macro-lattices act as a volumetric scaffold that can be fully infiltrated by the adhesive. Consequently, load transfer is no longer governed predominantly by adhesion at the adhesive-substrate interface; instead, stresses are redistributed within the infiltrated lattice-adhesive network, promoting cohesive failure rather than interfacial debonding while maintaining a lightweight design. The following discussion focuses on macro-lattices in the first scenario, where interfacial performance is primarily governed by mechanical interlocking rather than adhesive bonding.

Despite their limited diffusion, macro-lattices offer significant advantages, including a high strength-to-weight ratio and enhanced energy absorption. Moreover, the properties of these structures are highly dependent on their geometry, and tailored properties can often be achieved through only a single parameter adjustment within the unit-cell [15,58]. The design workflow typically starts with the selection of the unit-cell [61], after which macro-lattices are generally classified into three categories: *strut-based*, *planar-based*, and *surface-based*. The literature may present varying classifications, with additional distinctions based on topology, connectivity, and other factors [61]. This work adopts the classification most commonly used in mechanical interlocking applications.

Strut-based lattices consist of rod-like elements connected in different orientations to form three-dimensional unit-cells. Among them, cubic-derived configurations, such as Body-Centered Cubic (BCC) lattices, are frequently reported in the literature [20,60,62]. In several cases, a single layer of these structures oriented along the loading direction has proven sufficient to enhance interfacial strength over both conventional surface modification techniques and more complex lattice designs. Verma et al. [20], for instance, investigated the mechanical interlocking between PBF-LB processed 316 L lattice structures joined to Avaspire AV651 resin. Three strut-based geometries were evaluated: a BCC lattice reinforced along the vertical direction (BCCZ) (Fig. 13a), a Cubic Face-Centered (FCC) lattice (Fig. 13b), and a truncated octahedron (Kelvin cell) lattice (Fig. 13c). Their findings revealed that joints incorporating these structures, consisting of a single layer of unit cells with varying relative densities and an overall size of 5x5x1 mm^3, exhibited tensile strength values two to three times higher than those obtained through conventional surface modification techniques. The BCCZ lattice provided the highest interfacial strength. Nevertheless, geometric detailing plays a crucial role: the BCCZ lattice with 29% relative density and 0.25 mm strut diameter reached the highest tensile strength, while both the denser configuration, with 39% relative density and 0.30 mm strut diameter, and the less dense configuration, with 20% relative density and 0.20 mm strut diameter, showed lower performance. This demonstrates that bonding strength is governed by a balance between lattice structural integrity and secondary material penetration. Lower densities led to premature lattice failure due to thinner struts and manufacturing defects, whereas higher densities promoted secondary material failure due to reduced penetration in the lattice. Additionally, sharp corners at the node intersections were identified as preferential sites for stress concentration and crack initiation [63]. Accordingly, simplified lattice geometries with rounded struts and smooth node transitions are generally preferred.

Planar-based lattices are created by generating a periodic pattern in a two-dimensional plane and then extruding it in the third direction to form the three-dimensional structure. They face intrinsic limitations in mechanical interlocking, since they constrain only one or two of the three translational degrees of freedom [17,21,43]. Representative examples include periodic two-dimensional patterns with U-shape, T-shape, or dovetail shape features extruded in the third direction (Fig. 14). Kuipers et al. [21], for example, investigated dual-material MEX of PLA and PP, comparing the dovetail planar-based interlocking geometries with strut-based lattices. Their study showed that planar-based lattices, if not complemented by additional geometrical features, may allow relatively easy disassembly. Consequently, although planar-based lattices improve bonding compared to smooth or surface-modified interfaces, the interlocking mechanism primarily develops within the interface plane and can be overcome by in-plane deformation or sliding.

Surface-based lattices consist of surfaces generated from mathematical functions and represent an effective strategy for mechanical interlocking, primarily due to their continuous and smooth geometries, which mitigate stress concentrations. Among these, Triply Periodic Minimal Surface (TPMS) lattices are widely investigated. TPMS lattices are continuous, non-self-intersecting surfaces characterized by zero mean curvature at every point and periodicity along three orthogonal directions. Representative examples include Gyroid, Diamond, or

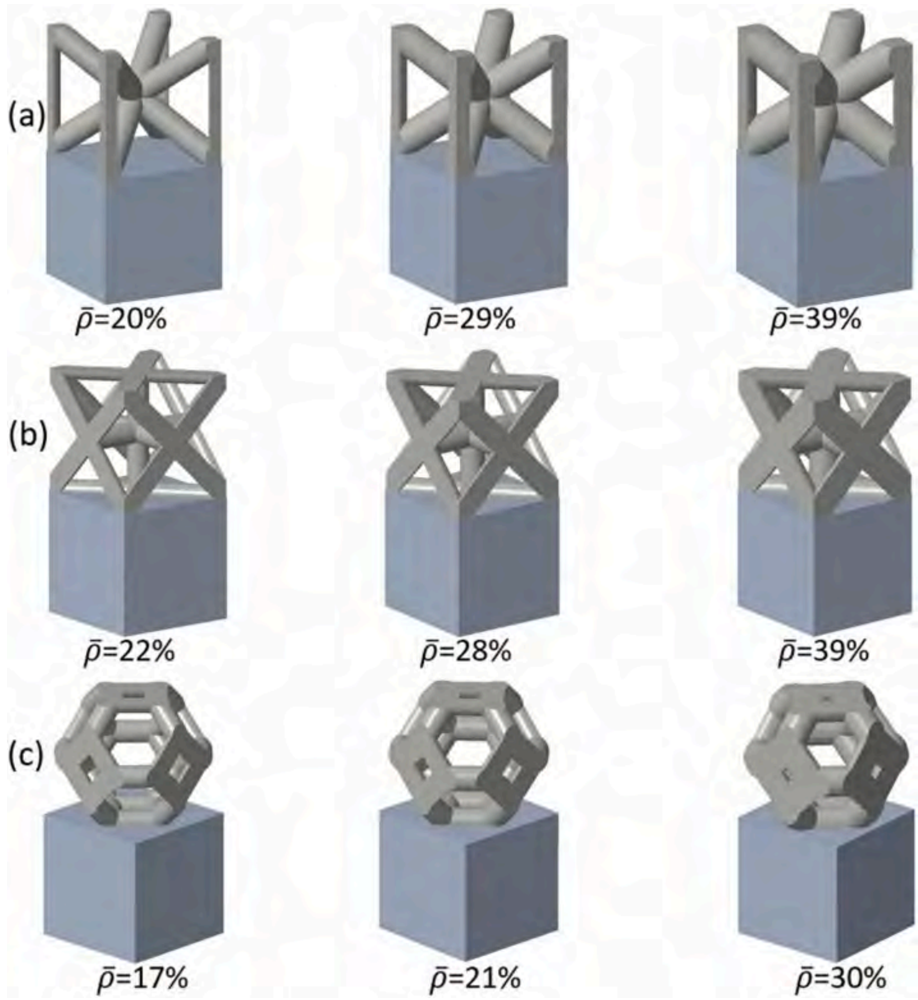

Fig. 13. Strut-based macro-lattices geometries: (a) Body-Centered Cubic lattice reinforced along the vertical direction (BCCZ); (b) Face-Centered Cubic (FCC) lattice; (c) truncated octahedron (Kelvin cell) lattice. For each unit-cell topology, the relative density is varied by modifying the strut diameter and the corresponding pore dimensions. Reprinted from [20], Copyright (2022), with permission from Elsevier.

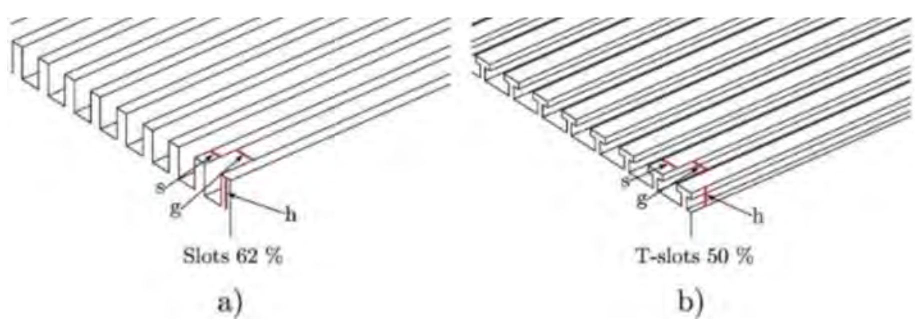

Fig. 14. Planar-based macro-lattice geometries obtained by extrusion of periodic two-dimensional patterns: (a) U-shape configuration; (b) T-shape configuration. Adapted from [43], under the terms of the Creative Commons CC BY 4.0 license.

Neovius geometries (Fig. 15c) [22,64]. Compared to strut-based and planar-based lattices, surface-based lattices generally exhibit superior mechanical performance. Ding et al. [22], for instance, explored mechanical interlocking between a rigid UV-curable acrylate resin, VeroClear, and a soft thermally curable silicone rubber, PDMS, combining PolyJet printing of the rigid component with subsequent molding and curing of the silicone. They compared U-shape pins with hierarchical features, BCC, and TPMS lattices. Their results demonstrated that TPMS lattices, specifically the diamond geometry, compared to control flat samples, enhanced the bonding strength by up to 28 times and the fracture energy by up to 217 times, due to their smooth, non-intersecting surfaces and more uniform stress distribution. Moreover, increasing the porosity of the diamond cells from 60% to 84% increased the ultimate bonding strength by about 73%.

When designing macro-lattices for mechanical interlocking, the geometry selection must consider manufacturing constraints, material compatibility, application requirements, and interlocking functionality. The design of the lattice is an important factor contributing to the strength of the bond [65]. A useful way to rationalize the relationship between lattice design and mechanical performance is to consider the

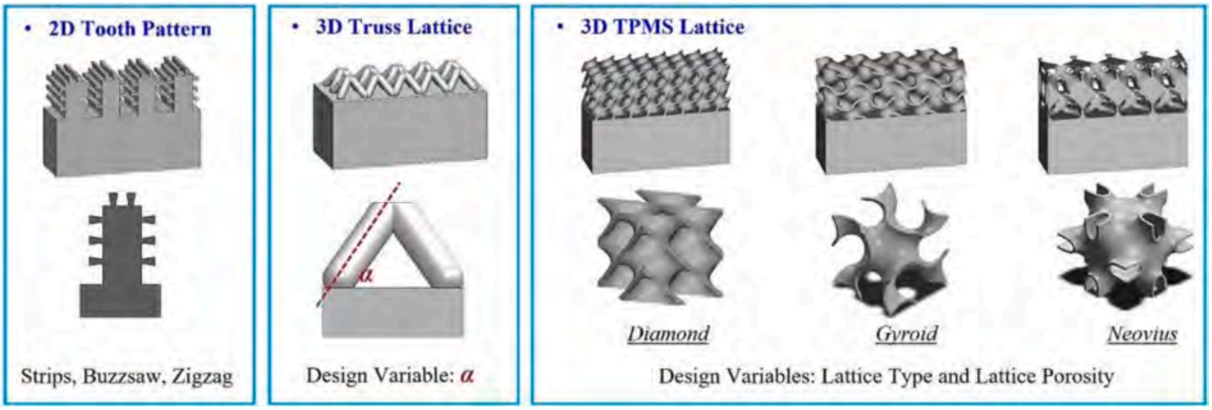

Fig. 15. Representative macro-interlocking structures: on the left, U-shape macro-pins with hierarchical micro-features; in the center, a strut-based macro-lattice, with a single layer corresponding to half BCC unit-cells; on the right, surface-based macro-lattices based on Triply Periodic Minimal Surfaces (TPMS), including Diamond, Gyroid, and Neovius geometries. Adapted from [22], Copyright (2024), with permission from Elsevier.

interlock as a system whose strength is governed by its weakest load-bearing region. Although Freund et al. [65] developed this framework in the context of Material Extrusion (MEX), the same principle can be extended to macro-lattices produced by different AM processes. In this view, the final joint strength is controlled by the concurrent contribution of the lattice structure, the infiltrated secondary material, and the connection between the lattice and the substrate. Therefore, increasing lattice complexity, connectivity, or relative density does not necessarily lead to higher joint strength. A denser lattice may improve the load-bearing capability of the structure, but it also reduces pore volume and may hinder complete infiltration of the secondary material. Conversely, a highly porous lattice can promote filling and stress redistribution, but excessively thin struts or shells may become sensitive to manufacturing defects, local fracture, or weak connection with the substrate. The optimal design is therefore process. and material-dependent and results from a balance between lattice robustness, secondary material penetration, stress distribution, and manufacturability.

Based on the literature [65], several recommendations can be identified:

- Unit cell topology, cell size, relative density and porosity, strut diameter or wall thickness, number of lattice layers, and orientation are the main design descriptors of macro-lattices and must be carefully considered.
- Comparing topology design, manufacturability constraints, and performance, strut-based lattices are generally easy to manufacture and offer effective load transfer due to their interconnected porosity and undercut features; nevertheless stress concentrations may arise at node intersection. Planar-based lattices are the simplest to fabricate, but they constrain only one or two translational degrees of freedom and may allow disassembly if not complemented by additional features. Surface-based lattices are generally preferred. They provide smooth, non-self-intersecting surfaces that mitigate stress concentration and promote enhanced bonding strength; however, their thin walls and complex internal channels may amplify manufacturability constraints.
- Cell size, strut diameter or wall thickness, and lattice porosity must be selected together, since they jointly control both manufacturability and connection strength. Higher porosity and larger pores generally facilitate the penetration of the secondary material and improve volumetric engagement, but may weaken the lattice structure if the struts or walls become too thin or approach the process resolution limit. Conversely, denser lattices improve lattice stiffness and strength, but reduce pore accessibility and may limit the mechanical contribution of the infiltrated material. Moreover, smaller cells increase the number of load-transfer points and the interfacial area, whereas larger cells improve filling efficiency and manufacturing reliability. Therefore, optimal performance is generally achieved within a process- and material-dependent design window, rather than by maximizing either density or porosity.
- The lattice should maximize load transfer within the smallest possible interfacial volume. Since interlocking is primarily established within the first layer, additional layers may introduce potential failure sites without proportionally increasing joint strength.
- Lattice orientation should align with the dominant loading mode to promote uniform stress distribution. Repetitive and symmetric geometries are preferable, whereas density gradient may introduce stiffness mismatches and stress concentrations, causing premature failure governed by the weakest structural region.

4. Materials and manufacturing techniques

This section provides a structured analysis of materials (Section 4.1) and manufacturing techniques (Section 4.2) for mechanically interlocked joints. These aspects are inherently interdependent, as material selection constrains the range of feasible fabrication and joining approaches, while the adopted processing strategies influence the achievable material combinations, interlocking configurations, and resulting interfacial behavior.

4.1. Materials

A comprehensive analysis of material families employed in mechanical interlocking structures is presented, making a clear distinction between the primary materials used to fabricate the interlocking structures and the secondary materials joined to these structures (Section 4.1.1). This approach enables the identification of prevalent material combinations, facilitating insights into current industrial trends and identifying existing gaps (Section 4.1.2).

4.1.1. Material families

Examining the previously defined mechanical interlocking categories – micro-features, macro-pins, and macro-lattices – it emerges from the literature that only two material families, metals and polymers, are currently employed as primary materials (Fig. 16). In contrast, secondary materials encompass metals, polymers, and composite families, particularly Fiber Reinforced Polymers (FRPs). Composite materials have not yet been reported as primary materials. This may be related to the intrinsic manufacturing constraints associated with fiber-reinforced materials, where the presence of continuous or oriented fibers can limit the geometric freedom required to fabricate complex three-dimensional interlocking structures. Ceramic materials, instead, are scarcely

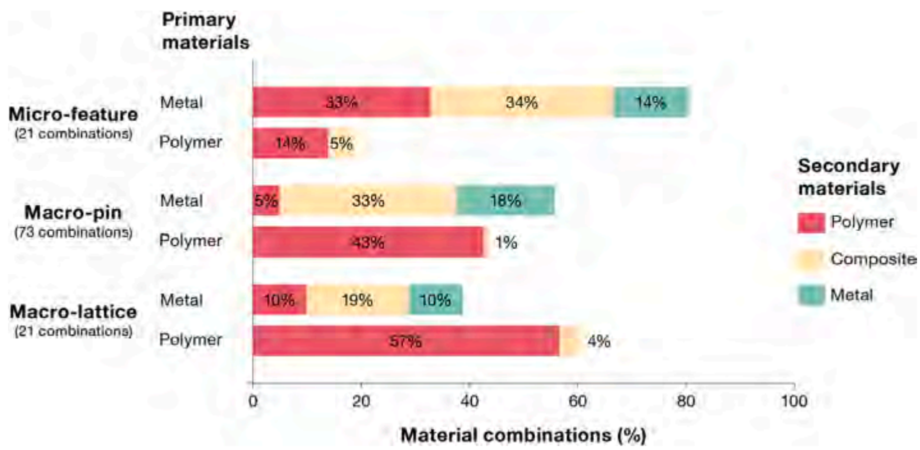

Fig. 16. Frequency analysis of material family combinations reported in the literature for micro-features, macro-pins, and macro-lattices. Percentages represent the relative occurrence within each category. The x-axis indicates the primary material families, while the bars represent its combinations with the corresponding secondary material familes.

investigated in either role, with only a single specific biomedical application reported among the analyzed studies [36,66] and therefore not included in the graph. In this case, a surface texture was produced on zirconia substrates to enhance bonding with secondary materials, namely dental resin or veneering ceramic, for dental restorations.

At the level of material families, combinations can be broadly organized into two principal groups: combinations within the same family (e.g., polymer–polymer) and combinations across different families (e.g., polymer-composite). Metals are utilized as primary materials in conjunction with all three secondary material families, while polymers predominantly pair with other polymers or composite materials. Polymer-metal combinations, with polymer serving as the primary material, have been suggested in the literature as a potentially interesting direction for future research [27].

A clearer trend becomes apparent when correlating material families with interlocking typologies (Fig. 16). In micro-features, metal interlocking structures combined with composite or polymeric secondary materials clearly dominate. Combinations involving polymers as primary material, in this case, remain infrequent. This tendency appears consistent with the predominant methods used to produce micro-features, such as anodizing or related treatments, which are well-established for metal AM components. In contrast, macro-pins and macro-lattices are largely characterized by polymer–polymer combinations, reflecting the broader adoption of polymers in AM and the maturity of their manufacturing techniques. The second most common combination involves metal interlocking structures paired with composite materials, aligning with the industrial drive toward lightweight, highly functional multi-material components. A detailed analysis of specific material combinations is presented in the next section.

4.1.2. Material combinations

Bubble maps illustrating the combinations of materials for each interlocking category are presented in Figs. 17–19. In these maps, node size corresponds to the frequency of individual material citations, whereas the thickness of the connecting lines indicates the prevalence of a specific material combination within the literature. The direction of the connecting lines represents the interlocking configuration: the tail corresponds to the primary material providing the interlocking

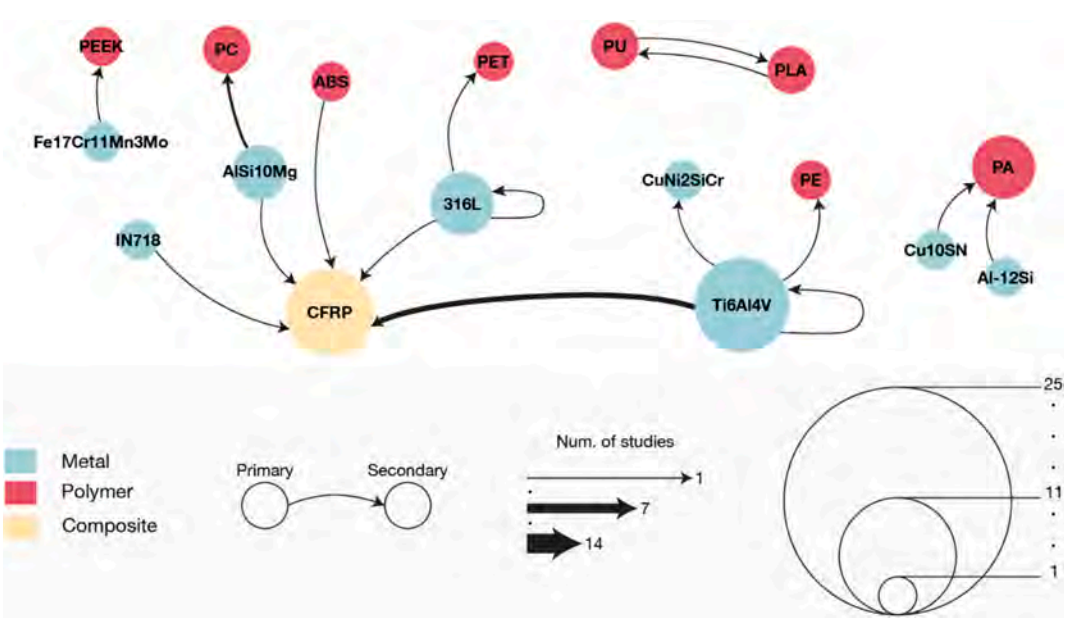

Fig. 17. Bubble map of material combinations for micro-features. Arrow direction indicates the interlocking configuration: the tail corresponds to the primary material, while the arrowhead points to the secondary material. Line thickness scales with the number of studies for a given combination. Node size is proportional to the number of citations of each material in the literature.

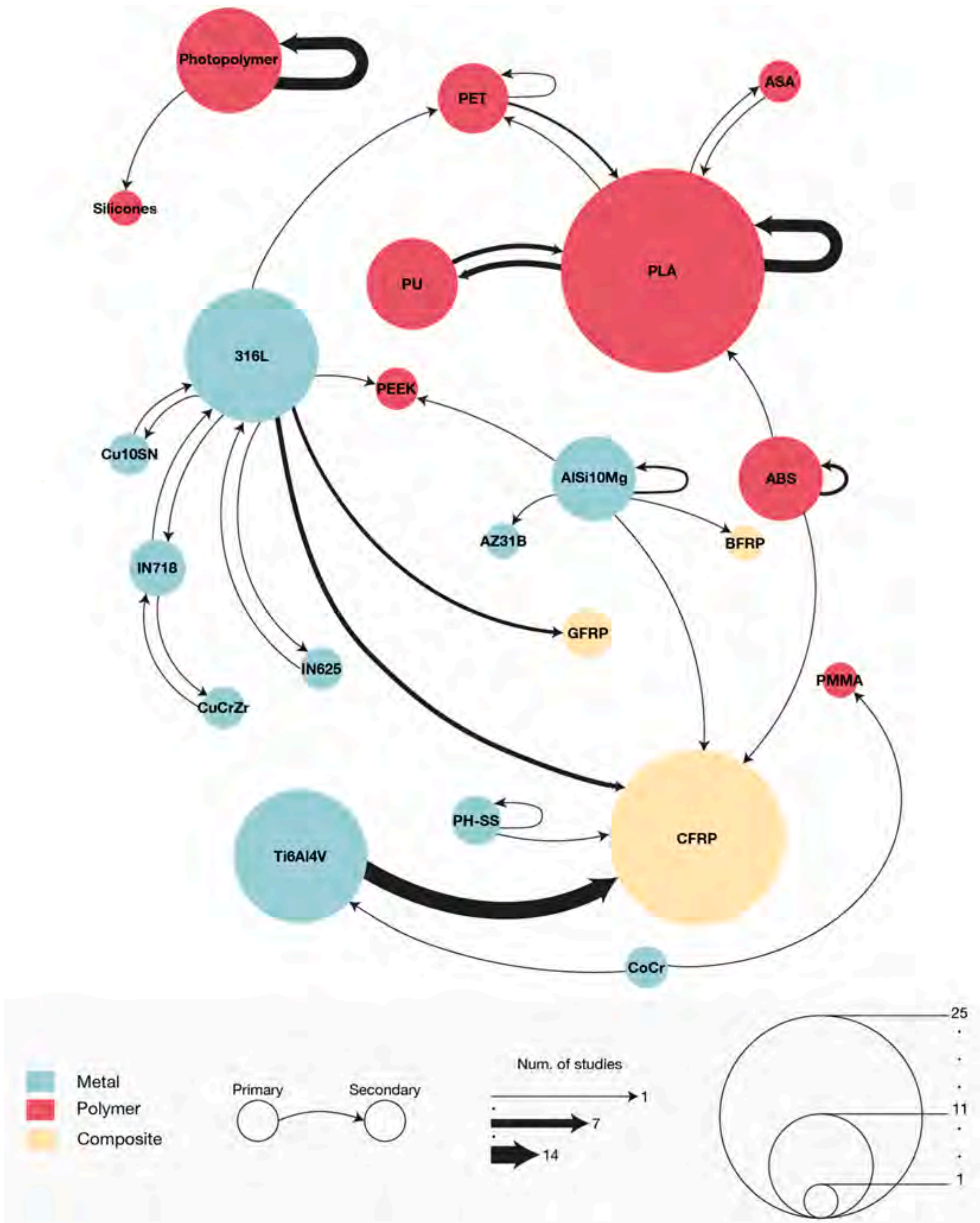

Fig. 18. Bubble map of material combinations for macro-pins. Arrow direction indicates the interlocking configuration: the tail corresponds to the primary material, while the arrowhead points to the secondary material. Line thickness scales with the number of studies for a given combination. Node size is proportional to the number of citations of each material in the literature.

structures, while the arrowhead points to the secondary material. The same scaling criteria are adopted across all three figures to ensure direct comparison.

One of the most frequently reported combinations across the three analyzed interlocking categories, and particularly pronounced in macro-pins, involves metallic primary materials, such as titanium alloys and steels, joined with CFRPs [3,17,31,33,34,51–55,63,67–77]. More than 75% of current CFRP production relies on thermoset matrices [8], while thermoplastic composites are progressively gaining industrial attention due to their short processing cycles and inherent recyclability. The considerable interest in CFRPs is primarily driven by their increasing adoption in industrial sectors, such as aerospace and automotive, where weight reduction is crucial for decreasing fuel consumption and minimizing CO_2 emissions [26]. Additionally, CFRPs exhibit excellent specific mechanical properties, although they present certain drawbacks, including high costs, limited energy absorption, and degradation of matrix-dominated properties at elevated temperatures. In contrast, GFRPs appear less frequently and are mainly observed in macro-pins and macro-lattices [18,50,78,79]. Natural fiber reinforced polymers also remain marginal, despite their increasing relevance in sustainable material development. To the best of the authors knowledge, the only reported example is provided by Miranda et al. [16], who combined AlSi10Mg macro-pins with BFRPs, highlighting the less energy-intensive production and superior environmental profile of basalt fibers compared to glass and carbon fibers, while maintaining competitive mechanical properties.

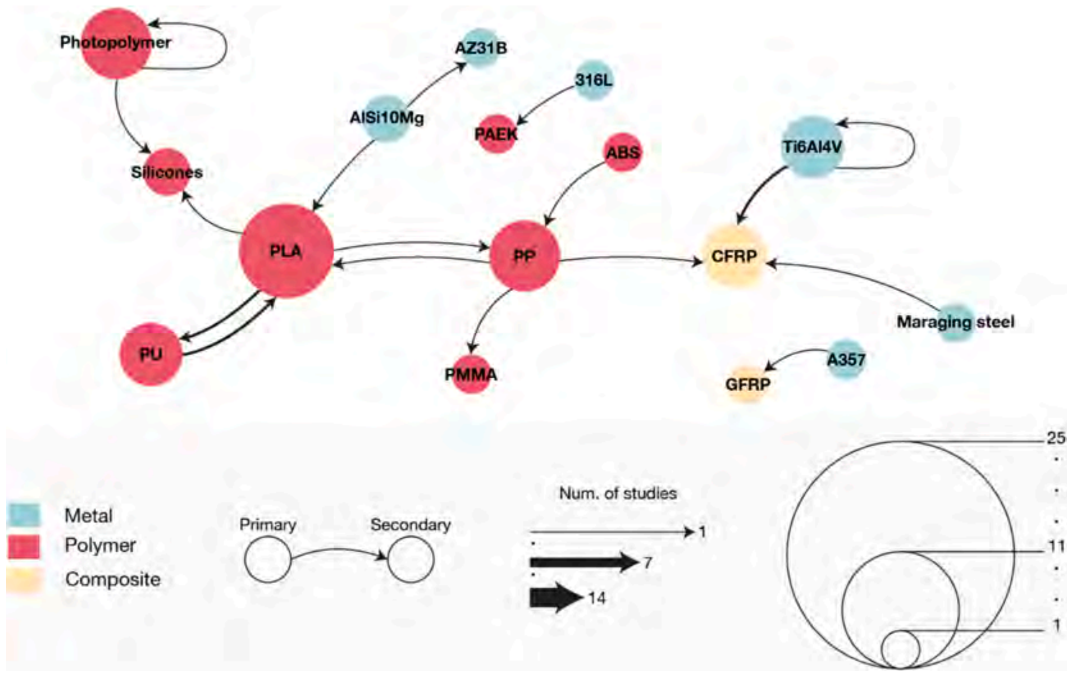

Fig. 19. Bubble map of material combinations for macro-lattices. Arrow direction indicates the interlocking configuration: the tail corresponds to the primary material, while the arrowhead points to the secondary material. Line thickness scales with the number of studies for a given combination. Node size is proportional to the number of citations of each material in the literature.

Among metallic materials, titanium alloys, aluminum alloys, and stainless steels have attracted extensive research interest for their well-known advantageous characteristics, such as good mechanical properties, stiffness, and thermal performance [75]. Within metal-polymer combinations, particularly evident in micro-features, metals paired with thermoplastic materials such as PA and PC are recurrent [19,20,27,30,37,39,40,43,80–82]. Metal-metal combinations are also reported. In some cases [17,83,84], the secondary material may coincide with the primary one, for example, AlSi10Mg joined with AlSi10Mg [44,85], often implemented through complementary interlocking configurations, in which macro-pins are produced on both materials prior to joining. Alternatively, dissimilar metallic combinations are explored [24,62,86–89], as in the case of Li et al. [86], who combined stainless steel 316 L, characterized by high ductility, with Inconel 625, exhibiting higher strength but reduced deformability. This specific combination aims to mitigate the conventional strength-ductility trade-off by promoting complementary deformation behavior, thereby improving energy absorption and extending applicability to high-temperature, harsh environments.

Finally, polymer–polymer combinations are particularly recurrent in macro-pins and macro-lattices [21,23,28,47,49,57,58,90–96]. Often reported materials include thermoplastic polymers such as PLA, PP, ABS, and PU, especially PLA-PU combinations, reflecting their processing versatility and accessibility [97–99]. However, when chemically dissimilar polymers are combined, reliable mechanical interlocking remains challenging due to poor interfacial adhesion, chemical incompatibility, and susceptibility to deformation-induced shape distortions. Comprehensive studies on interface characteristics remain limited, highlighting a notable research gap [100]. Photopolymer resins and silicone-based elastomers appear sporadically in the literature [22,59,101,102].

Overall, the material distributions reveal clear scale-dependent tendencies. Micro-features are largely characterized by metallic primary materials paired with polymeric or composite adherends; macro-pins exhibit a wide spectrum of combinations, including metal-composite systems, metal–metal complementary joints, and polymer–polymer pairings; macro-lattices display a marked prevalence of polymer–polymer combinations. The trends highlight several research gaps, including the limited exploration of natural fiber composites and the lack of systematic interfacial characterization in chemically dissimilar material pairings. Moreover, material selection is influenced not only by compatibility and application requirements, but also by the technological constraints and maturity of the AM processes, discussed in the following section.

4.2. Manufacturing techniques

The analysis of materials necessitates an integrated and comprehensive study of the corresponding manufacturing techniques, as presented in this section. In this review, the classification and terminology of the AM processes follow the ISO/ASTM 52900:2021(E) standard [101].

The manufacturing of mechanically interlocked multi-material components can be divided into two sequential phases [9]. The first involves the fabrication of the interlocking structures on primary material substrates (Section 4.2.1). In complementary interlocking configurations, such structures are typically produced on both materials prior to assembly; however, this represents a specific configuration that differs from the more conventional approach. Despite the intrinsic differences in the three interlocking categories – micro-features, macro-pins, and macro-lattices – the fabrication processes share a common objective: creating geometrical features that enable subsequent joining. The second phase consists of the actual joining process, in which the interlocking structures fabricated on the primary material are bonded to the secondary material (Section 4.2.2). The following sections provide an in-depth analysis of these two phases.

4.2.1. AM fabrication of mechanical interlocking structures

As depicted in Fig. 20, Powder Bed Fusion (PBF) and Material Extrusion (MEX) are the predominant technologies for producing interlocking structures across all analyzed categories. This trend is consistent with the material distributions presented in the frequency analysis and bubble maps discussed in Section 4.1. Conversely, the limited adoption of Directed Energy Deposition (DED), Material Jetting

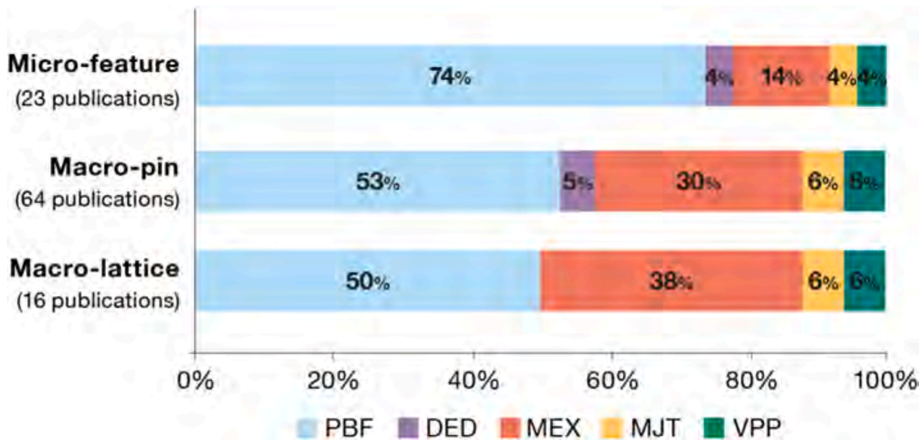

Fig. 20. Relative distribution of AM processes employed for the fabrication of mechanical interlocking structures. Percentages are calculated with respect to the total number of publications considered within each interlocking category.

(MJT), and Vat Photopolymerization (VPP) highlights the need for further investigation to expand their applicability to interlocking structures.

The marginal adoption of MJT and VPP, each accounting for approximately 4–6% of the reviewed literature, can be traced to three converging limitations. First, the available feedstock is mainly restricted to photo-curable resins, inks, or resin-based formulations, whose mechanical and thermal performance is generally lower than that of thermoplastics processed by MEX or metals processed by PBF, thereby limiting their suitability for load-bearing interlocking joints. Second, the properties of MJT- and VPP-printed parts are strongly influenced by curing and post-curing conditions, which may complicate the integration of the printed primary substrate with co-bonded or secondary bonded materials. Third, in MJT, the limited range of materials and the frequent need for support materials can restrict the feasibility of complex interlocking geometries, whereas in VPP the need to ensure resin drainage and complete curing can hinder the fabrication of closed or poorly accessible internal cavities. DED is also less represented in the surveyed literature, approximately 4–5%, although for different reasons. While DED is highly suitable for adding material onto existing substrates and for producing large-scale features, its lower geometrical resolution compared with PBF, larger melt pools, higher heat input, and greater susceptibility to distortion and residual stresses limit its use for small, accurately controlled interlocking features. These process-specific constraints explain why MJT, VPP, and DED are currently utilized in few studies, while also identifying clear research directions.

In the micro-feature category, PBF techniques represent the dominant approach, accounting for 74% of the reported cases. This prevalence is closely aligned with the frequent use of metallic alloys, such as Ti6Al4V and AlSi10Mg, and thermoplastic materials such as PA and PU, as illustrated in Fig. 17, which are well suited to PBF processing. Since controlling surface morphology at the micron scale is essential to achieving strong interfacial adhesion, the intrinsic resolution of PBF makes it particularly suitable for this application. Nevertheless, to further enhance interface performance, additional post-processing methods such as mechanical or chemical surface treatments may still be required, as already discussed in Section 3.1. In contrast, MEX (14%), DED, MJT, and VPP (4% each) are only marginally reported.

In contrast, the macro-pin category shows greater technological diversification. Although PBF remains prevalent (53%), employing both laser and electron beam energy sources, other technologies, including MEX (30%), DED (5%), MJT (6%), and VPP (6%), are also employed. This diversity is further reflected in the broader range of primary materials employed, including photopolymers and silicones (Fig. 18). Such findings suggest that macro-pins possess greater flexibility in dimensional and functional requirements, enabling the adoption of different manufacturing technologies. Moreover, the widespread investigation of macro-pins in the literature, compared to other interlocking categories, likely contributes to the exploration of their production via multiple technologies.

Consistent with the trends observed for macro-pins, the macro-lattice category displays a similar process distribution, with PBF (50%) and MEX (38%) prevailing, in line with the predominance of polymers in this type of structure (Fig. 19), and only marginal use of MJT and VPP (6% each).

Across all categories, the literature emphasizes that, despite the design flexibility offered by AM, intrinsic limitations and process constraints must be considered prior to fabrication [15]. A direct quantitative correlation between individual processing parameters and interlocking performance cannot yet be established, since the available studies differ markedly in terms of interlocking geometries, material pairs, joining strategies, and testing configuration. Nevertheless, a qualitative process-structure-performance relationship can be extracted by considering the features through which processing affects interlocking behavior, such as, for example, surface roughness for micro-features, dimensional accuracy for macro-pins, and support requirements for macro-lattices. Since PBF is the most frequently reported process in the reviewed literature, most available examples refer to powder-based technologies; however, the same rationale applies to other AM processes, each governed by its own process-sensitive variables, such as layer height, raster orientation, infill density, and extrusion temperature in MEX; heat input, deposition path, and feed rate in DED; curing, post-curing, support removal, and resin drainage in MJT and VPP.

For micro-features, surface roughness is a key factor governing bonding performance and must be controlled through the appropriate tuning of parameters such as power input, layer thickness, hatch spacing, and build orientation [76]. In the study by Nusom et al. [76], PBF-LB Ti6Al4V surfaces manufactured at different build angles showed distinct roughness patterns that directly affected bonding performance. In particular, the highest roughness condition, obtained at a 45° build angle with $R_a = 24.84$ µm, resulted in a 54.4% increase in bonding shear strength compared with the samples built at 90°, which exhibited a lower roughness of $R_a = 10.68$ µm. Likewise, in macro-pins, mechanical performance, particularly in terms of lap-shear strength and fracture behavior, is highly sensitive to process conditions [72]. In this case, the process-performance link is mediated by the dimensional accuracy of the pins, surface porosity and roughness, and the ability of the secondary material to flow around them during the joining step. From a dimensional perspective, the accurate reproduction of key geometrical details, including tips, bodies, and roots, is essential since these regions govern the effective mechanical engagement between two materials. The choice of the production system can therefore significantly affect the replication of small features. Systems using a larger spot size and layer thickness, for instance, tend to produce rougher surfaces, with partially melted particles or balling phenomena, as well as geometrical deviations in small features. Conversely, systems using a smaller laser spot size and layer thickness may enable the fabrication of more distinct shapes, improving surface quality. Thus, even when the designed interlocking geometry is successfully manufactured, process resolution and defect formation can alter the effective pin morphology and, consequently, the potential interlocking capacity. In macro-lattices, manufacturability constraints become even more critical, since the performance of the structure depends on the accurate reproduction of thin struts, open pores, and internal cavities. In powder-based techniques, laser power and scan speed can affect powder adhesion on struts and dimensional accuracy [103]. Moreover, macro-lattices are susceptible to residual powder entrapment [102], necessitating careful consideration of both geometry and process parameters. Similar attention is required to minimize excessive support structures [104] and to mitigate deformations caused by thermal expansion, shrinkage, or suboptimal processing conditions [103]. Consequently, designers must balance structural integrity, dimensional accuracy, cost-efficiency, and production time while ensuring compatibility with the subsequent joining phase.

In conclusion, PBF and MEX are currently the most commonly employed technologies for the fabrication of interlocking structures, although their effective use requires careful optimization of process parameters. This further confirms that material selection is often inherently linked to process availability and technological maturity. Moreover, the selection of a suitable manufacturing technique should be guided not only by material and structural complexity, but also by the specific requirements of the subsequent joining phase. Future research should aim to fully exploit the potential of AM technologies in this context.

4.2.2. Joining processes of materials

Joining processes refer to the phase in which the secondary material is bonded to the mechanical interlocking structures fabricated on the primary material. In this context, the distinction between micro-features, macro-pins, and macro-lattices becomes secondary, as joining processes are primarily dictated by the materials involved. For this reason, an analysis based on material combinations and typical application scenarios is conducted, as summarized in Table 3. Within each combination, a distinction can be drawn between co-bonding and secondary bonding methods. Co-bonding refers to processes wherein the production of the secondary material and its joining to the primary one occur simultaneously. Secondary bonding, in contrast, separates these two stages.

For metal-composite combinations, co-bonding approaches clearly derive from conventional composite manufacturing technologies. These include Vacuum-Assisted Resin Infusion (VARI) techniques [18,70], autoclave consolidation [3,17], and thermo-mechanical processes, including hot pressing and compression overmolding [34,76]. In these methods, the composite phase is consolidated while simultaneously penetrating and engaging the metallic interlocking features.

VARI involves resin infiltration into dry fibers facilitated by vacuum pressure within a flexible or closed mold setup [9]. It is a cost-sensitive process, suitable for large-area components. A known limitation of these infusion-based processes, particularly when applied to components with macro-pins, is their susceptibility to defects such as voids, cracks, debonding, and delamination [70]. Autoclave and thermo-mechanical processes are most commonly used in combination with prepreg composite materials. While both rely on controlled thermal and pressure cycles, autoclave processes apply pressure uniformly via a pressurized gas environment, whereas thermo-mechanical systems deliver direct pressure through heated plates. These methods currently represent the benchmark for manufacturing such components, as they tend to ensure

Table 3
Overview of joining processes for mechanically interlocked components, classified according to material combinations, and typical application scenarios. Processes are distinguished between co-bonding and secondary bonding.

Material combination	Co-bonding	Secondary bonding	Typical application scenarios
Metal-composite	VARI Autoclave Consolidation Thermo-mechanical Processes	Ultrasonic Joining	**VARI:** large-area or cost-sensitive parts with moderate consolidation requirements **Autoclave/Thermo-mechanical Processes**: high-performance parts requiring low void content and/or high fiber volume fraction **Ultrasonic Joining:** short-cycle, localized heat input (applicable only to composite with thermoplastic matrix)
Metal-polymer	Thermo-mechanical Processes MMAM Hybrid additive-subtractive Processes	Ultrasonic Joining	**Thermo-mechanical Processes:** metal-thermoplastic joints requiring controlled polymer softening and flow into interlocking features **MMAM:** integrated or sequential fabrication, reducing handling steps and enabling direct material deposition onto interlocking features **Hybrid Processes:** tailored undercuts and localized interlock **Ultrasonic Joining:** short-cycle, localized heat input (applicable only to thermoplastic polymers)
Metal–metal	MMAM	Adhesive Bonding Manual Bonding	**MMAM:** integrated or sequential fabrication, reducing handling steps and enabling direct material deposition onto interlocking features **Adhesive/Manual Bonding:** complementary interlocking configuration
Polymer–polymer	MMAM Thermo-mechanical Processes	Adhesive Bonding Ultrasonic Joining	**MMAM:** integrated or sequential fabrication, reducing handling steps and enabling direct material deposition onto interlocking features **Adhesive Bonding:** chemically dissimilar polymers **Thermo-mechanical Processes/Ultrasonic Joining:** applicable only to thermoplastic, although scarcely reported
Polymer-composite	Thermo-mechanical Processes	Adhesive Bonding	**Thermo-mechanical Processes:** applicable to thermoplastic-matrix composite, although scarcely reported **Adhesive Bonding:** most diffuse technique with structural adhesive

substantial reductions in void content and enable higher fiber volume fractions compared to VARI techniques. Nevertheless, their implementation entails strict process control and high investment costs [9].

Secondary bonding in metal-composite combinations involves the application of localized thermal energy to soften the matrix and facilitate the joining procedure. Ultrasonic joining [105,106] exemplifies this strategy, allowing short cycle times and high energy efficiency. Nevertheless, the process is restricted to composites with thermoplastic matrices and may present drawbacks, such as potential tool wear when joining hard alloys such as titanium [9], as well as possible inaccuracies and laminate swelling during assembly [70].

In metal-polymer combinations, co-bonding strategies include thermo-mechanical processes, Multi-Material Additive Manufacturing (MMAM) [27,30,43,80], and hybrid additive-subtractive processes [39]. Thermo-mechanical processes, including hot pressing [37,72,76] and compression molding [63], are widespread due to the frequent use of thermoplastic polymers such as PA, PLA, ABS, and PU. These processes enable strong mechanical interlocking through controlled thermal softening and material flow. However, inadequate parameter selection may result in incomplete penetration of the interlocking structures, residual stress, or interfacial defects.

MMAM systems constitute an interesting and emerging solution, as they enable the fabrication of both primary and secondary materials and their simultaneous joining within the same platform. These systems may be based on a single-process configuration, in which the same AM technology is employed to deposit different materials (e.g., multi-nozzle MEX [107] or multi-material PBF [87]). This approach is particularly suited for metal–metal or polymer–polymer pairings. Alternatively, particularly in metal-polymer combinations, MMAM may rely on multi-process configurations that integrate distinct AM manufacturing techniques within a single machine (e.g., a hybrid platform merging laser-based PBF and MEX [27]). These configurations reduce handling steps and processing time but remain technologically complex [23], requiring further research. Sequential AM approaches are also reported in the literature. In these cases, separate AM machines are employed to fabricate the interlocking structures and subsequently deposit and join the secondary material (e.g., a PBF system to fabricate metallic interlocking structures, followed by a separate MEX system to deposit polymer directly into the structures [43]).

Lastly, hybrid additive-subtractive processes may be adopted, combining subtractive creation of undercuts with subsequent additive deposition of the secondary material [108]. Within this category, the AddJoining technique (patent application DE 102016121267 [109]) deserves a mention. The process involves fixing a pre-manufactured metallic substrate onto the build platform, depositing an intermediate coating layer via MEX to promote adhesion, and subsequently depositing thermoplastic layers to complete the joint [110,111].

Secondary bonding in metal-polymer combinations is less prevalent and mainly involves ultrasonic joining [112], again limited to thermoplastic polymers.

Metal-metal combinations exhibit a limited set of joining processes. Co-bonding is achieved through MMAM systems [24,86–89], where multiple metallic materials are deposited within a single integrated manufacturing system.

Secondary bonding includes adhesive bonding [17] and manual mechanical assembly [44], particularly in complementary interlocking configurations. Although adhesive bonding is traditionally regarded as an independent joining method, it can serve as a complementary joining process in mechanically interlocked components. Several studies have shown that the combination of mechanical interlocking structures and adhesive bonding can enhance or reduce joint performance depending on loading conditions [34,49,51,113]. For example, under compression loading, joints with macro-pins and adhesive outperformed the corresponding interlocked joints without adhesive [49]. Conversely, in another study, the addition of a film adhesive reduced the Mode I toughening compared with macro-pins alone [51]. However, the integrated use of these two techniques is still at an early stage and requires further investigation [5].

Polymer-polymer combinations are frequently addressed through MMAM systems [21,23], with different thermoplastic materials sequentially deposited within the same process. However, when chemically dissimilar polymers are involved, interfacial adhesion becomes challenging due to limited molecular compatibility and mismatched thermal expansion behavior. In such cases, joining performance is highly sensitive to infiltration and dimensional accuracy.

For secondary bonding, adhesive application remains the most common approach [45,58]. When both polymers are thermoplastic, thermo-mechanical process or ultrasonic joining may be feasible, although such approaches are scarcely reported.

In polymer-composite combinations, co-bonding techniques are generally not documented. Also in this case, when thermoplastic matrices are involved, thermo-mechanical processes are feasible but remain scarcely reported [35]. Polymer-composite combinations, instead, are predominantly joined through secondary bonding, most commonly using structural adhesives [60].

Across all material systems, the selection of the joining process is strongly governed by the intrinsic behavior of the materials involved. Co-bonding approaches are prevalent, particularly when thermoplastic and composite materials are involved. In contrast, secondary bonding methods are less diffused and become necessary when materials are chemically dissimilar or thermally incompatible. Despite the variety of reported processes, comparative studies assessing joint performance remain scarce. Consequently, process selection must rely on case-specific evaluation, considering material compatibility, process feasibility, and application requirements.

5. Performance and test methods of mechanically interlocked joints

In this section, an in-depth overview of the performance of mechanically interlocked joints and of the experimental methods used to assess it is provided. Section 5.1 introduces the most frequently investigated performance metrics and the key parameters governing joint behavior. Building on this, Sections 5.2 and 5.3 review the most commonly adopted destructive and non-destructive testing methods used to quantify these metrics and characterize interfacial integrity. Finally, Section 5.4 discusses the main findings and recurring trends reported in the literature, with particular emphasis on the correlation between the design and performance of mechanically interlocked joints.

A major limitation that clearly emerges from the literature is the lack of standardized testing protocols specifically tailored for mechanical interlocking as a joining method. This issue becomes even more critical when AM is considered as the production route for the interlocking structures. As a result, a wide variety of specimen geometries, setups, and testing procedures have been proposed. This methodological diversity, while reflecting the early stage of research in the field, also prevents a direct comparison between studies, underscoring the need for a unified experimental framework.

5.1. Performance metrics

The performance of mechanically interlocked joints results from a complex interplay among geometry, materials, and process-related factors. These variables are strongly interdependent, making it difficult to isolate the contribution of any single factor. At the geometrical level, the design of the interlocking features, including shapes, dimensions, and distributions, governs the load-transfer path, stress localization, and the ensuing failure mechanisms. At the material level, intrinsic properties such as elastic modulus, strength, polarity, wettability, and thermal expansion coefficient control both the local stress state and the effectiveness of interfacial interactions. Manufacturing-related variables, including build orientation, energy input, and layer thickness in AM processes, as well as joining-related factors such as infiltration pressure or curing temperature, affect the quality of mechanical engagement and interfacial continuity. The combined influence of these factors determines the joint performance, which is quantified through different metrics reported in the literature. Moreover, the testing configuration adopted to measure them can also influence the observed joint response and is discussed in Section 5.2.

Several performance metrics are recurrently reported to evaluate joint performance. Apparent shear strength and failure load remain the most frequently adopted metrics, reflecting the need to quantify load-transfer efficiency at the interface. In the majority of studies, particularly those involving macro-pins, failure load is preferentially reported rather than stress-based metrics. This is due to the inherent difficulty in defining an effective bonding area in the presence of micro-features, macro-pins, and macro-lattices, together with the non-uniform stress distributions that characterize these structures [16,45,114,115]. In this context, comparing results across different studies becomes challenging due to the absence of a standardized design and testing framework. Consequently, results from different works may differ substantially and can even appear contradictory [14]. Tensile strength and interfacial fracture toughness are also commonly evaluated, as well as fatigue life and environmental durability (e.g., corrosion or humidity resistance). These mechanical outcomes are often correlated with morphological descriptors such as surface roughness, topology, porosity, defect distribution, and infiltration depth, establishing links between interface morphology and macroscopic response.

Describing interfacial strength is further complicated by the simultaneous action of multiple adhesion mechanisms. A useful interpretative map (Fig. 21) is provided by the adhesion-theory framework discussed by Freund et al. [23], in which interfacial bonding is classified into mechanical adhesion and specific adhesion. Mechanical adhesion is achieved through geometric interference between interlocking features. Specific adhesion, instead, is the result of polar interactions and chemisorption, both dependent on the polarity of the materials; adsorption, governed by intermolecular forces and wettability; diffusion, resulting from elements or chain mobility across the interface; and, to a lesser extent, weak boundary layer effects and electrostatic interactions. While these mechanisms co-act and are each sensitive to several variables, mechanical interlocking and material polarity emerge as particularly impactful levers. Focusing the present analysis on interlocking, therefore, allows examination of one dominant mechanism in depth while keeping sight of the multi-mechanism landscape.

Since test configuration and boundary conditions can amplify or suppress specific mechanisms, a clear understanding of testing methods is essential for interpreting joint performance. The following sections, therefore, review the most commonly adopted destructive and non-destructive testing methods used to quantify the performance metrics discussed above.

5.2. Destructive testing

Destructive testing methods employed for mechanically interlocked joints are commonly derived from procedures originally developed for adhesive bonding. These methods can be adapted to better capture the specific features of mechanical interlocking, reflecting the absence of consolidated testing protocols for this class of joints. According to the literature, the most common approaches, applicable to micro-features, macro-pins, and macro-lattices, are mechanical tests complemented by morphological inspections and fracture analyses. A summary of the main reported tests, including output metrics, applicability to different interlocking categories, and main limitation, is reported in Table 4.

Among mechanical tests, the lap shear configuration, particularly the single-lap shear test, is the most frequently adopted, owing to its ease of fabrication and testing efficiency in evaluating adhesion performance [49]. The lap shear test consists of bonding the primary and secondary materials, together referred to as adherends, through an overlap region where the load is transferred. The standards most often referenced for single-lap shear tests are those originally defined for adhesive bonding under different material combinations and conditions (e.g., ASTM D1002 [116], D3165 [117], D5868 [118], ISO 19095 [119], ISO 13445 [120]). However, in many studies, the reference standard is not explicitly mentioned, and substantial flexibility is observed in specimen dimensions. The overlap length, for instance, can range from the 12.7 mm prescribed by ASTM D1002 and D3165 [39] up to 25 mm or more [18,34], depending on the case study. Increasing the overlap length generally leads to higher failure loads, since the load is distributed over a larger region. Yet, as demonstrated for adhesive joints [121], this improvement is nonlinear: beyond a certain length, the increase tends to

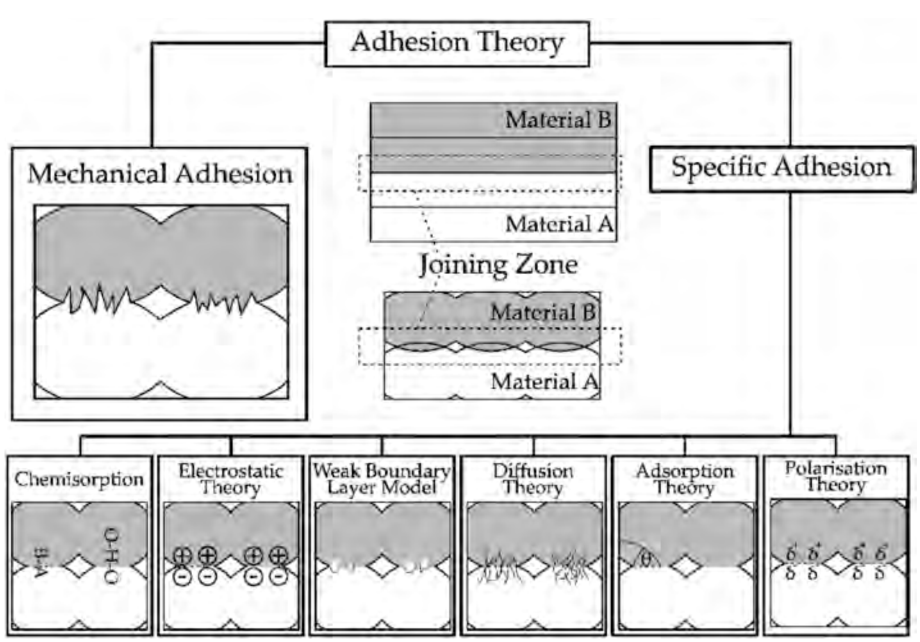

Fig. 21. Schematization of the adhesion mechanisms that govern interface strength. Reprinted from [23], under the terms of the Creative Commons CC BY 4.0 license.

Table 4
Summary of the destructive and non-destructive testing methods used to characterize mechanically interlocked joints, highlighting output metrics, main applicability and limitations.

Testing category	Testing technique	Main output/metric	Main applicability	Main limitations
Destructive Testing	Single-lap shear	Maximum load, apparent shear strength, displacement, failure mode	Most common for micro-features and macro pins for comparative assessment under dominant shear loading	Non-uniform stress distribution, peel and bending effects, local stress concentrations at overlap edges and geometric transitions, strong dependence on overlap length, adherend thickness, and stiffness mismatch
	Double-lap shear and custom shear fixtures	Maximum load, apparent shear strength, failure mode	Suitable for micro-features and macro-pins, when a symmetric shear loading condition is required	Complex specimen preparation and alignment, fixture and specimen geometry often study-specific, possible local stress concentrations in geometric transitions
	Tensile, pull-out, compression	Tensile strength, pull-out force, energy absorption	Most common for macro-pins and macro-lattices, where out-of-plane anchoring, pin extraction, and infiltration efficiency are critical	Results strongly depend on feature geometry, embedded length, loading direction, and infiltration quality
	Double cantilever beam and end notch flexure	Mode I and Mode II interfacial fracture toughness	Useful for assessing crack opening and crack sliding resistance, especially in macro-pins	Requires controlled pre-crack insertion, mainly applicable to relatively planar joint configurations
	Fatigue	Load-cycle response, fatigue life, residual strength	Relevant for evaluating cyclic durability and progressive interfacial degradation in micro-features and macro-pins	Stress-based comparisons are difficult because of heterogeneous stress fields
	Impact	Damage tolerance, delamination resistance, crack deflection	Reported mainly for macro-pins and potentially relevant for macro-lattices subjected to dynamic loading	Rarely reported and difficult comparison across studies because of different impact energies and configurations
Complementary characterization and in-test monitoring	Digital image correlation and optical monitoring	Surface strain fields, crack initiation, deformation localization	Useful during mechanical testing to correlate deformation with failure mechanisms, reported for all categories	Cannot directly detect internal defects, requires optical access and surface preparation
	Surface morphology (OM, SEM, profilometry, confocal microscopy)	Roughness features, surface defects, micro-feature quality	Useful for all categories	Provides mainly surface information, does not directly assess the final interfacial quality
	Cross-sectional analysis	Infiltration quality, voids, interface continuity, material distortion, local defects	Useful for all categories	Limited to selected sections and may not represent the whole joint volume
	Fractography (OM, SEM, EDS, EBSD, XRD)	Failure mode, crack path, elemental composition, microstructural changes	Useful to interpret mechanical test results and identify failure type for all categories	Local observations require careful interpretation
	Micro-indentation	Local interfacial integrity, hardness variation	Useful for probing local property gradients near the interface, mainly reported for micro-features	Local and not directly representative of global joint performance
Non-destructive testing	Micro-computed tomography	Porosity, voids, incomplete infiltration, internal geometry, dimensional deviations, penetration depth	Particularly useful for macro-pin and macro-lattices with complex internal features	Resolution depends on specimen size, limited contrast between dissimilar materials, artefacts, scan time, cost, data-processing effort, and mostly laboratory-scale use
	Ultrasonic testing	Debonding, delamination, internal discontinuities, interface defects	Potentially scalable to larger components, mostly reported for macro-pins	Resolution limited by wavelength, signal attenuation and scattering increase in dissimilar materials, non-planar interfaces
	AI-assisted morphological analysis	Quantitative descriptors of surface defects and morphological features	Useful for automated analysis across all categories	Strongly dependent on image quality, dataset size, annotation quality, and model validation

plateau, as most of the load is still carried near the overlap edges, where stress concentrations occur. This behavior results from the eccentric load path inherent to the single-lap geometry, which introduces, in addition to the intended shear load, bending moments that generate normal stresses along the overlap edges, producing local peel effects. Variations also emerge in the thickness of the adherends. Some authors, such as Nguyen et al. [3], proposed adjusting the thickness to account for stiffness mismatch between dissimilar materials, according to the following relationship:

$$t_2 = \sqrt[3]{\frac{E_1}{E_2}} \times t_1$$

where t is the adherends thickness and E is the elastic modulus in the specimens longitudinal direction. Conversely, Banea [122] recommended keeping both adherends identical in thickness, arguing that maintaining geometric symmetry is more critical than balancing stiffness, as it minimizes bending moments and load eccentricity. Moreover, thickness also affects the joint performance, since thicker adherends can reduce peel effects and increase load-carrying efficiency, although this effect likewise saturates beyond a certain threshold [122,123]. Overall, the interplay among these parameters is one of the key factors governing how effectively the load is transferred through the interface, and thus the joint performance. While these considerations are well established for adhesively bonded joints, they can be reasonably extended to mechanically interlocked joints, although specific studies confirming these trends are still scarce.

Single lap shear tests can be carried out under various conditions to investigate different aspects of joint behavior. These tests can be conducted, for example, at quasi-static loading rates or under high-strain-rate conditions, as proposed by Graham et al. [18], particularly when dealing with composite materials, whose mechanical response is often strain-rate sensitive. Alternatively, environmental conditions can be modified to assess bond stability under different service scenarios. Moritz et al. [34], for instance, combined lap shear tests with a salt spray exposure for 1000 h (DIN EN ISO 9227 [124]). The results showed that corrosion resistance is strongly affected by the joining method. The configuration using pins combined with an adhesive layer exhibited the highest durability, as the adhesive acted as a barrier to moisture diffusion and corrosion.

However, as mentioned above, single-lap shear tests generate a non-uniform stress distribution along the bond line, with the highest peaks typically concentrated at the overlap edges [49]. To mitigate these issues, alternative configurations have been proposed. An example is the double-lap shear test, which provides a symmetric, non-eccentric loading condition that leads to a more uniform stress distribution, reducing the peel effects.

In addition to its mechanical advantages, the double-lap geometry has also been used to investigate other influencing factors. Grothe et al. [75], for instance, adopted a double-lap setup based on the ASTM D3528-96 standard [125] to study the role of temperature and processing conditions on joint performance. Their results showed that manufacturing-related factors, particularly residual stresses induced during the process, had a more significant impact on joint strength than the temperature variations during the tests. In particular, samples cured at lower temperature exhibited higher failure load even under cryogenic conditions, whereas those cured at higher temperature failed earlier, likely due to thermally induced residual stresses associated with shrinkage and differential thermal expansion. These findings underline the importance of thermal management during processing and the need to focus on residual stress effects, which are an unexplored aspect in the literature.

Beyond standardized configurations, customized testing setups can be designed to better reflect functional and application-specific conditions. Chueh et al. [27], for instance, designed a custom fixture system, which clearly aimed to ensure direct shear load across the bonded region, avoiding bending or tensile components (Fig. 22). Similarly, Freund et al. [60] developed a dedicated experimental methodology with a tailored specimen and a C-shaped fixture to prevent bending during shear loading, while a printed rim around the interlocking area controlled material infiltration and enabled repeatable testing.

Other, less common test configurations have also been explored, offering valuable insights despite their limited diffusion. Among these, one notable example is the scarf configuration proposed by Spaggiari and Favali [91], typically adopted when it is useful to compare the joint properties with those of the monolithic material. In this case, the adherends are joined through inclined surfaces, maintaining a continuous and uniform thickness along the joint. The absence of a distinct overlap zone eliminates stress concentrations and ensures a more homogeneous load transfer.

Lap-shear tests are widely adopted for assessing the performance of joints featuring micro-features and macro-pins, whereas their application to macro-lattices remains far less common. In macro-lattices, the joining process requires the secondary material to infiltrate the entire lattice volume. As a result, load transfer is not confined to the interface but occurs through the lattice structure itself, making the interpretation of lap-shear results less straightforward than for micro-features or macro-pins. Moreover, achieving complete and uniform infiltration in these systems can be more challenging, since the secondary material must penetrate through the full lattice thickness. This may lead to defects not only in the overlap region but also in the first layers of the secondary material. Corrado et al. [77], for instance, observed that, despite achieving high shear stress in single-lap shear tests applied to macro-lattices, premature failure occurred through delamination between the first CFRP plies, likely caused by resin starvation.

Hence, joints with macro-lattices are more commonly evaluated through compression and tensile/pull-out tests (terms that are often used interchangeably in the literature) [20,58,59]. Also in this case, these tests, which are likewise employed for macro-pins [94,96], lack a clearly defined reference standard. When specified, the ASTM D638 [126] is typically adopted [48], and classical dog-bone specimens could be employed [107], although this remains relatively uncommon.

In addition to these tests, other experimental methods are employed to evaluate the interfacial toughness of the joints. For instance, Bagnato et al. [51] utilized the Double Cantilever Beam (ASTM D5528-13 [127]) and End Notch Flexure (ESIS protocol) tests, both performed on specimens with a pre-crack inserted along the interface. In these tests, a non-stick PTFE film is introduced to ensure a controlled and repeatable initiation of debonding. The double cantilever beam test assesses crack opening, promoting the separation of the adherends along the interface, while the end notch flexure test measures crack sliding under flexural loading. Results showed that the effectiveness of the joining methods

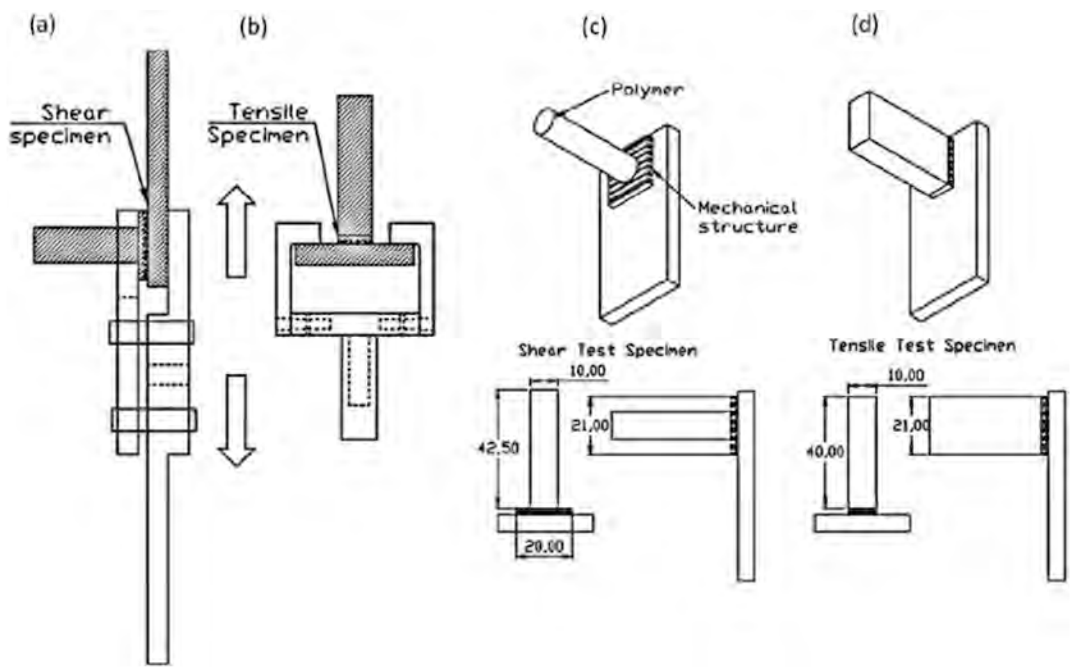

Fig. 22. Customized testing setups for evaluating mechanically interlocked joints under controlled shear (a,c) and tensile (b,d) loading conditions. Reprinted from [27], Copyright (2020), with permission from Elsevier.

depends on the loading mode: the presence of pins drastically increased resistance to crack opening, whereas the combined pin-adhesive configuration performed best under flexural conditions. Overall, deeper investigations of combined loading scenarios are still needed.

Moving to dynamic testing, fatigue performance is typically evaluated through cyclic lap shear tests (ASTM D3166 [128]), often complemented by additional protocols to account for environmental effects (e.g., ASTM D2295 [129], D1183 [130]), such as thermal cycling, humidity, and chemical exposure. It emerged again that, due to the coexistence of multiple interacting factors, a highly heterogeneous stress distribution develops at the interface, making conventional stress-based fatigue analyses unreliable [73]. For this reason, load-number of cycles curves are recommended instead of standard stress-number of cycles curves, allowing a more accurate representation of the mechanical response. Fatigue investigations showed that mechanically interlocked joints can sustain long cyclic loading, while exhibiting progressive interfacial degradation, especially under environmental exposure [18,73]. Finally, although less frequently reported, impact tests have also been used to evaluate damage tolerance. Graham et al. [18], for example, conducted impact tests, revealing that macro-pins effectively limit delamination and deflect crack propagation.

Mechanical testing is consistently complemented by additional analyses aimed at gaining deeper insight into joint behavior. These can include morphological characterizations [27,34], fractography analyses, performed through optical or electron microscopy [72,76], and damage monitoring techniques such as Digital Image Correlation (DIC) [34,110].

Morphological analyses play a crucial role, particularly in the studies involving micro-features. These analyses can be divided into two stages: surface characterization prior to joining, aimed at describing the morphology of the interlocking features, and post-joining analyses, aimed at evaluating the quality of the formed interface.

Prior to joining, surface morphology is typically characterized to assess topographical features, which strongly influence adhesion and interfacial strength. Optical and electron-based techniques are commonly employed, including confocal laser scanning microscopy, surface profilometry, Optical Microscopy (OM), and Scanning Electron Microscopy (SEM) [23,38,43]. Wang et al. [38], for instance, developed a systematic methodology to produce uniform, well-defined micro-features on metal surfaces, analyzing the influence of process parameters through SEM observations.

Post-joining analyses are mainly performed through cross-sectional investigations to evaluate the quality of the interfacial region and the degree of material infiltration within the interlocking structures. Several studies have reported incomplete infiltration or void formation, which may arise from the joining process, the geometry of the interlocking features, or the material selection [34,39,74]. For example, the high viscosity of polymeric components can hinder the complete filling of metallic surface structures [39]. Similar issues have also been observed when bonding metals with fibre-reinforced composites using pins, as their presence and geometry can strongly influence both the resin flow and the local fibre architecture, ultimately affecting joint performance [34,74]. In addition, SEM observations can be coupled with Energy Dispersive Spectroscopy (EDS) or Electron Backscatter Diffraction (EBSD) to investigate the elemental composition and crystallographic texture at the interface [86]. X-ray Diffraction (XRD) is also used to identify phase transformations or the formation of brittle secondary phases, which may affect joint performance [86].

Finally, micro-indentation methods, such as Vickers hardness-based interfacial testing, have been employed to locally probe interfacial integrity and evaluate bonding quality [86,87].

5.3. Non-destructive testing

Non-destructive techniques are often employed alongside destructive testing as supplementary tools. While destructive testing remains the primary method to determine joint strength and identify failure mechanisms, non-destructive testing plays a crucial role in investigating internal features and damage evolution without altering the integrity of the joint. An overview of the main reported tests, including metrics, main applicability and constraints, is reported in Table 4.

Among the available techniques, Micro-Computed Tomography (μCT) is increasingly adopted to investigate the internal morphology of interlocked joints, providing insights not only into porosity and manufacturing defects, but also into penetration depth within the interlocking structures. Englert et al. [43], for instance, used μCT to evaluate the infiltration of polymer into metallic macro-pins, revealing that penetration into undercut regions strongly depends on pin geometry and nozzle-substrate distance. Similarly, Popp et al. [78] combined μCT analysis with stereomicroscopy and a MATLAB-based image-processing script to investigate the fibre displacement during pin insertion, showing that compaction beneath the pin tips and matrix-rich zones around the pins are strongly influenced by pin diameter. Overall, μCT observations confirm that the joining process itself can substantially modify the local morphology, with direct implications for the mechanical integrity of the interface.

Advanced monitoring techniques, such as ultrasonic testing, have also been utilized for the evaluation of mechanically interlocked joints. For example, Parkes et al. [31] employed immersion pulse-echo ultrasonic testing to monitor interfacial debonding through variations in reflected acoustic energy. Using the same technique, Jasiūnienė et al. [70] proposed a novel signal post-processing algorithm capable of reconstructing the joint interface and improving the detection of internal defects. Although demonstrated using an immersion pulse-echo setup, the technique could be extended to more practical configurations, such as water-jet inspection, for industrial applications.

More recently, experimental investigations have increasingly been complemented by numerical modelling, statistical approaches, and machine learning-based methods [81,110]. In a recent study [81], conventional microscopy-based morphological inspection was integrated with a Region-based Convolutional Neural Network to quantitatively analyze the balling features typical of PBF-LB surfaces. These features, usually considered detrimental defects, were reinterpreted as potential anchoring sites for mechanical interlocking. This data-driven approach enabled the extraction of geometric descriptors, which were then correlated with finite-element predictions of interlocking strength, marking a shift toward quantitative and Artificial Intelligence (AI) assisted morphological characterization of AM surfaces.

Nevertheless, the application of non-destructive techniques to mechanically interlocked joints remains challenging. The presence of complex internal geometries, non-planar interfaces, and multi-material systems can significantly affect signal propagation and image interpretation, limiting defect detectability and quantitative accuracy. In particular, μCT analyses can be affected by artifacts and limited contrast resolution between phases. Ultrasonic techniques may suffer from signal scattering and attenuation at material interfaces, while AI-based analyses remain constrained by dataset quality, model validation, and image resolution. These limitations underscore that non-destructive techniques have not yet been fully adapted to the structural complexity of mechanically interlocked joints. Since such joints cannot be disassembled without damage, the development of reliable and tailored non-destructive inspection strategies remains an important research direction. The main experimental findings emerging from the testing methods discussed above are summarized in the following section.

5.4. Influence of mechanical interlocking structures geometry on joint performance

The experimental results obtained from the testing methods discussed above reveal several recurring trends, highlighting the significant role that the geometry of the interlocking structures plays in determining joint performance. Although the literature is still fragmented and testing conditions vary across studies, common relationships can be identified between feature size, shape, and spatial distribution and the resulting failure modes.

Failure modes in mechanically interlocked joints are described using different classifications, reflecting the inherent complexity of these systems. Miranda et al. [16] proposed a classification by adapting the failure modes commonly used for adhesive bonding to mechanical interlocking structures (Fig. 23a). According to this approach, failures can be categorized as adhesive failure, corresponding to interfacial debonding; cohesive failure, occurring within the interlocked region; and mixed failure, characterized by the coexistence of both mechanisms. The transition from adhesive to cohesive or mixed failures is generally associated with improved interfacial adhesion and more efficient load transfer. Alternative descriptions have also been proposed to account for mechanisms associated with specific interlocking structures. De Carvalho et al. [73], for instance, identified additional mechanisms such as pin pull-out, referring to the extraction of the pins without fracture; through-thickness reinforcement failure, associated with pin breakage; and net-tension failure, which occurs when rupture takes place in the unreinforced zone of the adherends.

When focusing on macro-pins, the correlation between geometry, load transfer, and failure behavior becomes particularly evident. While similar relationships can also be identified for micro-features and macro-lattices, the available studies remain more limited, and the resulting trends are therefore less clearly established. Nguyen et al. [68] developed a numerically and experimentally validated map correlating the pin aspect ratio L/D (length-to-diameter) and loading mode with the dominant failure mechanism, providing a useful tool for geometry optimization (Fig. 23b). Since pin pull-out represents a progressive failure mechanism within the cohesive failure mode, in which load is dissipated through friction and deformation along the pin, the authors suggest that it is generally preferred over brittle pin breakage. Their analysis revealed that the critical L/D ratio required to promote complete pin pull-out strongly depends on the loading mode, decreasing from about 6 in tension-dominated conditions to approximately 3.5 under shear-dominated loading. When the aspect ratio exceeds the critical value, the pin tends to fracture at the root due to increased bending stresses, limiting the energy absorption capacity of the joint. Similarly, Peralta Marino et al. [49] demonstrated that modifying the shape and height of the pins can effectively homogenize the stress distribution along the interface.

Further studies highlight that not only the geometry but also the spatial distribution of pins affects the load transfer and failure mode. De Carvalho and Amancio-Filho [112] showed that failure often initiates near the first row of pins and typically involves a combination of cohesive and adhesive mechanisms. Consistent observations were also reported by Graham et al. [18], who observed that pin failure is spatially non-uniform, with pins near the edges of the overlap carrying higher loads and failing earlier. To alleviate these effects and redistribute the load, the authors introduced a graded pin distribution, using fewer pins at the edges and a higher density toward the center of the overlap region (3 in the first row, 4 in the second, and 6 in the remaining four rows).

Overall, several design-oriented trends can be identified to guide the optimization of mechanically interlocked joints:

- Increasing the effective bonding area through mechanical interlocking structures generally leads to improved strength and toughness by promoting more effective mechanical engagement and load transfer at the interface. However, these improvements strongly depend on achieving complete material infiltration between the adherends, which must therefore be carefully considered when selecting materials and joining processes.
- Appropriately designed interlocking features, tailored to the expected loading conditions, can mitigate interfacial debonding, crack initiation and propagation, redistribute stresses, and promote cohesive failure mode.
- Geometrical transition regions within the interlocking structures often act as stress concentration sites [131]. Consequently, careful design of feature shapes is essential to avoid premature failure.
- In macro-pins, both pin geometry and distribution strongly influence joint performance. Thin and elongated pins tend to improve energy absorption and fatigue resistance, whereas shorter and wider pins increase stiffness and ultimate strength. Moreover, the spatial distribution of pins must reflect the stress distribution within the joint. Higher stress regions may benefit from a lower pin density to avoid local overloading, potentially combined with longer pins to improve load transfer. Conversely, regions experiencing lower stress can accommodate a higher density of shorter pins, allowing the load to be shared more effectively.

Establishing a clear relationship between interlocking geometry, load transfer mechanisms, and failure behavior is essential for the reliable integration of these joining strategies into structural multi-material components. The potential applications of mechanically interlocked joints across different industrial sectors are discussed in the following section, highlighting how the design principles identified above can be translated into practical solutions.

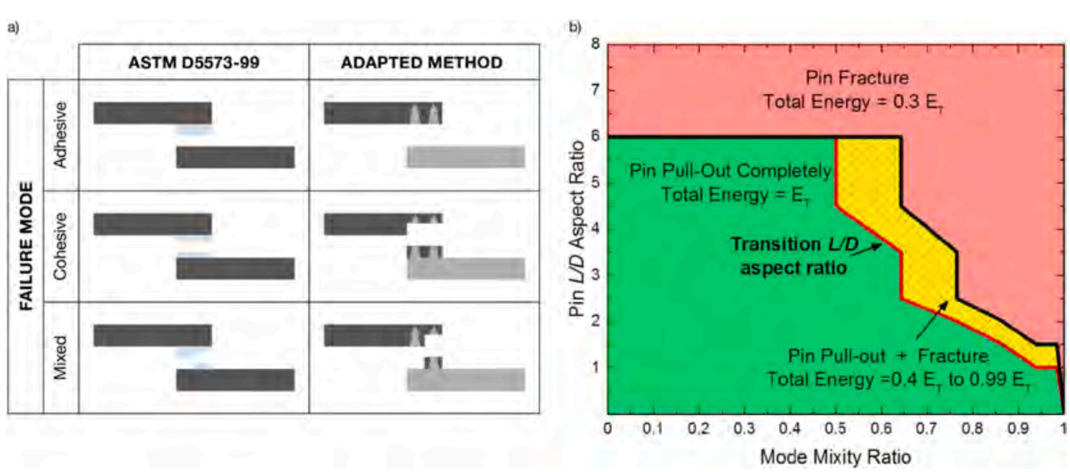

Fig. 23. Failure mechanisms in mechanically interlocked joints: (a) schematic classification of failure modes adapted from adhesive joints. Reprinted from [16], under the terms of the Creative Commons CC-BY-NC-ND license. (b) Failure map correlating pin aspect ratio (L/D) and loading mode with the dominant failure mechanism. Reprinted from [68], Copyright (2018), with permission from Elsevier.

6. Applications of mechanical interlocking structures

The adoption of AM-enabled mechanical interlocking structures has the potential to unlock new opportunities for developing complex, high-value, multi-material components. However, the analysis of current literature indicates that industrial uptake remains a distant prospect. The field is relatively recent and, consequently, the limited existing body of works is predominantly oriented towards understanding fundamental mechanisms and conducting laboratory-scale tests. Furthermore, the absence of robust design rules and standardized procedures limits the repeatability and reliability of the proposed solutions. In addition, AM processes impose practical constraints on build volume, productivity, and material, making scalability a major challenge [18]. Economic considerations also influence feasibility. Production costs depend on multiple parameters, including machine characteristics, material selection, build volume, and batching efficiency [79]. However, evaluating cost-effectiveness would require comprehensive life-cycle analyses, which fall outside the scope of this review and exceed the current maturity level of the technology. As a result, the available literature illustrates promising directions rather than fully validated industrial solutions, providing insights into which application areas may benefit from AM-enabled mechanical interlocking structures once the underlying manufacturing routes become more robust and scalable.

Only a limited number of studies explicitly address application-driven developments, which can be classified into five thematic areas: aerospace, automotive and lightweight mobility, biomedical devices, robotics and electronics, and secondary structural functions.

Aerospace applications reflect the sector longstanding pursuit of lightweight, high-performance multi-material structures and the need to realize reliable interfaces between specific material combinations such as Al/CFRP and Ti/CFRP, commonly employed in wing panels, helicopter blades, and other aeronautical components [26]. The widespread use of multi-material configurations in aerospace is exemplified by the Boeing 787 aircraft, which strategically combines CFRPs in weight-critical regions with metallic components in areas requiring greater impact and wear resistance [72]. This illustrates the structural demand for a robust joining approach capable of accommodating material incompatibilities, ensuring efficient load transfer, and meeting durability constraints. In this context, interlocking-based joining has been explored for load-bearing structural assemblies [67], serving as a fastening strategy in components such as trailing edge mechanisms and undercarriage door structures [44,52]. Further applications could include lightweight sandwich panel architectures [132], as well as aerospace-specific systems, such as thermal protection assemblies designed for harsh environments (Fig. 24) [133].

Applications in automotive and lightweight mobility reflect the increasing demand for energy-efficient and weight-optimized components – a priority shared across the entire transportation sector. Reducing mass directly lowers CO_2 emissions over the vehicle service life and helps compensate for additional weight introduced, for example, by electrification [134]. Consequently, multi-material solutions are already well established in this field, although reliable joining remains a critical challenge. Within this context, AM-enabled mechanical interlocking structures have been explored for structural automotive components such as seatback frames, where metal-composite regions have demonstrated up to 20% weight reduction while maintaining comparable stiffness to the baseline metallic design (Fig. 25) [134]. Beyond conventional automotive applications, lightweight mobility also encompasses alternative transportation systems such as bicycles. In this framework, fully customized, ergonomic handles with improved grip comfort have already been proposed, showcasing the potential of this joining strategy for tailored, high-performance assemblies [59].

In biomedical applications, mechanical interlocking enables the development of advanced implants, prosthetic components, and drug-delivery systems by facilitating the integration of dissimilar materials, including bio-functional materials. This sector particularly benefits from AM capability to tailor interfacial geometries to patient-specific anatomical conditions and to integrate mechanical anchoring with controlled functional gradients. Representative applications include bioinspired microneedles with microbarbs designed to enhance tissue anchorage and facilitate transdermal drug delivery [135,136]; orthopedic prosthetic components, such as hip implants and acetabular cups (Fig. 26), integrating dissimilar materials to achieve region-dependent mechanical or therapeutic functionality [27,88]; customized multi-material devices, such as mouthguards, that enhance impact absorption while improving patient-specific comfort [90,93], or dental restorations with engineered surface textures to improve functional performance and patient-specific adaptation [36,66]. Although examples remain at the prototype level, the biomedical field shows strong translational potential due to its inherent need for customization and interface reliability.

In the robotics and electronics field, mechanical interlocking plays a key role in enabling the local integration of materials with markedly different stiffness, which is essential for soft robotic actuators, grippers, wearable devices, and embedded electronics. A representative example in this domain is the soft robotic finger proposed by Rossing et al. [59], in which interlocking structures were used to mechanically anchor thermoplastic fingers to silicone, ensuring stable load transfer while preserving flexibility at the active fingertip. Interlocking structures have also been demonstrated in pressure sensors for robotic and

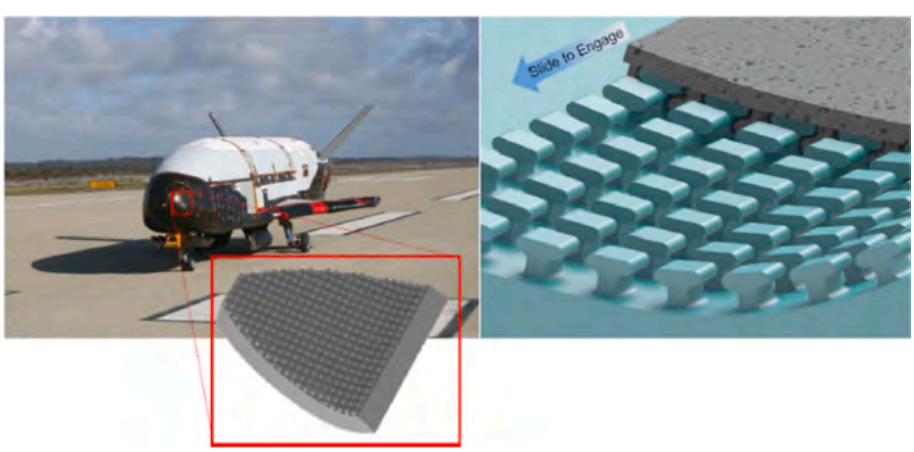

Fig. 24. Example of aerospace application of mechanical interlocking structures. Thermal protection tiles used in spacecraft such as the X-37B (left) may be attached to the underlying vehicle structure through macro-pins (right), allowing secure fixation while accommodating thermal expansion and mechanical loads. Reprinted from [133], under the terms of the Creative Commons CC BY 4.0 license.

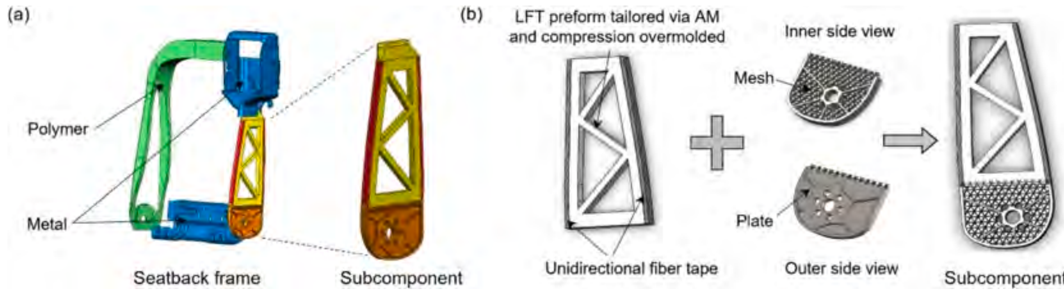

Fig. 25. Example of automotive application of mechanical interlocking structures. Topology-optimized seatback frame (a) incorporating a metal-composite sub-component joined through micro-features (b), enabling weight reduction while maintaining structural performance. Reprinted from [134], Copyright (2024), with permission from Elsevier.

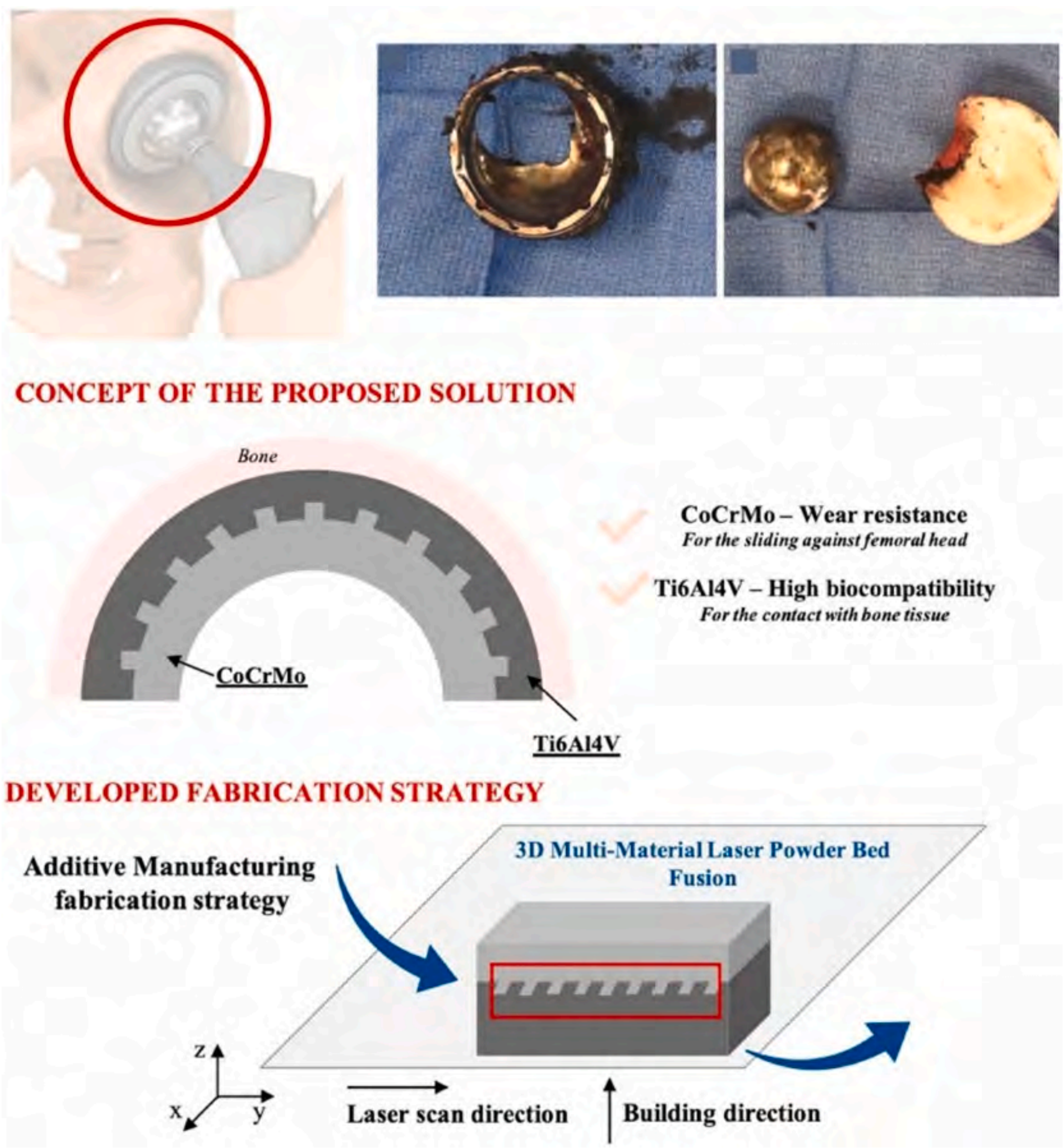

Fig. 26. Example of biomedical application of mechanical interlocking structures. Acetabular cup concept combining dissimilar metals through planar-based macro-lattices, enhancing mechanical performance at the interface. Reprinted from [88], Copyright (2023), with permission from Elsevier.

human–machine interaction applications, supporting reliable force detection across a wide range of loading conditions (Fig. 27) [137]. These examples show how AM-enabled interlocking can support hybrid soft-rigid mechanisms that are difficult to achieve with conventional bonding methods.

Finally, secondary structural functions encompass a diverse set of potential applications in which interlocking is not intended as the primary load-bearing mechanism, but to support adhesives or other joining technologies, such as inserts, mounting elements, and ancillary components. One recurrent example is the reinforcement of adhesive joints

Fig. 27. Example of electronic application of mechanical interlocking structures. Flexible piezoresistive sensor inspired by the structure of human fingerprints, incorporating micro-features between soft-rigid polymers to enhance sensing performance and mechanical stability. Adapted with permission from [137]. Copyright 2024 American Chemical Society.

with micro-features inspired by gecko toe morphology to increase the shear strength of the bond (Fig. 28) [83,138].

In summary, these five domains illustrate the breadth of opportunities offered by AM-enabled mechanical interlocking structures, demonstrating how sector-specific requirements, from structural efficiency to soft-rigid materials integration, can be addressed through geometrically tailored interfaces that complement and overcome specific limitations of traditional joining technologies.

7. Current limitations and future perspectives

The analysis conducted throughout this review demonstrates that mechanical interlocking has emerged as a promising strategy for joining dissimilar materials. The adoption of AM technologies has further expanded the range of achievable architectures, enabling control over surface morphology, geometric complexity, and multi-material integration. By examining micro-features, macro-pins, and macro-lattices, along with the related material combinations, manufacturing strategies, and performance metrics, it becomes clear that AM-enabled

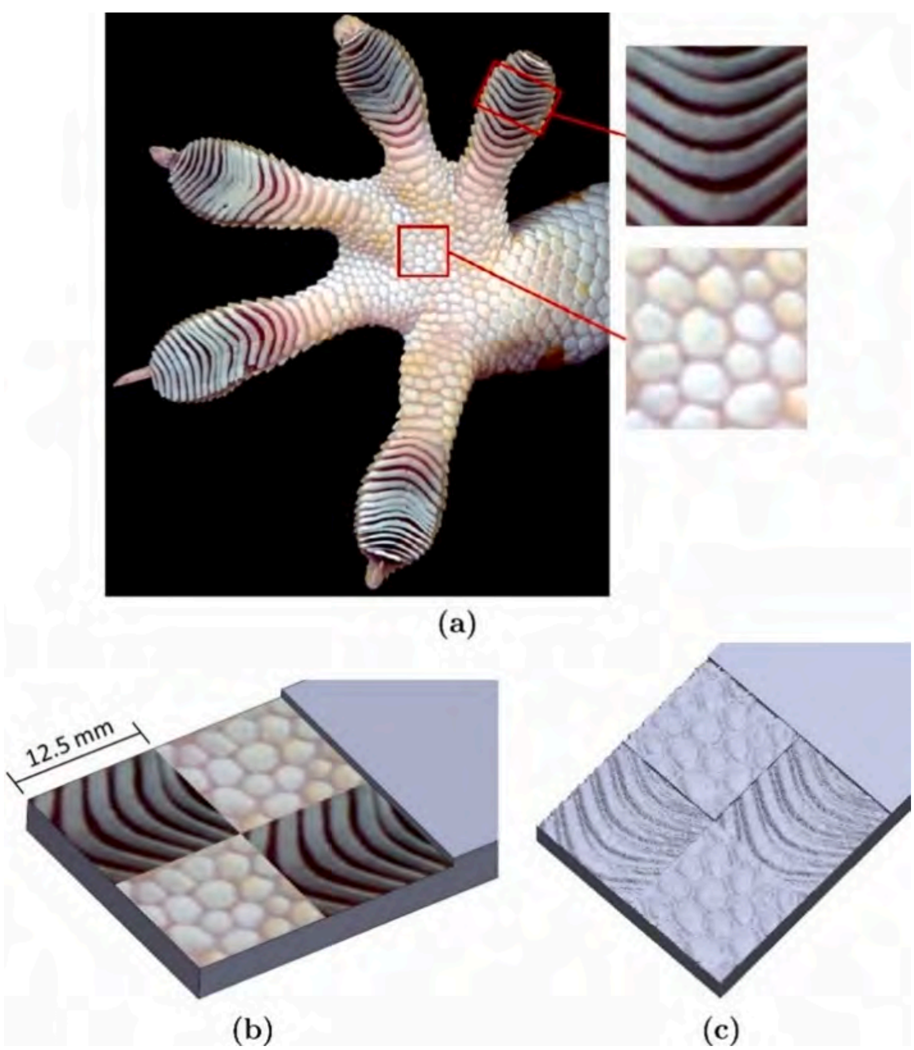

Fig. 28. Example of secondary structural function of mechanical interlocking structures. Bio-inspired micro-features derived from gecko toe morphology (a), applied to the overlap region of a component to enhance adhesion and increase the shear strength of adhesive joints (b-c). Reprinted from [83], Copyright (2025), with permission from Elsevier.

mechanically interlocked joints offer a viable route to complement and overcome several limitations of conventional joining methods. This strategy is especially attractive for joining material combinations that are difficult to bond through conventional methods due to differences in thermal expansion, surface chemistry, or mechanical properties. Despite the encouraging performance trends observed, the technological maturity of this strategy remains low. The available literature is still highly fragmented, methodologies diverge, and only a few studies provide demonstrators approaching real application requirements. Taken together, these factors reveal a set of persistent challenges that must be addressed to consolidate the field and unlock its full potential.

In this context, a primary challenge is the lack of standardized procedures for both the design and testing of mechanically interlocked joints. Geometries, material combinations, process strategies, test configurations, and reported metrics vary widely, hindering cross-study comparison and the establishment of robust and generalizable rules. Consequently, the reliability and repeatability of the obtained joints are affected, limiting the capacity to validate performance trends and derive transferable conclusions. The field would therefore greatly benefit from consolidated guidelines and unified methodological frameworks. Moreover, current studies often investigate isolated interlocking configurations, whereas the potential of hybrid approaches necessitates further investigations.

A further limitation arises from the restricted combination of materials investigated to date. As the industrial sector continues to evolve, there is a growing trend toward the use of materials such as composites reinforced with natural fibers. These materials offer promising functional and mechanical characteristics; however, their integration within this domain remains scarce. Sustainability and recyclability should be also considered in this sense. Multi-material components complicate material separation and end-of-life management, making recyclability a critical aspect to be addressed already at the design stage [92]. While monolithic components benefit from well-established recovery pathways and environmental data, multi-material solutions introduce complexity, particularly in composite-based structures, for which mature recycling technologies remain limited [139,140]. The sustainability of mono- versus multi-material components is a complex and context-dependent issue that requires full life-cycle evaluation. Comprehensive studies on this topic are still largely lacking.

An additional challenge concerns the further development and extension of AM technologies to support multi-material components. While future research should aim to fully exploit the potential of existing AM techniques, additional progress is expected from the emergence of dedicated MMAM platforms. In parallel, the development of specific design tools will be essential to fully leverage these technologies [141]. Beyond manufacturing, testing and quality assessment also remain critical barriers, due to the intrinsic complexity of mechanically interlocked joints. The local evolution of stresses, deformation, and material flow during manufacturing, as well as process-related factors, has been shown to exert a strong influence on the final quality and mechanical reliability of the interlocked interface. Since mechanical interlocking structures are not intended to be disassembled, robust non-destructive inspection strategies and post-process controls are essential [58,100]. However, the current literature has only begun to address these capabilities.

Finally, it is evident that the technology is in an early stage of development and not yet sufficiently mature for widespread practical implementation. The majority of studies are confined to laboratory-scale specimens, meaning that current manufacturing routes lack the stability and reproducibility needed for industrial workflows. Progress in this direction will require intermediate steps, including the consolidation of scalable processes and the development and validation of pilot-scale demonstrators.

At the current stage, practical research actions include:

- Establish mechanism-oriented datasets that correlate interfacial descriptors, such as roughness amplitude, pore size, feature spacing, and surface morphology, with mechanical performance. These datasets should also report failure modes using consistent criteria, in order to distinguish the different type of fracture.
- Develop equivalent datasets for measurable macro-scale descriptors, including L/D ratio, pin distribution, lattice topology, cell size, strut or wall thickness. This should be supported by unified testing framework, design-of-experiments campaigns, simulations, or machine-learning models to generate design-performance maps. As an initial step, this could focus on the most relevant metal-polymer and metal-composite systems highlighted in this review.
- Establish quantitative correlations between dissimilar joining techniques applied to the same interlocking category. This would help clarify which joining route is most suitable for each type of geometry, while also considering material compatibility and process-related constraints.
- Validate non-destructive inspection and quality-assessment protocols specifically tailored to mechanically interlocked interfaces. Particular attention should be paid to the detection of incomplete infiltration, lack of contact, internal porosity, pin defects, lattice damage, and local debonding, since these features can strongly affect the reliability of the joint but are not always visible from external inspection.
- Develop and validate pilot-scale demonstrators that move beyond laboratory coupons by incorporating realistic geometries and application requirements.

CRediT authorship contribution statement

Federica Valenza: Writing – original draft, Methodology, Investigation. **Eleonora Atzeni:** Writing – review & editing, Supervision, Funding acquisition. **Alberta Aversa:** Writing – review & editing, Supervision. **Sara Biamino:** Writing – review & editing, Supervision, Funding acquisition. **Alessandro Salmi:** Writing – review & editing, Visualization, Supervision.

Declaration of competing interest

The authors declare the following financial interests/personal relationships which may be considered as potential competing interests: Sara Biamino, Politecnico di Torino DISAT reports financial support was provided by Ministero dell'Università e della Ricerca (MUR). If there are other authors, they declare that they have no known competing financial interests or personal relationships that could have appeared to influence the work reported in this paper.

Acknowledgements

The research was funded by MUR (Ministero dell'Università e della Ricerca) under the grant scheme PRIN2020 with the project TARGET "addiTive mAnufactuRing for liGhtwEight joinTs" (grant number 2020E3XL47).

Data availability

Data will be made available on request.

References

[1] A. Kausar, I. Ahmad, S.A. Rakha, M.H. Eisa, A. Diallo, State-of-the-art of sandwich composite structures: manufacturing—to—high performance applications, J. Compos. Sci. 7 (2023) 102, https://doi.org/10.3390/jcs7030102.

[2] H.-J. Um, H.-J. Rho, N.-H. Jeon, J.-H. Shin, H.-S. Kim, Mechanical performance of novel curved sandwich structures featuring 3D printed continuous carbon fiber/polyamide 6 composite corrugated core with rail interlocking, Compos. B 295 (2025) 112222, https://doi.org/10.1016/j.compositesb.2025.112222.

[3] A.T.T. Nguyen, C.K. Amarasinghe, M. Brandt, S. Feih, A.C. Orifici, Loading, support and geometry effects for pin-reinforced hybrid metal-composite joints, Compos. A 98 (2017) 192–206, https://doi.org/10.1016/j.compositesa.2017.03.019.
[4] M. Mariam, M. Afendi, M.S. Abdul Majid, M.J.M. Ridzuan, A.G. Gibson, Tensile and fatigue properties of single lap joints of aluminium alloy/glass fibre reinforced composites fabricated with different joining methods, Compos. Struct. 200 (2018) 647–658, https://doi.org/10.1016/j.compstruct.2018.06.003.
[5] P.H. Hari Krishna, T. DhilipKumar, K.V. Shankar, M.P. Hariprasad, A.P. Murali, A. El-Rayyes, K.G. Prashanth, Review on nature-inspired interfaces and mechanical interlocking techniques in additively manufactured adhesively bonded joints, J. Mater. Res. Technol. 39 (2025) 998–1016, https://doi.org/10.1016/j.jmrt.2025.09.150.
[6] S. Maggiore, M.D. Banea, P. Stagnaro, G. Luciano, A review of structural adhesive joints in hybrid joining processes, Polymers 13 (2021) 3961, https://doi.org/10.3390/polym13223961.
[7] P. Kah, R. Suoranta, J. Martikainen, C. Magnus, Techniques for joining dissimilar materials: metals and polymers, Rev. Adv. Mater. Sci. 36 (2014) 152–164.
[8] K. Ramaswamy, R.M. O'Higgins, M.C. Corbett, M.A. McCarthy, C.T. McCarthy, Quasi-static and dynamic performance of novel interlocked hybrid metal-composite joints, Compos. Struct. 253 (2020) 112769, https://doi.org/10.1016/j.compstruct.2020.112769.
[9] E.E. Feistauer, J.F. dos Santos, S.T. Amancio-Filho, A review on direct assembly of through-the-thickness reinforced metal–polymer composite hybrid structures, Polym. Eng. Sci. 59 (2019) 661–674, https://doi.org/10.1002/pen.25022.
[10] A. Galińska, C. Galiński, Mechanical joining of fibre reinforced polymer composites to metals—a review. Part II: Riveting, clinching, non-adhesive form-locked joints, pin and loop joining, Polymers 12 (2020) 1681, https://doi.org/10.3390/polym12081681.
[11] M.J. Page, D. Moher, P.M. Bossuyt, I. Boutron, T.C. Hoffmann, C.D. Mulrow, L. Shamseer, J.M. Tetzlaff, E.A. Akl, S.E. Brennan, R. Chou, J. Glanville, J. M. Grimshaw, A. Hróbjartsson, M.M. Lalu, T. Li, E.W. Loder, E. Mayo-Wilson, S. McDonald, L.A. McGuinness, L.A. Stewart, J. Thomas, A.C. Tricco, V.A. Welch, P. Whiting, J.E. McKenzie, PRISMA 2020 explanation and elaboration: updated guidance and exemplars for reporting systematic reviews, BMJ 372 (2021) n160, https://doi.org/10.1136/bmj.n160.
[12] M.J. Page, J.E. McKenzie, P.M. Bossuyt, I. Boutron, T.C. Hoffmann, C.D. Mulrow, L. Shamseer, J.M. Tetzlaff, E.A. Akl, S.E. Brennan, R. Chou, J. Glanville, J. M. Grimshaw, A. Hróbjartsson, M.M. Lalu, T. Li, E.W. Loder, E. Mayo-Wilson, S. McDonald, L.A. McGuinness, L.A. Stewart, J. Thomas, A.C. Tricco, V.A. Welch, P. Whiting, D. Moher, The PRISMA 2020 statement: an updated guideline for reporting systematic reviews, BMJ 372 (2021) n71, https://doi.org/10.1136/bmj.n71.
[13] N. Sarantinos, V. Kostopoulos, G. Di Vita, G. Campoli, L. Bricout, Micro-pins: the next step in composite–composite and metal–composite joining, CEAS Space J. 11 (2019) 351–358, https://doi.org/10.1007/s12567-019-00251-1.
[14] N. Sarantinos, S. Tsantzalis, S. Ucsnik, V. Kostopoulos, Review of through-the-thickness reinforced composites in joints, Compos. Struct. 229 (2019) 111404, https://doi.org/10.1016/j.compstruct.2019.111404.
[15] A. Seharing, A.H. Azman, S. Abdullah, A review on integration of lightweight gradient lattice structures in additive manufacturing parts, Adv. Mech. Eng. 12 (2020) 1687814020916951, https://doi.org/10.1177/1687814020916951.
[16] R. Miranda, F. Valenza, F.D. Franco, M. Santamaria, A. Aversa, E. Atzeni, S. Biamino, F. Sarasini, V. Fiore, Influence of pin distribution and anodizing on strength of co-bonded joints between additive AlSi10Mg and basalt fibre epoxy composite, Mater. Des. 260 (2025) 114967, https://doi.org/10.1016/j.matdes.2025.114967.
[17] A.T.T. Nguyen, M. Brandt, A.C. Orifici, S. Feih, Hierarchical surface features for improved bonding and fracture toughness of metal–metal and metal–composite bonded joints, Int. J. Adhes. Adhes. 66 (2016) 81–92, https://doi.org/10.1016/j.ijadhadh.2015.12.005.
[18] D.P. Graham, A. Rezai, D. Baker, P.A. Smith, J.F. Watts, The development and scalability of a high strength, damage tolerant, hybrid joining scheme for composite–metal structures, Compos. A 64 (2014) 11–24, https://doi.org/10.1016/j.compositesa.2014.04.018.
[19] A.A. Alsheghri, O. Alageel, M. Amine Mezour, B. Sun, S. Yue, F. Tamimi, J. Song, Bio-inspired and optimized interlocking features for strengthening metal/polymer interfaces in additively manufactured prostheses, Acta Biomater. 80 (2018) 425–434, https://doi.org/10.1016/j.actbio.2018.09.029.
[20] S. Verma, C.-K. Yang, C.-H. Lin, J.Y. Jeng, Additive manufacturing of lattice structures for high strength mechanical interlocking of metal and resin during injection molding, Addit. Manuf. 49 (2022) 102463, https://doi.org/10.1016/j.addma.2021.102463.
[21] T. Kuipers, R. Su, J. Wu, C.C.L. Wang, ITIL: interlaced topologically interlocking lattice for continuous dual-material extrusion, Addit. Manuf. 50 (2022) 102495, https://doi.org/10.1016/j.addma.2021.102495.
[22] Y. Ding, H. Jiang, M.L. Dunn, K. Yu, 3D interfacial material-locking structures to promote bonding strength of dissimilar materials, J. Manuf. Processes 112 (2024) 92–102, https://doi.org/10.1016/j.jmapro.2024.01.031.
[23] R. Freund, H. Watschke, J. Heubach, T. Vietor, Determination of influencing factors on interface strength of additively manufactured multi-material parts by material extrusion, Appl. Sci. 9 (2019) 1782, https://doi.org/10.3390/app9091782.
[24] A. Marques, A. Cunha, M. Gasik, O. Carvalho, F.S. Silva, F. Bartolomeu, 3D multi-material laser powder bed fusion: Ti6Al4V–CuNi2SiCr parts for aerospace applications, Prog. Addit. Manuf. 9 (2024) 391–400, https://doi.org/10.1007/s40964-023-00460-5.
[25] E. Ertürk, B. Musil, G. Diez, C. Felber, P. Höfer, Surface morphology influences of PBF-LB manufactured Ti6Al4V parts on adhesive bond strength—investigation of as-built and surface-treated conditions, Prog. Addit. Manuf. 8 (2023) 719–731, https://doi.org/10.1007/s40964-023-00450-7.
[26] R. Sandeep, A. Natarajan, Advances in joining technologies for the innovation of 21st century lightweight aluminium-CFRP hybrid structures, Proc. Inst. Mech. Eng., Part E: J. Process Mech. Eng. 236 (2022) 1239–1255, https://doi.org/10.1177/09544089211073027.
[27] Y.-H. Chueh, C. Wei, X. Zhang, L. Li, Integrated laser-based powder bed fusion and fused filament fabrication for three-dimensional printing of hybrid metal/polymer objects, Addit. Manuf. 31 (2020) 100928, https://doi.org/10.1016/j.addma.2019.100928.
[28] B. Goetzendorfer, T. Mohr, R. Hellmann, Hybrid approaches for selective laser sintering by building on dissimilar materials, Materials 13 (2020) 5285, https://doi.org/10.3390/ma13225285.
[29] G. Martins, C.M.S. Vicente, M. Leite, Polymer-metal adhesion of single-lap joints using fused filament fabrication process: aluminium with carbon fiber reinforced polyamide, Appl. Sci. 13 (2023) 4429, https://doi.org/10.3390/app13074429.
[30] S. Yu, S. Park, D.Y. Kang, G.S. Shin, M.W. Lee, S.Y. Moon, J.Y. Hwang, Strategic dual laser 3D printing of structural metal-plastic hybrid materials, Compos. B 261 (2023) 110794, https://doi.org/10.1016/j.compositesb.2023.110794.
[31] P.N. Parkes, R. Butler, J. Meyer, A. de Oliveira, Static strength of metal-composite joints with penetrative reinforcement, Compos. Struct. 118 (2014) 250–256, https://doi.org/10.1016/j.compstruct.2014.07.019.
[32] E. Ertürk, J.G. Diez, P. Vitale, P. Höfer, Surface morphology influences on the adhesive bond performance of PBF-LB manufactured Ti6Al4V parts – investigation of quasi-static and fatigue loading conditions, J. Adhes. 101 (2025) 1219–1251, https://doi.org/10.1080/00218464.2024.2441886.
[33] N. Zoesmar, D. Fuchs, I. Taha, Treatment of additively manufactured AlSi10Mg surfaces for improved bonding with fiber reinforced composites for sandwich applications, J. Sandw. Struct. Mater. 24 (2022) 1152–1168, https://doi.org/10.1177/10996362211035431.
[34] J. Moritz, P. Götze, T. Schiefer, L. Stepien, A. Klotzbach, J. Standfuß, E. López, F. Brückner, C. Leyens, Additive manufacturing of titanium with different surface structures for adhesive bonding and thermal direct joining with fiber-reinforced polyether-ether-ketone (PEEK) for lightweight design applications, Metals 11 (2021) 265, https://doi.org/10.3390/met11020265.
[35] P.K. Rajamani, T. Ageyeva, J.G. Kovács, Personalized mass production by hybridization of additive manufacturing and injection molding, Polymers 13 (2021) 309, https://doi.org/10.3390/polym13020309.
[36] K. Dai, J. Wu, Z. Zhao, H. Yu, Z. Zhao, B. Gao, Surface texture designs to improve the core–veneer bond strength of zirconia restorations using digital light processing, Materials 16 (2023) 6072, https://doi.org/10.3390/ma16186072.
[37] X. Zou, L. Huang, K. Chen, M. Jiang, S. Zhang, M. Wang, X. Hua, A. Shan, Surface structuring via additive manufacturing to improve the performance of metal and polymer joints, Metals 11 (2021) 567, https://doi.org/10.3390/met11040567.
[38] T. Wang, K. Yasuda, H. Nishikawa, Fabrication of micron-sized protrusions on metal surface for metal/polymer easy-disassembly joining by selective laser melting technology, Mater. Des. 220 (2022) 110873, https://doi.org/10.1016/j.matdes.2022.110873.
[39] G.H.M. Oliveira, C. Belei, W.S. de Carvalho, L.B. Canto, S.T. Amancio-Filho, On the fully additive manufacturing of PC/AlSi10Mg hybrid structures, Mater. Lett. 330 (2023) 133378, https://doi.org/10.1016/j.matlet.2022.133378.
[40] G.H.M. Oliveira, V.F. Sciuti, R.B. Canto, S. Arneitz, L. Minkowitz, S.T. Amancio-Filho, L.B. Canto, Additive manufacturing of surface structured metal parts for high strength lightweight injection overmolded polymer-metal hybrid joints, Int. J. Adhes. Adhes. 141 (2025) 104045, https://doi.org/10.1016/j.ijadhadh.2025.104045.
[41] S.G. Kim, A. Suzuki, N. Takata, M. Kobashi, Control of surface micro−structure for Al alloy/polymer joining fabricated by laser process using Al−Ti−C powders: effect of powder composition, J. Adv. Joining Process. 4 (2021) 100068, https://doi.org/10.1016/j.jajp.2021.100068.
[42] X.-P. Zheng, Y.-P. Cao, B. Li, X.-Q. Feng, S.-W. Yu, Surface wrinkling of nanostructured thin films on a compliant substrate, Comput. Mater. Sci 49 (2010) 767–772, https://doi.org/10.1016/j.commatsci.2010.06.020.
[43] L. Englert, A. Heuer, M.K. Engelskirchen, F. Frölich, S. Dietrich, W.V. Liebig, L. Kärger, V. Schulze, Hybrid material additive manufacturing: interlocking interfaces for fused filament fabrication on laser powder bed fusion substrates, Virtual Phys. Prototyp. 17 (2022) 508–527, https://doi.org/10.1080/17452759.2022.2048228.
[44] N. Yunzhu, H. Bai, Z. Wang, H. Liao, W. Wu, Bio-inspired, metal additive manufacturing interlocked structures: geometrically design and fracture performance analysis, Compos. Struct. 321 (2023) 117220, https://doi.org/10.1016/j.compstruct.2023.117220.
[45] E. Alvarez, S. González, L. Lopez, E. Niebles Nuñez, Experimental study of adhesive joints with mechanical interlocking of acrylonitrile butadiene styrene (ABS) parts fabricated for fused filament (FFF), Rapid Prototyp. J. 29 (2023) 1984–2000, https://doi.org/10.1108/RPJ-04-2023-0146.
[46] D.F. Silva, I.M. Bragança, C.M. Silva, L.M. Alves, P.A. Martins, Joining by forming of additive manufactured 'mortise-and-tenon' joints, Proc. Inst. Mech. Eng., Part B: J. Eng. Manuf. 233 (2019) 166–173, https://doi.org/10.1177/0954405417720954.

[47] R.J. Nash, Y. Li, Experimental and numerical analysis of 3D printed suture joints under shearing load, Eng. Fract. Mech. 253 (2021) 107912, https://doi.org/10.1016/j.engfracmech.2021.107912.
[48] M. Ribeiro, O. Sousa Carneiro, A. Ferreira da Silva, Interface geometries in 3D multi-material prints by fused filament fabrication, Rapid Prototyp. J. 25 (2018) 38–46, https://doi.org/10.1108/RPJ-05-2017-0107.
[49] G. Peralta Marino, S. De la Pierre, M. Salvo, A. Díaz Lantada, M. Ferraris, Modelling, additive layer manufacturing and testing of interlocking structures for joined components, Sci. Rep. 12 (2022) 2526, https://doi.org/10.1038/s41598-022-06521-z.
[50] D.P. Graham, A. Rezai, D. Baker, P.A. Smith, J. Watts, A hybrid joining scheme for high strength multimaterial joints, ICCM International Conferences on Composite Materials (2011). https://iccm-central.org/iccm-18/.
[51] T. Bagnato, A.R. Ravindran, A. Mirabedini, R.B. Ladani, E. Kandare, A.C. Orifici, P. Chang, J. Wang, A.P. Mouritz, Superior interfacial toughening of hybrid metal-composite structural joints using 3D printed pins, Compos. A 168 (2023) 107479, https://doi.org/10.1016/j.compositesa.2023.107479.
[52] A.T.T. Nguyen, M. Brandt, S. Feih, A.C. Orifici, Pin pull-out behaviour for hybrid metal-composite joints with integrated reinforcements, Compos. Struct. 155 (2016) 160–172, https://doi.org/10.1016/j.compstruct.2016.07.047.
[53] D. Huelsbusch, M. Haack, A. Solbach, C. Emmelmann, F. Walther, Influence of pin size on tensile and fatigue behavior of TI-CFRP hybrid structures produced by laser additive manufacturing, International Conference on Composite Materials, ICCM (2015), http://doi.org/10.5281/zenodo.15444615.
[54] L. Raimondi, L. Tomesani, A. Zucchelli, Enhancing the robustness of hybrid metal-composite connections through 3D printed micro penetrative anchors, Appl. Compos. Mater. 31 (2024) 1275–1293, https://doi.org/10.1007/s10443-024-10224-1.
[55] P.N. Parkes, R. Butler, D.P. Almond, Growth of damage in additively manufactured metal-composite joints. ECCM 2012 - Composites at Venice, Proceedings of the 15th European Conference on Composite Materials, 2012.
[56] J. Rivera, M.S. Hosseini, D. Restrepo, S. Murata, D. Vasile, D.Y. Parkinson, H. S. Barnard, A. Arakaki, P. Zavattieri, D. Kisailus, Toughening mechanisms of the elytra of the diabolical ironclad beetle, Nature 586 (2020) 543–548, https://doi.org/10.1038/s41586-020-2813-8.
[57] M. Frascio, A. Zafferani, M. Monti, M. Avalle, Investigating enhanced interfacial adhesion in multi-material filament 3D printing: a comparative study of t and Mickey Mouse geometries, Prog. Addit. Manuf. 9 (2024) 2113–2122, https://doi.org/10.1007/s40964-024-00570-8.
[58] R. Freund, F.M. Sallach, T. Vietor, Design freedoms of lattice structures for interlock bonding, Fut. Autom. Prod. Conf. 2022 (2023) 156–169, https://doi.org/10.1007/978-3-658-39928-3_12.
[59] L. Rossing, R.B.N. Scharff, B. Chömpff, C.C.L. Wang, E.L. Doubrovski, Bonding between silicones and thermoplastics using 3D printed mechanical interlocking, Mater. Des. 186 (2020) 108254, https://doi.org/10.1016/j.matdes.2019.108254.
[60] R. Freund, S. Koch, H. Watschke, E. Stammen, T. Vietor, K. Dilger, Utilization of additively manufactured lattice structures for increasing adhesive bonding using material extrusion, J. Adhes. 100 (2024) 340–361, https://doi.org/10.1080/00218464.2021.1983431.
[61] A. Ahmad, L. Belluomo, M. Bici, F. Campana, Bird's eye view on lattice structures: design issues and applications for best practices in mechanical design, Metals 13 (2023) 1666, https://doi.org/10.3390/met13101666.
[62] T. Wang, Q. Chen, C. Wang, X. Wang, C. Liu, Design and fabrication of Al-Mg bimetallic interface structures via synergistic additive manufacturing and powder hot pressing, Mater. Today Commun. 49 (2025) 114295, https://doi.org/10.1016/j.mtcomm.2025.114295.
[63] D.K. Pokkalla, A.A. Hassen, D. Nuttall, N. Tsiamis, M.L. Rencheck, V. Kumar, P. Nandwana, C.B. Joslin, P. Blanchard, S.L. Tamhankar, P. Maloney, V. Kunc, S. Kim, A novel additive manufacturing compression overmolding process for hybrid metal polymer composite structures, Addit. Manuf. Lett. 5 (2023) 100128, https://doi.org/10.1016/j.addlet.2023.100128.
[64] W. Shi, Y. Wang, C.L. Bi, H. Xu, Y.F. Zheng, C. Zhe Li, B. Li, B. Xie, Microstructure and properties of interlocking Cu/Al bimetallic composites by porous lattice additive combined with vacuum liquid infiltration, J. Alloys Compd. 1032 (2025), https://doi.org/10.1016/j.jallcom.2025.181142.
[65] R. Freund, K. Hilbig, T. Vietor, A systematic evaluation of design freedoms and restrictions of lattice structures used as interlock bonds, Designs 8 (2024) 97, https://doi.org/10.3390/designs8050097.
[66] J. Chen, Z. Yan, K. Tang, J. Li, X. Lyu, Z. Zhao, F. Li, J. Chen, F. Wang, Micropore texture design enhancing zirconia-resin bonding of additively manufactured zirconia, Surf. Interfaces 77 (2025) 108008, https://doi.org/10.1016/j.surfin.2025.108008.
[67] C. Kralovec, A. Dengg, M. Schagerl, A. Schiller, C. Bisagni, M. Loebbecke, J. Haubrich, R. Hanelt, Static strength and fatigue life of pinned hybrid titanium-composite single-lap-shear joints, Compos. Struct. 354 (2025) 118765, https://doi.org/10.1016/j.compstruct.2024.118765.
[68] A.T.T. Nguyen, N. Pichitdej, M. Brandt, S. Feih, A.C. Orifici, Failure modelling and characterisation for pin-reinforced metal-composite joints, Compos. Struct. 188 (2018) 185–196, https://doi.org/10.1016/j.compstruct.2017.12.043.
[69] J. Moritz, P. Götze, T. Schiefer, A. Klotzbach, J. Standfuß, E. Lopez, F. Brueckner, C. Leyens, Joining of additively manufactured titanium with different surface structures with fiber-reinforced PEEK for lightweight design applications, international conference hybrid, Mater. Struct. (2020), in: https://hybrid2020.dgm.de/the-conference/proceedings/.
[70] E. Jasiūnienė, L. Mažeika, V. Samaitis, V. Cicėnas, D. Mattsson, Ultrasonic non-destructive testing of complex titanium/carbon fibre composite joints, Ultrasonics 95 (2019) 13–21, https://doi.org/10.1016/j.ultras.2019.02.009.
[71] G. De Pasquale, F.E. Altunok, Multiphase modeling of matrix/fiber-related damaging mechanism in multimaterial additively manufactured joints with 3D interlocking, Eng. Fail. Anal. 170 (2025) 109272, https://doi.org/10.1016/j.engfailanal.2025.109272.
[72] K. Shirasu, M. Mizutani, N. Takano, H. Yoshinaga, T. Oguri, K.-I. Ogawa, T. Okabe, S. Obayashi, Lap-shear strength and fracture behavior of CFRP/3D-printed titanium alloy adhesive joint prepared by hot-press-aided co-bonding, Int. J. Adhes. Adhes. 117 (2022) 103169, https://doi.org/10.1016/j.ijadhadh.2022.103169.
[73] W.S. De Carvalho, J. Draper, T. Terrazas-Monje, A. Toumpis, A. Galloway, S. T. Amancio-Filho, Fatigue life assessment and fracture mechanisms of additively manufactured metal-fiber reinforced thermoplastic hybrid structures produced via ultrasonic joining, J. Mater. Res. Technol. 26 (2023) 5716–5730, https://doi.org/10.1016/j.jmrt.2023.08.305.
[74] B. Castro, A.C. Orifici, P. Muscat, A.A. Khatibi, The effect of pin angle on the microstructure of resin-infused pin-reinforced metal-composite hybrid joints, Hybrid Adv. 5 (2024) 100182, https://doi.org/10.1016/j.hybadv.2024.100182.
[75] R. Grothe, M. Pohl, J. Troschitz, C. Weidermann, K.P. Weiss, M. Gude, Characterization of intrinsic interfaces between fibre-reinforced composites and additively manufactured metal for designing hybrid structures, J. Adv. Joining Process. 9 (2024) 100209, https://doi.org/10.1016/j.jajp.2024.100209.
[76] Y. Nusom, S. Srimanosaowapak, V. Uthaisangsuk, Effects of 3D-printing surface morphologies on interfacial bonding strength between Ti–6Al–4V and CFRTP with PMCs interlayer, Int. J. Adhes. Adhes. 121 (2023) 103313, https://doi.org/10.1016/j.ijadhadh.2022.103313.
[77] A. Corrado, R. De Biasi, D. Rigotti, F. Stecca, A. Pegoretti, M. Benedetti, Hybrid single lap joints between 3D printed titanium lattices and CFRP composites: experimental and numerical insights, Metals 14 (2024) 268, https://doi.org/10.3390/met14030268.
[78] J. Popp, T. Kleffel, D. Römisch, T. Papke, M. Merklein, D. Drummer, Fiber orientation mechanism of continuous fiber reinforced thermoplastics hybrid parts joined with metallic pins, Appl. Compos. Mater. 28 (2021) 951–972, https://doi.org/10.1007/s10443-021-09892-0.
[79] S. Graziosi, F. Cannazza, M. Vedani, A. Ratti, F. Tamburrino, M. Bordegoni, Design and testing of an innovative 3D-printed metal-composite junction, Addit. Manuf. 36 (2020) 101311, https://doi.org/10.1016/j.addma.2020.101311.
[80] Y.-H. Chueh, X. Zhang, J.-C.-R. Ke, Q. Li, C. Wei, L. Li, Additive manufacturing of hybrid metal/polymer objects via multiple-material laser powder bed fusion, Addit. Manuf. 36 (2020) 101465, https://doi.org/10.1016/j.addma.2020.101465.
[81] M. Aladag, I. Zglobicka, M. Cyriac, L. Stepien, E. Lopez, K. Jan Kurzydlowski, Analysis of mechanical interlocking of as-printed LPBF surfaces, Next Mater. 9 (2025) 101151, https://doi.org/10.1016/j.nxmate.2025.101151.
[82] B. Ma, Y. Yang, Y. Wang, Y. Xu, L. Bi, Experimental investigation on microstructure and properties of Al alloy-PEEK joint with different surface structure obtained by hot-pressing, J. Adhes. Sci. Technol. 38 (2024) 2085–2099, https://doi.org/10.1080/01694243.2023.2283997.
[83] M.G. Atahan, I. Maskery, I. Ashcroft, M.K. Apalak, A. Pappas, Effect of bio-mimicked surface texturing on the shear strength of additively manufactured metal single-lap joints: an innovative approach, Eng. Fail. Anal. 174 (2025) 109460, https://doi.org/10.1016/j.engfailanal.2025.109460.
[84] Y.-R. Kim, E.-A. Kim, J.P. Choi, T. Ha, S. Won, J.B. Jeon, S.-H. Kwon, H.-S. Lee, Assessment of joinability in additively manufactured interlocking structures, Crystals 13 (2023) 1575, https://doi.org/10.3390/cryst13111575.
[85] Y. Ni, Z. Wang, H. Bai, Q. Zeng, H. Liao, W. Wu, Investigations of the failure mode for additive manufactured interlocked interface structure based on X-Ray CT image guided finite element analysis and experimental comparisons, Eng. Fract. Mech. 284 (2023) 109220, https://doi.org/10.1016/j.engfracmech.2023.109220.
[86] X. Li, P. Jiang, M. Nie, Z. Liu, M. Liu, Y. Qiu, Z. Chen, Z. Zhang, Enhanced strength-ductility synergy of laser additive manufactured stainless steel/Ni-based superalloy dissimilar materials characterized by bionic mechanical interlocking structures, J. Mater. Res. Technol. 26 (2023) 4770–4783, https://doi.org/10.1016/j.jmrt.2023.08.217.
[87] C. Wei, L. Li, X. Zhang, Y.-H. Chueh, 3D printing of multiple metallic materials via modified selective laser melting, CIRP Ann. 67 (2018) 245–248, https://doi.org/10.1016/j.cirp.2018.04.096.
[88] F. Bartolomeu, O. Carvalho, M. Gasik, F.S. Silva, Multi-functional Ti6Al4V-CoCrMo implants fabricated by multi-material laser powder bed fusion technology: a disruptive material's design and manufacturing philosophy, J. Mech. Behav. Biomed. Mater. 138 (2023) 105583, https://doi.org/10.1016/j.jmbbm.2022.105583.
[89] L. Liu, D. Wang, T. Wang, C. Han, Y. Li, H. Tan, W. Zhou, X. Yan, L. Lei, Y. Yang, Laser additive manufacturing of multimaterials with hierarchical interlocking interface via a flexible scraper-based method, Int. J. Mach. Tools Manuf 205 (2025) 104236, https://doi.org/10.1016/j.ijmachtools.2024.104236.
[90] N. Nasrollahzadeh, M. Broome, D.P. Pioletti, A new approach to the design and fabrication of customized multi-material mouthguards to maximize athletes' safety and comfort, J. Manuf. Process. 136 (2025) 282–290, https://doi.org/10.1016/j.jmapro.2025.01.042.
[91] A. Spaggiari, F. Favali, Evaluation of polymeric 3D printed adhesively bonded joints: effect of joint morphology and mechanical interlocking, Rapid Prototyp. J. 28 (2022) 1437–1451, https://doi.org/10.1108/RPJ-09-2021-0259.

[92] C. Leupold, M. Petersen, Approach to an automated method for load-optimized design of multimaterial joints for additive manufacturing, Ind. Addit. Manuf. (2024) 115–129, https://doi.org/10.1007/978-3-031-42983-5_8.
[93] N. Nasrollahzadeh, D.P. Pioletti, M. Broome, Design of customized mouthguards with superior protection using digital-based technologies and impact tests, Sports Med. - Open 10 (2024) 64, https://doi.org/10.1186/s40798-024-00728-2.
[94] W. Wang, Y. Sun, Y. Lu, J. Wang, Y. Cao, C. Zhang, Tensile behavior of bio-inspired hierarchical suture joint with uniform fractal interlocking design, J. Mech. Behav. Biomed. Mater. 113 (2021) 104137, https://doi.org/10.1016/j.jmbbm.2020.104137.
[95] D. Wu, Z. Zhao, P. Wang, Y. Pei, H. Chen, H.J. Qi, D. Fang, Structured interfaces for improving the tensile strength and toughness of stiff/highly stretchable polymer hybrids, Adv. Mater. Technol. 5 (2020) 2000652, https://doi.org/10.1002/admt.202000652.
[96] D. Dairabayeva, A. Perveen, D. Talamona, Investigation on the mechanical performance of mono-material vs multi-material interface geometries using fused filament fabrication, Rapid Prototyp. J. 29 (2023) 40–52, https://doi.org/10.1108/RPJ-07-2022-0221.
[97] G.L. Goh, S. Lee, S.H. Cheng, D.J.S. Goh, P. Laya, V.P. Nguyen, B.S. Han, W. Y. Yeong, Enhancing interlaminar adhesion in multi-material 3D printing: a study of conductive PLA and TPU interfaces through fused filament fabrication, MSAM 3 (2024). https://doi.org/10.36922/msam.2672.
[98] B. Liu, Y. Xu, W. Cao, P. Lu, C. Huang, Cooperative enhancement of multi-material interface strength by mechanical interlocking structures and FDM path planning, Int. J. Adv. Manuf. Technol. 134 (2024) 4099–4115, https://doi.org/10.1007/s00170-024-14398-7.
[99] B. Vins, A. Gupta, S. Suri, A. Kishor, A. Chandrasekar, Optimizing adhesion in fused filament fabrication-printed thermoplastic polyurethane–polylactic acid composites: effects of penetration, overlapping, and void reduction, J. Mater. Eng. Perform. (2025), https://doi.org/10.1007/s11665-025-12437-2.
[100] Z. Qiang, S. Yan, Z. Zeang, A brief review of mechanical designs for additive manufactured soft materials, Soft Sci. 2 (2022) 2. http://doi.org/10.20517/ss.2021.22.
[101] ISO/ASTM 52900:2021: Additive manufacturing - General principles - Fundamentals and vocabulary, Geneva, Switzerland, 2021.
[102] B. Jetté, V. Brailovski, M. Dumas, C. Simoneau, P. Terriault, Femoral stem incorporating a diamond cubic lattice structure: design, manufacture and testing, J. Mech. Behav. Biomed. Mater. 77 (2018) 58–72, https://doi.org/10.1016/j.jmbbm.2017.08.034.
[103] S.L. Sing, W.Y. Yeong, F.E. Wiria, B.Y. Tay, Characterization of titanium lattice structures fabricated by selective laser melting using an adapted compressive test method, Exp. Mech. 56 (2016) 735–748, https://doi.org/10.1007/s11340-015-0117-y.
[104] C. Yan, L. Hao, A. Hussein, P. Young, D. Raymont, Advanced lightweight 316L stainless steel cellular lattice structures fabricated via selective laser melting, Mater. Des. 55 (2014) 533–541, https://doi.org/10.1016/j.matdes.2013.10.027.
[105] W.S. de Carvalho, N.F. Colvin, A. Benatar, S.T. Amancio-Filho, Ultrasonic joining of additively manufactured metal-composite hybrid joints: a comparison between vertical and horizontal vibration modes, Metals 13 (2023) 319, https://doi.org/10.3390/met13020319.
[106] W.S. de Carvalho, G.S. Vacchi, C.A.D. Rovere, S.T. Amancio-Filho, Joining of additively manufactured fiber-reinforced thermoplastic and metals by ultrasonic energy: mechanical and corrosion behavior, Mater. Des. 234 (2023) 112342, https://doi.org/10.1016/j.matdes.2023.112342.
[107] I. Mustafa, T.H. Kwok, Development of intertwined infills to improve multi-material interfacial bond strength, J. Manuf. Sci. Eng. 144 (2021) 1–10, https://doi.org/10.1115/1.4051884.
[108] E. Weflen, M.C. Frank, Hybrid additive and subtractive manufacturing of multi-material objects, Rapid Prototyp. J. 27 (2021) 1860–1871, https://doi.org/10.1108/RPJ-06-2020-0142.
[109] S.d.T. Amancio-Filho, R.M.M. Falck, Method for producing a layered component. DE Patent DE102016121267A1. 2018.
[110] C. Belei, R. Pommer, S.T. Amancio-Filho, Optimization of additive manufacturing for the production of short carbon fiber-reinforced polyamide/Ti-6Al-4V hybrid parts, Mater. Des. 219 (2022) 110776, https://doi.org/10.1016/j.matdes.2022.110776.
[111] R. Falck, S.M. Goushegir, J.F. dos Santos, S.T. Amancio-Filho, AddJoining: a novel additive manufacturing approach for layered metal-polymer hybrid structures, Mater. Lett. 217 (2018) 211–214, https://doi.org/10.1016/j.matlet.2018.01.021.
[112] W.S. De Carvalho, S.T. Amancio-Filho, On the feasibility of joining additively-manufactured 316L stainless steel and poly-ether-ether-ketone by ultrasonic energy, Addit. Manuf. Lett. 3 (2022) 100098, https://doi.org/10.1016/j.addlet.2022.100098.
[113] P. Golewski, T. Sadowski, M. Nowicki, Mechanical response of adhesive and hybrid joints containing novel additive manufacturing adherends, Constr. Build. Mater. 379 (2023) 131230, https://doi.org/10.1016/j.conbuildmat.2023.131230.
[114] Z. Dawei, Z. Qi, F. Xiaoguang, Z. Shengdun, Review on joining process of carbon fiber-reinforced polymer and metal: applications and outlook, rare met, Mater. Eng. 48 (2019) 44–54, https://doi.org/10.1016/S1875-5372(19)30018-9.
[115] T. Abreu, R.M. Leal, C. Leitão, I. Galvão, Metal–polymer joining by additive manufacturing: effect of printing parameters and interlocking design, J. Manuf. Mater. Process. 8 (2024) 228, https://doi.org/10.3390/jmmp8050228.
[116] ASTM D1002-10R19: Standard Test Method for Apparent Shear Strength of Single-Lap-Joint Adhesively Bonded Metal Specimens by Tension Loading (Metal-to-Metal), West Conshohocken, PA, USA, 2019.
[117] ASTM D3165-07R14: Standard Test Method for Strength Properties of Adhesives in Shear by Tension Loading of Single-Lap-Joint Laminated Assemblies, West Conshohocken, PA, USA, 2014.
[118] ASTM D5868-01R14: Standard Test Method for Lap Shear Adhesion for Fiber Reinforced Plastic (FRP) Bonding, West Conshohocken, PA, USA, 2014.
[119] ISO 19095-1:2015: Plastics - Evaluation of the adhesion interface performance in plastic-metal assemblies, Geneva, Switzerland, 2015.
[120] ISO 13445:2003: Adhesives - Determination of shear strength of adhesive bonds between rigid substrates by the block-shear method, Geneva, Switzerland, 2003.
[121] M. Banea, L.F.M. Silva, Adhesively bonded joints in composite materials: An overview, Proc. Inst. Mech. Eng., Part L: J. Mater.: Des. Appl. 223 (2009) 1–18, https://doi.org/10.1243/14644207JMDA219.
[122] M. Banea, Influence of adherend properties on the strength of adhesively bonded joints, MRS Bull. 44 (2019) 625–629, https://doi.org/10.1557/mrs.2019.180.
[123] F. Bianchi, Y. Liu, A.M. Joesbury, D. Ayre, X. Zhang, A finite element model for predicting the static strength of a composite hybrid joint with reinforcement pins, Materials 16 (2023) 3297, https://doi.org/10.3390/ma16093297.
[124] ISO 9227:2017: Corrosion tests in artificial atmospheres - Salt spray tests, Geneva, Switzerland, 2017.
[125] ASTM D3528-96R16: Standard Test Method for Strength Properties of Double Lap Shear Adhesive Joints by Tension Loading, West Conshohocken, PA, USA, 2016.
[126] ASTM D638-14: Standard Test Method for Tensile Properties of Plastics, West Conshohocken, PA, USA, 2014.
[127] ASTM D5528-13: Standard Test Method for Mode I Interlaminar Fracture Toughness of Unidirectional Fiber-Reinforced Polymer Matrix Composites, West Conshohocken, PA, USA, 2013.
[128] ASTM D3166-99R20 Standard Test Method for Fatigue Properties of Adhesives in Shear by Tension Loading (Metal/Metal), West Conshohocken, PA, USA, 2020.
[129] ASTM D2295-96R16: Standard Test Method for Strength Properties of Adhesives in Shear by Tension Loading at Elevated Temperatures (Metal-to-Metal), West Conshohocken, PA, USA, 2016.
[130] ASTM D1183-03R19: Standard Practices for Resistance of Adhesives to Cyclic Laboratory Aging Conditions, West Conshohocken, PA, USA, 2019.
[131] K. Davaasambuu, Y. Dong, A. Pramanik, A.K. Basak, Mechanisms and performance of composite joints through adhesive and interlocking means—a review, J. Compos. Sci. 9 (2025) 359, https://doi.org/10.3390/jcs9070359.
[132] Y. Liu, Z. Wang, B. Yi, Enhancing mechanical performances of material extrusion additively manufactured composite sandwich structures via multi-scale interfacial bonding strategies, Polym. Compos. 46 (2025) 17041–17055, https://doi.org/10.1002/pc.70094.
[133] B. Young, O. Bolmin, B. Boyce, P. Noell, Synergistic strengthening in interlocking metasurfaces, Mater. Des. 227 (2023) 111798, https://doi.org/10.1016/j.matdes.2023.111798.
[134] D.K. Pokkalla, N. Garg, M. Paramanathan, V. Kumar, M.L. Rencheck, P. Nandwana, V. Kunc, A.A. Hassen, S. Kim, Design optimization of lightweight automotive seatback through additive manufacturing compression overmolding of metal polymer composites, Compos. Struct. 349–350 (2024) 118504, https://doi.org/10.1016/j.compstruct.2024.118504.
[135] Z. Chen, Y. Lin, W. Lee, L. Ren, B. Liu, L. Liang, Z. Wang, L. Jiang, Additive manufacturing of honeybee-inspired microneedle for easy skin insertion and difficult removal, ACS Appl. Mater. Interfaces 10 (2018) 29338–29346, https://doi.org/10.1021/acsami.8b09563.
[136] R.K. Pirlo, C. McCrea, L. Carothers, K. Shrader, E. Johnson, T. Tilly, Additive manufacturing of high-resolution solid microneedles via continuously variable stacked extrusion (CVSE) of conductive thermoplastic using a fused filament fabrication (FFF) printer, Manuf. Lett. 44 (2025) 1–5, https://doi.org/10.1016/j.mfglet.2025.01.005.
[137] W. Tang, B. Lv, Z. Pei, Z. Fu, C. Zhang, Y. Zeng, K. Wang, Q. Zhang, Bioinspired soft pressure sensors with interlocked structures based on 3D printing methods, ACS Appl. Polym. Mater. 6 (2024) 11575–11585, https://doi.org/10.1021/acsapm.4c02224.
[138] N. Naat, K. Hajlaoui, S. Mezlini, L.F.M. da Silva, Enhanced mechanical interlocking in adhesive joints through precision-engineered surface patterns on 3D-printed PLA adherends, Int. J. Adhes. Adhes. 142 (2025) 104132, https://doi.org/10.1016/j.ijadhadh.2025.104132.
[139] F. Borda, G. Ambrogio, L. Filice, F. Gagliardi, Integrated costs and environmental impacts optimization for production of a multi-material component, Proc. CIRP 122 (2024) 587–592, https://doi.org/10.1016/j.procir.2024.02.017.
[140] S. Ura, A. Fuji, A. Kubo, J. Tamaki, Analyzing the sustainability of bimetallic components, Int. J. Autom. Technol. 8 (2014) 745–753. https://doi.org/10.20965/ijat.2014.p0745.
[141] D.J. Roach, C.M. Hamel, C.K. Dunn, M.V. Johnson, X. Kuang, H.J. Qi, The m4 3D printer: a multi-material multi-method additive manufacturing platform for future 3D printed structures, Addit. Manuf. 29 (2019) 100819, https://doi.org/10.1016/j.addma.2019.100819.